A Functional Characterization of the Mouse Huntingtin N-terminus in the Adult Brain

Elise Marie Braatz
Charlottesville, Virginia

B.S. Interdisciplinary Studies with a Concentration in
Neuroscience, Chemistry Minor, College of William and Mary,
2015

A Dissertation presented to the Graduate Faculty of the
University of Virginia in Candidacy for the
Degree of Doctor of Philosophy

Department of Neuroscience

University of Virginia
December, 2021

Abstract

The N-terminus of the Huntingtin (HTT) protein is comprised of three functional domains encoded by exon 1 of the *Huntingtin* (*HTT*) gene. The polyglutamine stretch (polyQ), which is expanded in Huntington's disease (HD), is flanked by the first 17 amino acids (N17) and the proline rich region (PRR). In vitro, the N17 domain can regulate HTT's subcellular localization in response to increased oxidative stress [1], and the PRR is a protein-protein interaction domain [2, 3]. Mice lacking regions of the Htt N-terminus are born at the expected Mendelian frequency, suggesting that the Htt N-terminus is not required for Htt's critical role during embryonic development [4-7]. In aged mice, deletion of the polyQ domain results in an increase in autophagy markers [8], while deletion of the N17 domain results in a reduction in thalamostriatal glutamatergic synapses [4]. The behavioral consequences of single- or double-domain deletions within the Htt N-terminus, however, are not consistent [4-6], suggesting that these domains do not function in isolation. Characterizing a model with a deletion in all three Htt N-terminal domains should contribute to our understanding the function of the Htt N-terminus in vivo.

I have characterized a mouse model with a deletion of the N17, polyQ, and PRR domains of the Htt N-terminus ($Htt^{\Delta E1}$), and found that while the progeny from $Htt^{\Delta E1/+}$ intercrosses were born at the expected Mendelian frequency, there was a sex-specific distortion in the number of $Htt^{\Delta E1/\Delta E1}$ and $Htt^{+/+}$ progeny. I performed longitudinal examinations of motor and spatial learning and memory performance in $Htt^{\Delta E1/\Delta E1}$, $Htt^{\Delta E1/+}$, and $Htt^{\Delta E1/-}$, $Htt^{+/+}$, and $Htt^{+/-}$ mice, and found that $Htt^{\Delta E1/\Delta E1}$ mice exhibit a non-progressive rotarod deficit compared to $Htt^{+/+}$ mice. Additionally, I investigated Htt subcellular localization, DNA damage repair, oxidative stress markers, synapse numbers, and autophagosome marker levels in $Htt^{\Delta E1/\Delta E1}$ and $Htt^{+/+}$ mice, and found no differences between genotypes. I did, however, observe an increase in DNA double strand breaks (DSBs) in the cortex and striatum of 3-month-old mice along with elevated pan-nuclear levels of the DNA DSB repair protein 53bp1.

I have also characterized the *Htt*$^{\Delta E1}$ allele in trans to an HD model allele (*Htt*$^{140Q/\Delta E1}$), and found that the *Htt*$^{\Delta E1}$ allele modifies HD phenotype progression. *Htt*$^{140Q/\Delta E1}$ mice exhibit delayed onset of HD mouse model motor phenotypes including reduced grip strength and hypoactivity. The *Htt*$^{\Delta E1}$ allele did not modify spatial learning and memory performance. Additionally, Htt subcellular localization and autophagy levels were not significantly altered and levels of synaptic markers were not consistently changed in *Htt*$^{140Q/\Delta E1}$ mice compared to *Htt*$^{140Q/+}$ mice, or in single- or double-domain deletion mice (*Htt*$^{140Q/\Delta Q}$, *Htt*$^{140Q/\Delta QP}$, or *Htt*$^{140Q/\Delta N17}$) compared to *Htt*$^{140Q/+}$ mice.

Based on these results, I conclude that the Htt N-terminus is not required for Htt's critical functions in development and in the brain, but instead may modulate the efficiency of some Htt functions both under basal conditions and in the presence of an HD model allele.

Acknowledgements

I would like to thank Scott Zeitlin for providing advice and support throughout my time in graduate school, Jeh-Ping Liu for sharing technical expertise, and Emily André for developing the mouse model that this project is based on. To my committee members, Iggy Provencio, George Bloom, Madaline Harrison, and John Lukens, thank you for providing invaluable guidance and encouragement. Thank you to the past members of the Zeitlin lab who helped me with mouse genotyping, Sharon Garrot, Amanda Peck, Jong Shin, Allen Jo, and Matt Barnes. Thank you to the members of the NGP, the UVA Neuroscience Department, and BIG Center for many helpful discussions, and to Josh Milstein and Heather Ferris for sharing protocols and materials. I would also like to thank Valerie Spencer and the vivarium staff, NGP Coordinator Nadia Cempré, and NGP Directors Manoj Patel, Chris Deppmann, and Alban Gaultier. Thank you to my mom, dad, brother, and my extended family for their love, support, and understanding. To my friends, thank you for reminding me to laugh and for helping me to maintain perspective. And to Kevin, thank you for being there for me through it all.

Financial support was provided by NIH training grant 4T32GM008328 and NIH/NINDS NS077926 and NS090914.

Table of Contents

Chapter I: Introduction

Huntington's disease (HD) is caused by an autosomal dominant trinucleotide repeat mutation in the *Huntingtin (HTT)* gene [9, 10]. In HD, an expansion of the CAG repeats within exon 1 of *HTT* results in an elongated polyglutamine (polyQ) stretch in the N-terminus of the Huntingtin protein (HTT). Beyond a pathogenic threshold of 36-39Q, this expansion results in the formation of nuclear and cytoplasmic HTT aggregates within neurons and other postmitotic cells [11-13]. There are currently no treatments available that can effectively prevent HD onset or progression. Loss of normal HTT function likely contributes to HD pathogenesis, as conditional knockout of *Htt* in the brains of mice leads to neurodegeneration [14] and absence of wild type *Htt* expression affects disease severity in HD model mice [15]. Additionally, HTT functions in many cellular processes that are altered in HD. Determining the normal function of HTT is therefore critical for understanding HD pathogenesis and progression.

Huntington's disease

The hallmark pathological feature of HD is progressive neurodegeneration of the medium spiny neurons (MSNs) of the striatum and, in later stages of the disease, pyramidal neurons in layers V/VI of the cortex. HD has a prevalence of ~2.71 per 100,000 worldwide. European populations (~5.70 per 100,000) are more affected than Asian populations (~0.40 per 100,000) [16]. Symptoms usually manifest between ages 35 and 50, although the age of onset is correlated with the length of the polyQ expansion, so juvenile-onset HD cases can occur when CAG repeat lengths are extremely long [17]. HD causes a wide range of motor, cognitive, and psychiatric symptoms. The most distinctive symptom of HD is chorea, an involuntary writhing and dance-like movement; however, HD patients can also experience psychiatric and

cognitive symptoms such as depression, anxiety, apathy, irritability, and dementia [18]. HTT is expressed throughout the body, and HD symptoms such as weight loss, skeletal muscle degeneration, and osteoporosis may be due to mutant HTT (mHTT) expression in the periphery [19]. Treating psychiatric HD symptoms with common pharmacological interventions such as antidepressants is often successful. However, in late disease stages, voluntary movement is disrupted and the most likely cause of death in HD patients is aspiration pneumonia caused by difficulty swallowing [20].

Huntingtin structure

The *HTT* gene is located on the short arm of chromosome 4 at position 16.3, and its translated product was identified in 1993 as a large (~350kDa) protein with a variable polyQ stretch [9]. HTT is a multifunctional protein that acts as a scaffold for a variety of cellular processes [21-24]. HTT is comprised of multiple alpha-helical solenoid domains, known as HEAT (Huntingtin, elongation factor 3, protein phosphatase 2A, and TOR1) repeats, that are known to modulate protein-protein interactions [25].

HTT's primary amino acid sequence is similar to the yeast proteins Atg23, Vac8, and Atg11 at the N-terminus, middle, and C-terminus of HTT, respectively. In yeast, these proteins function as components of the cytoplasm-to-vacuole targeting pathway, and HTT is thought to function in a similar manner during autophagy [22]. In addition, the HTT N-terminal region may interact with the C-terminus of HTT. Fragments of these two HTT segments can co-immunoprecipitate, and their hypothesized yeast orthologs, Atg11 and Atg23, can also interact with each other [22].

Huntingtin N-terminus structure

HTT's N-terminus is comprised of three functional domains encoded by the first exon of *HTT*: the first 17 amino acids (N17), the polyglutamine domain (polyQ), and the proline-rich region (PRR). The PRR, which evolved in vertebrates and is present in all mammals [26], can associate with proteins containing a Src homology 3 (SH3) [2] or tryptophan (WW) domain [3]. The polyQ region may modulate HTT's ability to bind directly to DNA [27]. Many transcription factors contain a polyQ stretch, and Spinocerebellar Ataxia 17—another trinucleotide repeat disease—is the result of a polyQ expansion in the TATA binding protein, which is a crucial component of transcriptional machinery. The HTT polyQ domain first appeared in deuterostomes and has increased in length throughout evolution, reaching its longest length in humans [26]. It is hypothesized to act as a flexible hinge, allowing for interactions between the N17 and PRR domains [28]. The N17 domain forms an alpha helix that is highly conserved among vertebrates [26], and may regulate HTT's subcellular localization [1, 29, 30]. Evolutionarily, the HTT N-terminus emerged as nervous systems became more complex, and it is proposed to have specialized nervous system functions [26].

Post-translational modifications

HTT has the potential to undergo a variety of post-translational modifications including phosphorylation, acetylation, sumoylation, ubiquitination, and palmitoylation. Within the HTT N17 domain, serines S13 and S16 are targets for phosphorylation, which signal for HTT translocation to the nucleus [23]. In addition, methionines M1 and M8 within the N17 domain are susceptible to oxidization, contributing to HTT's ability to react to oxidative stress [1]. S13 and S16 phosphorylation reduces HTT aggregation in HD models, and promotes HTT clearance [31, 32]. Threonine T3 is also a target for

phosphorylation within HTT's N17 domain, and T3 phosphorylation may modulate HTT structure and mutant HTT aggregation properties [33].

Both mutant and normal HTT can be cleaved by caspases and calpains between amino acids 400 and 600 to form N-terminal fragments prior to HD onset [34, 35]. Since unexpanded HTT N-terminal fragments are also found in unaffected brains, this cleavage is likely a part of HTT's normal catabolic processing [34] but may be increased in the context of HD [35]. In the presence of mHTT, N-terminal fragments of HTT with unexpanded polyQ domains can be detected in aggregates along with mHTT [36-38].

Huntingtin function in health and disease

HTT is a scaffolding protein with multiple protein-protein interaction domains that allow it to participate in a variety of protein complexes. HTT contributes to embryonic and CNS development, transcriptional regulation, intracellular transport, metabolism, synaptic function, autophagy, and DNA damage repair. In a study defining the HTT interactome in vivo, 747 binding partners were identified that participate in organelle and vesicle trafficking, synaptic function, and nucleotide-binding [39].

Embryonic development

Htt knockout leads to early embryonic lethality before neurulation at embryonic day (E)8.5 [40-42]. Ubiquitous conditional *Htt* knock-out in 2-month-old mice results in death within 10 days from acute pancreatitis that is not dependent on the Htt N-terminus, however, if *Htt* inactivation is postponed to 4 months of age, the majority of mice survive the first 10 days after loss of *Htt* expression [43]. Conditional knockout of *Htt* in the

forebrain at either E15 or postnatal day (P)5 results in progressive neurodegeneration and a decreased lifespan [14]. In addition, stem cells from *Htt* knockout mice are unable to differentiate into neuronal precursors [44], suggesting a role for HTT in nervous system development.

Nervous system development

When *Htt* expression is knocked down in mice starting during early embryonic development and continuing until P21, these animals exhibit striatal degeneration at 12 months of age [45]. Abnormal neurogenesis as a result of decreased HTT levels has been observed both in mouse models [46] and in vitro [44, 46]. HTT's role in regulating the angle of the mitotic spindle in dividing neuronal progenitor cells may contribute to defects in neurogenesis. During neurogenesis, the angle of the mitotic spindle relative to the apical surface of the ventricular zone during cell division determines the fate of the resulting daughter cells, and changes in spindle orientation can have long-term consequences in the brain. Removing or knocking down HTT can also result in mislocalization of dynein, the $p150^{Glued}$ subunit of dynactin, and the large nuclear mitotic spindle apparatus (NuMA), all of which are necessary for proper cytoskeletal organization during mitosis [46]. In vivo studies in mouse models with genetically depleted *Htt* expression show that spindle misorientation causes cleavage plane alternations in dividing cortical progenitor cells, resulting in an increase in horizontal division and a decrease in vertical division. This dysregulation causes early depletion of progenitor cells by E14.5 and an abnormally large number of differentiated neurons at E18.5 [46]. Spindle misorientation, as well as microtubule-associated motor subunit and plus-end-associated protein mislocalization, are apparent in HD mouse model cells [47] and in neural stem cells produced from HD human embryonic stem cells [48].

Transcriptional regulation

HTT contains a polyQ stretch, which is a common feature among DNA-binding proteins including transcription factors [49]. Both an N-terminal fragment of mHTT encoded by exon 1 and full-length mHTT can bind directly to DNA and increasing the length of the polyQ stretch increases DNA binding affinity [27]. When bound to DNA, HTT can modulate DNA structure and compete with transcription factors for binding sites. RNAseq experiments using HD cells show that there is a greater number of genes transcribed in cells that express mHTT compared to wild type, and that the levels of genes that are expressed under normal conditions are reduced in mHTT-expressing cells compared to wild-type controls [27]. HTT also interacts directly with transcription factors. Mutant HTT can sequester other polyglutamine-containing transcription factors in aggregates, including the TATA binding protein and the CREB binding protein, which are involved in the transcription of a wide variety of genes [50]. Interaction between the transcription factor SP1 and the TAF4 subunit of TFIID, and the RAP30 and RAP74 subunits of TFIIF, are disrupted by polyQ expansions in HTT [51]. This interaction also requires the PRR domain within the HTT N-terminus, and mHTT interferes with normal transcriptional activity [51].

Intracellular transport

HTT is important for microtubule-based vesicular transport, and nuclear transport may be disrupted by mHTT. A region of HTT between amino acids 600 and 698 directly interacts with the intermediate chain of dynein, a motor protein that facilitates vesicular transport toward the minus end of microtubules in a complex with dynactin and Huntingtin-associated protein-1 (HAP-1) that is required for proper HTT localization within the cell [24]. Brain-derived neurotrophic factor (BDNF), a necessary pro-survival

signal, is also transported along microtubules [52]. BDNF is not expressed in the striatum [53], and striatal BDNF signaling depends on anterograde trafficking of BDNF from cortical neurons [54] that is dependent on a complex in which HAP-1 acts as a link between HTT and the $p150^{Glued}$ subunit of dynactin [52]. BDNF transport is compromised both in the presence of mutant HTT and when HTT levels are low [52].

HTT also participates in other pathways required for the successful transport of cellular cargo. For example, HTT has been implicated in regulating the capture of dense core vesicles carrying neuropeptides to the presynaptic bouton [55]. Additionally, mHTT interferes with nuclear transport in several ways. Crucial subunits of the nuclear pore complex, including NUP62 and Gle1, as well as RanGAP1, which is necessary for the release of exported cargo from the nuclear shuttling protein Ran and its subsequent return to the nucleus, are sequestered in mutant HTT nuclear aggregates [56, 57]. Furthermore, the nuclear envelope is structurally compromised in both HD mouse models and in HD postmortem brain tissue [57]. These factors all contribute to the disruption of active and passive nuclear transport, including both protein transport and mRNA export [56, 57].

Body weight and metabolism

HD patients exhibit progressive weight loss [19]. In animal models, Htt expression levels are positively correlated with body weight. Overexpression of full-length Htt results in increased IGF-1 levels [58] and increased body weight in mice [58-60]. This effect is independent of polyQ length, and overexpression of only an N-terminal fragment of Htt does not affect IGF-1 levels [58]. Conversely, mice expressing only one allele of *Htt* exhibit reductions in body weight [60]. *Htt* overexpression does not result in

changes in food intake [60] or in leptin production per gram of fat [58], although total fat levels are increased in *Htt* overexpressing model mice [60], resulting in an increase in total leptin levels [58].

The striatum may be particularly susceptible to metabolic disruptions. In mice, injections of the TCA cycle inhibitor 3-nitropropionic acid (3-NP) have been used to model HD pathogenesis, and cause HD-like motor symptoms and selective lesions in the dorsal striatum [61]. Mutant HTT's effect on metabolism, however, has not been well defined. While studies using embryonic stem cells (mESCs) [62], striatal neurons differentiated from induced pluripotent stem cells (iPSCs) [63], or neurons and mitochondria isolated from HD model mice [64] report few if any changes in mitochondrial function, other studies using iPSCs derived from HD patients [65] or striatal cell lines derived from HD mouse models [66] report metabolic deficits. In addition to mitochondrial function, mHtt may affect mitochondrial dynamics. Mutant Htt can associate with mitochondria, causing mitochondrial trafficking to neuronal processes to be impaired [67]. In addition to mitochondrial trafficking, transport of proteins into mitochondria is disrupted in HD models [68], and mHtt can bind to the mitochondrial fission protein DRP1, increasing its activity and resulting in fragmented mitochondria [69]. Htt's polyQ domain may influence metabolism even in the absence of an expansion mutation. Cultured fibroblasts from mice homozygous for a polyQ domain deletion display increased levels of ATP [5]. In contrast, Htt knockout mESCs exhibit severe metabolic deficiencies, suggesting that Htt may influence mitochondrial function in healthy cells [62].

Synapses and circuitry

In HD, striatal and cortical dysfunction contribute to movement symptoms primarily through dysfunction of the normal basal ganglia circuitry, which is comprised of a direct and an indirect pathway. The striatum receives excitatory glutamatergic inputs from the cortex. In the direct pathway, when the striatum is activated it sends inhibitory signals to the internal globus pallidus, which in turn inhibits the thalamus. The thalamus activates the motor cortex, leading to an overall increase in movement. The indirect pathway sends inhibitory signals from the striatum to the external globus pallidus, which in turn inhibits the subthalamic nuclei. The subthalamic nuclei then inhibit the thalamus, which activates the motor cortex. Therefore, activity in the indirect pathway results in a decrease in movement. In cortical and striatal neuronal co-culture, corticostriatal synapses are reduced after 14 days in vitro using murine HD cells expressing 129Q-HTT. These cultures exhibit a reduction of mini excitatory postsynaptic potentials that were not observed if either the cortical or the striatal neurons were wild type [70]. In mice expressing 140Q-Htt, corticostriatal synapses in the direct pathway from the dorsolateral striatum are reduced at 12 months of age, but not in younger mice. Indirect pathways synapses, however, are not changed [71]. In contrast, thalamostriatal synapses in both the direct and indirect pathway from the dorsolateral striatum are reduced at both 4 and 12 months of age [71]. In HD model mice, corticostriatal synapse loss correlated with altered activity in an open field test, but thalamostriatal loss did not affect activity levels [71]. Loss of thalamostriatal synapses in mice through reduction of the presynaptic protein Vglut2, however, results in rotarod deficits with little change to learning and memory behavior [72].

In vitro, thalamostriatal co-cultures of neurons isolated from a 129Q-Htt HD mouse model exhibit alterations in their firing properties, and brain slices from these mice have an increase in glutamate release in the thalamostriatal pathway [73]. Excitotoxicity in HD may be mediated through the HTT N-terminus. HTT interacts with PSD95 through PSD95's SH3 domain. SH3 domains interact with the PRR domain in the HTT N-terminus, and N-terminal fragments of HTT co-immunoprecipitate with PSD95 [74]. This interaction, however, is reduced in the presence of an expanded polyQ domain [74, 75]. PSD95 instead has increased interactions with the NR2B subunit of the NMDA receptor causing increased glutamate signaling and excitotoxicity [74, 75].

Both HTT and mHTT can affect the number of synapses in the brain as well as their function. In mice with a conditional knockout of *Htt* in cortical neurons, both corticocortical and corticostriatal synapse numbers are increased at 3 weeks of age. In the striatum, this effect is maintained at 5 weeks of age [76]. No differences were observed in thalamostriatal synapses in cortex-specific *Htt* conditional knockout mice at 3 weeks of age, although at 5 weeks, these mice exhibited an increase in thalamostriatal synapses [76]. In addition to cortical Htt, striatal Htt may also affect synapse number and function. Conditional *Htt* knockout in either direct- or indirect- pathway striatal neurons results in altered projections to the globus pallidus, altered activity levels, and decreased neuron counts in aged mice [77]. The Htt N-terminus may also affect synapse numbers. 24-month-old mice with a homozygous N17 domain deletion exhibit a reduction in thalamostriatal synapses [4]. Changes in synapse number are the result of alterations in the length and complexity of dendritic branches both in *Htt* loss-of-function and in HD models [73, 76, 78], suggesting that Htt-mediated alterations in neuronal development

and morphology may influence synapse numbers. Htt may act directly at the synapse to influence synapse numbers, but it may also act indirectly. For example, *Htt* knock-out embryonic stem cells exhibit increased transcription of *Sdc2* [44], which encodes for the protein syndecan 2, a regulator of dendritic arborization [79].

Autophagy

HTT may act at several stages of the selective macroautophagy pathway. To trigger selective macroautophagy, the protein unc-5-like autophagy activating kinase 1 (ULK1) is released from a complex with mTOR. HTT also binds with ULK1 in a manner that is mutually exclusive from mTOR binding [21], suggesting that HTT may compete with mTOR for ULK1 binding, which allows for activation of ULK1 and initiation of selective macroautophagy. HTT may also play a role in the recognition of cargo selected for degradation. During autophagosome formation, LC3-I (diffusely localized in the cytosol) is conjugated to phosphatidylethanolamine (becoming LC3-II). LC3-II associates with the autophagosomal double membrane that forms around ubiquitinated cargo [80]. The autophagy protein p62/SQSTM1 (p62) is an autophagy cargo adaptor that has a C-terminal ubiquitin (Ub)-binding domain and a short LC3-interacting region [81], which allow p62 to recognize and target ubiquitinated cargo for degradation by selective macroautophagy [81]. Because LC3-II and p62 are both degraded by autophagy, the number of LC3-II^{+}p62^{+} autophagosomes and the steady-state levels of LC3-II and p62 can be affected by alterations in the autophagy pathway. HTT interacts with p62, and a reduction in HTT levels can prevent p62 from binding to proteins with ubiquitination dependent on lysine 63 of ubiquitin, but not ubiquitin conjugation mediated by a lysine 48

linkage [21]. This scenario results in both a buildup of p62, as well as a population of autophagosomes that do not contain any cargo.

Selective macroautophagy is the primary clearance method of mHTT, however autophagy is disrupted in cells with an expanded HTT polyQ domain, possibly through multiple mechanisms. Analysis of autophagosomes in HD cells has revealed a deficit in cargo recognition [82]. Additionally, studies of autophagosome dynamics show a deficit in autophagosome trafficking to the lysosome [83]. In an HD mouse model, deletion of the normal Htt polyQ region in trans increased autophagy levels [8]. Ubiquitination of the N17 domain at lysines K5, K9, and K15 can alleviate toxicity by promoting clearance, while sumoylation at these sites can increase HTT-mediated toxicity by competing with ubiquitination [84]. However, the efficiency of total autophagosome flux, including basal as well as selective autophagy, may not be influenced by normal HTT, since LC3-II levels are not changed when HTT is absent [21].

DNA damage repair

Recent evidence has uncovered a role for normal HTT in both base excision repair (BER) [23] and transcription-coupled DNA damage repair [85], HTT can sense oxidative stress through oxidation of methionines within the N17 domain of the HTT N-terminus. This process causes translocation of HTT to the nucleus, possibly through a conformational change that allows for HTT dissociation from the membrane, exposing S13 and S16 of HTT for phosphorylation [1]. Once in the nucleus, HTT will accumulate at areas of DNA damage and associate with the ATM complex, potentially assisting in DNA damage repair complex assembly by functioning as a scaffolding protein. HTT co-

localization with ATM at sites of DNA damage is dependent on N17 phosphorylation [23].

DNA damage is elevated in cells from HD patients compared to unaffected controls after induction of DNA damage [23]. In HD, mHTT may not only prevent DNA damage repair, but also contribute to DNA damage by disrupting nuclear envelope integrity and nuclear transport, which can cause an increase in DNA damage [57]. A genome-wide association study (GWAS) of HD patients found a correlation between disease progression and a gene locus that is likely to be associated with the *FAN1* (FANCD2- and FANCI-associated nuclease 1) gene [86], which encodes for FAN1, a protein that participates in DNA damage repair [87]. FAN1 can bind directly to mHTT, reduce somatic expansion of the CAG repeat, and modify disease age-of-onset and severity [88]. In vitro studies using cells from an HD mouse model found that after treatment with hydrogen peroxide (H_2O_2) to induce DNA damage, HD cells exhibited both a delay in the accumulation of the DNA double strand break repair marker γH2AX and an increase in total γH2AX signaling, suggesting a deficit in either DNA damage recognition or repair in HD cells [89]. Reducing levels of the DNA damage response protein ATM has been shown to ameliorate HD pathology both in vitro and in vivo, providing further evidence that dysregulation of the DNA damage response pathway may contribute to HD pathogenesis [89].

<u>The contribution of the HTT N-terminus to normal HTT function in the adult brain</u>

Because of HTT's critical role during development [40-43], the majority of HTT's normal functions have been studied using cell culture models rather than animal model

systems, limiting the identification and characterization of HTT's functions in the adult brain. Based on prior studies in mice, the Htt N-terminus is not likely to be required for embryonic development or survival [4-7] but may have some specialized functions in the nervous system [26]. Characterization of a mouse model with a deletion of the endogenous Htt N-terminus may therefore be able to provide new information about Htt's functions in the adult brain.

Chapter II: Materials and Methods

Chapters II and III are modified and expanded from the following manuscript: Braatz EM, André EA, Liu JP, Zeitlin SO. Characterization of a Knock-In Mouse Model with a Huntingtin Exon 1 Deletion. J Huntingtons Dis. 2021 Aug 25. doi: 10.3233/JHD-210494. Epub ahead of print. PMID: 34459410.

Mouse husbandry

Mice were housed in a temperature-and humidity-controlled facility on a 12-hour light-dark cycle with unrestricted access to food and water. Whole body γ-irradiation was administered with a J.L. Shepherd Mark 1 Model 68A Cesium-137 irradiator located in the vivarium. $KBrO_3$ was added in the drinking water at the concentration of 2 g/liter for 7 days. All experiments using mice were approved by the University of Virginia Animal Care and Use Committee. Both male and female mice in the C57BL/6J congenic background were used for all experiments, except for behavioral testing where only male mice were used to eliminate the potential effects of the estrus cycle on behavior. Experimenters were blinded to genotype during data collection and analysis when appropriate.

PCR genotyping

PCR was performed using the primers listed below:

To detect the *Htt*$^{\Delta E1}$ allele: HdEpi-1: 5'-GCGTAGTGCCAGTAGGCTCCAAG-3' and 140Reverse: 5′-GAAGGCACTGGAGTCGTGAC-3′

No product is generated from the *Htt*$^{+}$ allele because the PRR is G/C-rich. A 233 bp product is generated from the *Htt*$^{\Delta E1}$ allele.

To detect the *Htt*$^{\Delta E1}$ or *Htt*^{140Q} allele and the *Htt*$^{+}$ allele:

140Forward: 5´-CTGCACCGACCGTGAGTCC-3´ and 140Reverse (see above)

The *Htt*$^{+}$ allele generates a 236 bp product. A shortened 152 bp product is generated from the *Htt*$^{\Delta E1}$ and *Htt*^{140Q} alleles due to an intronic 84 bp deletion.

For detection of the MC1-neo positive selection cassette present in the *Htt* null allele: MC1-1 (forward): 5′-AACACCGAGCCGACCCTGCAG-3′ and Neo-3 (reverse): 5′-AGAGCAGCCGATTGTCTGTTGT-3′ (*Htt*-: 130 bp product)

To estimate the length of the CAG repeat in the *Htt*^{140Q} allele: HDEpi-1: (see above) and LacOM3'-1: 5'-CTGCGGCGGCGGCTGAGGAAG-3' (*Htt*^{140Q}: ~593bp product)

Behavioral analyses

Motor behavioral analysis using the accelerating rotarod, open field, and forelimb grip strength apparatuses were performed at 3, 6, 12, and 18 months of age. Mice were weighed at each time point. Morris water maze testing was performed at 10, 14, and 19 months of age. Testing was performed between 8:00AM and 2:00PM (light phase). Littermate controls were included when possible. The wild type control group for the HD mouse model experiments, however, were obtained from *Htt*$^{+/+}$ x *Htt*$^{+/+}$ intercrosses. (N=17-20/genotype).

Open Field Testing

Open field testing was performed with the VersaMax Animal Activity Monitoring System (AccuScan Instruments). Activity for each mouse was recorded for 5 min. The open field chamber was cleaned after each trial, and each mouse was subjected to open

field testing once at each experimental time point. VersaMax software was used to analyze activity outputs.

Rotarod

An Economex accelerating rotarod (Columbus Instruments) was used to assess motor performance. A training period consisting of a 1-min trial balancing on a stationary rod and a 1-min trial on a rod rotating at 2 rpm was completed before the initial experimental trial (trial day 1 at 3 months of age). If a mouse failed either trial it was given two more chances to complete it. For experimental trials, the latency to fall from a rod accelerating at 0.1 rpm/sec from an initial speed of 2 rpm was recorded for each trial, and trials were spaced at least 15 minutes apart. Three experimental trials were performed per day for each mouse over three consecutive days, and analyses were performed using the average latency to fall over the three trials.

Forelimb Grip Strength

Forelimb grip strength was assessed using a grip strength meter (San Diego Instruments). Each mouse was suspended by the tail and allowed to grip a metal grid attached to the force meter with both forelimbs. Once their grip had been firmly established the mice were pulled at a 45° angle away from the grip strength meter until they released their forepaws from the grid. Each mouse was tested on one day per experimental time point, and the average force required to break the mouse's grip over 3 trials was recorded.

Morris water maze

Morris water maze testing consisted of an 8-day experimental protocol including an acquisition phase (4 days), probe trial (1 day), reversal phase (2 days), and a visible platform control trial (1 day). Water maze testing was performed in a circular pool (Maze Engineer, 122 cm diameter) filled with opaque water (22 ± 1°C) to hide a circular platform >1 cm below the surface. Three visual reference cues were positioned on the side of the pool, and the experimenter was hidden by a curtain during data acquisition. Visual reference cues were not altered at any point during testing. All data was collected from a Basler ace color Gig-E camera centered above the pool using EthoVision XT 13 software (Noldus Information Technology). The maze was divided into quadrants during testing, and the platform was placed in the center of one quadrant. During testing, the mice were placed in the maze at designated locations outside of the platform quadrant. Placement locations varied between trials. After each trial, mice were removed from the maze, dried with paper towels, and allowed to rest in their home cage for at least 45 minutes before the next trial.

Acquisition phase

The acquisition phase consisted of four trials per day over four days. Mice were placed in the maze facing the wall of the pool and allowed to explore for 60 seconds. Mice who successfully climbed onto the hidden platform were removed from the maze after 20 seconds. Mice who failed to climb onto the hidden platform during the trial were guided onto the platform and removed after 20 seconds. The latency to the platform was recorded for each successful trial, and a latency of 60 seconds was recorded for mice who failed to find the platform.

Probe trial

The hidden platform was removed from the maze on the fifth day of testing and each mouse was allowed to explore the maze for 60 seconds. The amount of time the mouse spent in the maze quadrant that had previously contained the platform and the average swim velocity over the 60 second trial were recorded.

Reversal phase

On the sixth and seventh days of testing, the hidden platform was returned to the maze, but was moved to the center of a different quadrant. Mice were allowed to learn the new location of the platform for four 60 second trials per day over two days (similar to the acquisition trials).

Visible platform task

The visible platform test consisted of a single 60 second trial. A visible marker was placed on the hidden platform, which was moved to a different location in the pool. The latency to the platform was recorded for each mouse.

Brain tissue lysate preparation and subcellular fractionation

Whole brain lysates from 3-, 6-, 12- or 24-month-old mice were separated into enriched nuclear, microsomal, and cytosolic fractions as described [4] with the following modifications. The 800 xg supernatant was either centrifuged at 100k xg for 60 min at 4^{o}C to obtain a total microsomal (pellet) and a cytosolic (supernatant) fractions or centrifuged first at 9k xg for 10 min at 4^{o}C to obtain a heavy microsomal fraction (P1), the supernatant was then centrifuged at 100k xg for 60 min at 4^{o}C to obtain a light microsomal fraction (P2), and the remaining supernatant is the cytosolic fraction. To

obtain a nuclear-enriched pellet, the 800 xg pellet was resuspended in 1.3 M sucrose buffer, layered on a cushion of the same buffer, and centrifuged for 45 min at 3k xg.

The microsomal pellets were resuspended in 25 mM Tris (pH 7.6), 150 mM NaCl, 1% NP40, 1% SDS, 1% sodium deoxycholate, 1 mM EDTA, 1 mM DTT, 5 mM NaF, 1 mM $NaVO_4$, and Halt protease inhibitor, then centrifuged at 15,000g for 15 min at 4℃ to obtain the microsomal fraction (supernatant). The nuclear pellets were resuspended in 25mM Tris (pH 7.6), 400 mM NaCl, 1 mM EDTA, 1 mM DTT, 5 mM NaF, 1 mM $NaVO_4$, and Halt protease inhibitor, and then sonicated at 4℃ on a 10 seconds on/20 seconds off paradigm using a Fisher Scientific Sonic Dismembrator (FB-505) equipped with a cup horn attachment until a homogenous nuclear lysate was obtained, approximately 2-3 min. Following sonication, NP40 (1% f.c.), SDS (0.1% f.c.), and sodium deoxycholate (1% f.c.) were added to the nuclear lysate. The samples were centrifuged at 15,000g for 15 min at 4℃ to obtain the nuclear fraction (supernatant).

For detection of protein carbonyls, cortical and striatal tissues were dissected and homogenized in 25 mM Tris (pH 7.9), 500 mM NaCl, 1 mM EDTA, 1% NP40, 0.1% SDS, 1% sodium deoxycholate, 1 mM DTT, 5 mM NaF, 1 mM NaVO4, and Halt protease inhibitor (Thermo Scientific 78425). Samples were centrifuged at 15k xg for 15 min at 4^{o}C and the supernatant was collected.

For detection of 53bp1, cortical tissue was dissected and homogenized in 25 mM Tris (pH 7.9), 500 mM NaCl, 1 mM EDTA, 1 mM DTT, 5 mM NaF, 1 mM NaVO4, 1% TritonX-100 and Halt protease inhibitor. The homogenate was sonicated for 3 minutes

(10 sec on/20 sec off) at 4ºC (Fisher Scientific Sonic Dismembrator, Fisherbrand Model 505), centrifuged at 15k xg for 15 min at 4ºC, and the supernatant was collected.

For cortical and striatal cytosolic and microsomal fractions, tissues were dissected, homogenized, and resuspended in the same buffers used in the whole brain fractionation (see above), except the supernatant from the 800 xg spin was centrifugated at 15k xg to obtain the microsomal fraction (pellet) and cytosolic fraction (supernatant).

Protein levels were estimated using a Thermo Fisher Pierce BCA Protein Assay kit (PI23227).

Western blotting

Western blotting was performed as described [4], with the following modifications. 60 µg protein was fractionated on Mini-PROTEAN TGX 4-15% gradient gels (Bio-Rad) for synaptic marker and whole brain p62 detection, on 7% acrylamide gels for brain-regional p62 detection, or on 15% acrylamide gels for LC3 detection, and then transferred onto 0.2 µm nitrocellulose membranes (Bio-Rad, 1704158) using a Bio-Rad Transblot Turbo transfer system.

To detect Htt, 30 µg protein from cytosolic, heavy microsomal (P1), and light microsomal (P2) fractions and 90 µg nuclear proteins from *Htt*$^{\Delta E1/+}$ brains or 60 µg of cytosolic, total microsomal, and nuclear proteins from *Htt*$^{+/+}$, *Htt*$^{\Delta E1/+}$, *Htt*$^{\Delta E1/\Delta E1}$, *Htt*$^{+/-}$, *Htt*$^{\Delta E1/-}$, *Htt*$^{140Q/+}$, *Htt*$^{140Q/\Delta E1}$, *Htt*$^{140Q/-}$, *Htt*$^{140Q/\Delta Q}$, *Htt*$^{140Q/\Delta QP}$, and *Htt*$^{140Q\Delta N17}$ brains were fractionated on 4.4% acrylamide gels and transferred electrophoretically onto Immun-Blot Low Fluorescence PVDF membranes (Bio-Rad 162-0263) at 30 V overnight using a mini TransBlot system (BioRad) at 4ºC.

To quantify cortical 53bp1 levels, 60 µg of total protein were fractionated on 2-step 4.4%/8.8% acrylamide gels and transferred electrophoretically onto Immun-Blot Low Fluorescence PVDF membranes at 100 V for 2.5 hrs at 4°C.

To examine protein carbonyl levels, 15 µg of total cortical and striatal protein were fractionated on 7% acrylamide gels and transferred onto Immun-Blot Low Fluorescence PVDF membranes using the Transblot Turbo transfer system. Derivatization of carbonyl groups with 2,4-dinitrophenylhydrazine (DNPH) and immunoblotting with a DNP antibody were performed using the OxiSelect Protein Carbonyl Kit (Cell BioLabs STA-308) and signals were detected with Thermo Scientific SuperSignal WestDura substrate (PI34076). Blots were then re-probed with β-actin antibody.

Primary antibodies used were: Huntingtin (aa181-810) (Millipore MAB 2166, 1:3000), Huntingtin (aa1-17) (Sigma-Aldrich H7540, 1:1500), 53bp1 (Abcam 175933, 1:5000), LC3 (Novus NB100-2220, 1:1000), p62 (American Research Products 03-GP62-C; 1:2000), β-actin (Cell Signaling 3700; 1:1000), Vglut1 (Millipore AB5905 1:10,000), PSD95 (Cell Signaling 2507; 1:1000), Vglut2 (Millipore AB2251; 1:10,000), mTOR (Cell Signaling 2972, 1:1000) and DNP (Cell BioLabs 230801). IRDye 800CW and IRDye 680RD conjugated secondary antibodies were purchased from Li-Cor (926-32212, 926-68073, 925-68070, 925-32211) and Alexa Fluor 680 and 790 donkey anti-guinea pig conjugated secondary antibodies were purchased from Jackson ImmunoResearch (706-625-148, 706-655-148). Blots were imaged on a Li-Cor Odyssey Fc system and analyzed using Li-Cor ImageStudio software.

Immunohistochemistry

For immunohistochemistry, 2-, 3-, 4-, 12-, or 18-month-old mice were anesthetized and perfused with 10% sucrose in PBS for 1 min (5 ml/min)using a peristaltic pump (Cole-Parmer Master flex L/S pump equipped with a model 77200-60 pump head), followed by 4% paraformaldehyde-10% sucrose in 0.1 M phosphate buffer for 5 min. Brains were removed and post-fixed for 2 hr, rinsed in 10% sucrose in PBS, incubated for 1 hr in 0.125 M glycine-10% sucrose in PBS, and washed 3 times in 10% sucrose in PBS (including one overnight wash, all steps were performed at 4^{o}C). Tissue was then frozen in O.C.T. compound (Tissue-Tek 4583). Frozen forebrains were sectioned coronally at 14 or 20 µm, while cerebella were sectioned sagittally at 14 µm, and processed as described [4]. For samples to be labeled with primary antibodies generated in mice, an additional blocking step with a monovalent FAB anti-mouse antibody (Jackson ImmunoResearch, 715-007-003) at 1:100 was performed for 1 hr at RT.

Primary antibodies used: γH2AX (Abcam 26350, 1:8000), 53bp1 (Abcam 175933, 1:5000), p62 (American Research Products 03-GP62-C; 1:900), LC3 (Cell Signaling 12741; 1:900), Vglut1 (Millipore AB5905 1:3750), Vglut2 (Millipore AB2251;1:5000), PSD95 (Cell Signaling 3409; 1:800), NeuN (Millipore ABN90P, 1:500), calbindin (Novus NBP2-50028, 1:4000). Secondary antibodies were purchased from Jackson ImmunoResearch Laboratories (715-165-151, 711-165-152, 706-165-148, 715-545-151, 711-545-152, 706-545-148, 703-175-155). DAPI (Sigma-Aldrich, D9542) was used to label nuclei.

Images of brain sections were obtained using an Olympus FV1200 confocal system with a 60x objective. Coronal sections were collected for synapse quantification: from bregma -0.555 mm to 1.245 mm (dorsal striatum) and bregma -1.155 mm to 1.245 mm (motor cortex layers I and II) (20 μm sections at 200 μm intervals, 10-13 sections/mouse), for autophagy marker quantification: from bregma -0.18 mm to 1.42 mm (20 μm sections at 200 μm intervals, 9 sections/mouse), and for DNA damage marker quantification: from bregma -0.26 mm to 1.42 mm (14 μm sections at 210 μm intervals, 8-9 sections/mouse). Images of sagittal cerebellar sections were collected from 1.10 mm to 2.78 mm lateral to the midline (14 μm sections at 210 μm intervals, 9 sections/mouse, 3 images/section).

For Purkinje cell density quantification, images of sagittal cerebellar sections were obtained using a Keyence BZ-X800E fluorescence microscope with a 20x objective. Images were acquired from 1.10 mm to 2.99 mm lateral to the midline (14 μm sections at 630 μm intervals, 4 sections/mouse) and stitched into a single image per section.

Comet assay and nuclear immunostaining

Cortex, striatum, thalamus, and cerebellum were dissected from mice at 3 or 13-16 months of age and homogenized in 250 mM sucrose, 20 mM HEPES (pH 7.3), 1 mM $MgCl_2$, 1% DMSO, and Halt protease inhibitor. Homogenates were centrifuged at 800 xg for 4 min at 4°C. Pellets were gently resuspended in 250 mM sucrose, 20 mM HEPES (pH7.3), 1 mM $MgCl_2$, 25 mM KCl, 1% DMSO, and Halt protease inhibitor. Iodixanol solution (Optiprep, Sigma-Aldrich D1556) was added to 25%, and the samples were

layered on top of an 29%-35% iodixanol cushion and centrifuged at 3k xg for 30 min at 4^{o}C. The nuclear-enriched band between the 25% and 29% iodixanol layers was removed and added to 3x volume of PBS and centrifuged at 1k xg for 5 min at 4^{o}C. Excess PBS was removed and the nuclei were resuspended in the remaining PBS and counted using a hemocytometer.

For comet assays, ~5,500 nuclei in 10 μl PBS were mixed with 100 μl of 1% low-melting agarose, plated onto agarose-coated slides, covered with a 22 mm x 50 mm coverslip, and then allowed to solidify for 30 min at 4^{o}C. Coverslips were removed and slides were incubated in a lysis buffer (20 mM Tris, 50 mM EDTA, 1.2 M NaCl, 1% sarkosyl, and 2% DMSO) at either neutral (pH 8) or alkaline (pH 10) pH for 30 min at 4^{o}C to lyse the nuclei. The slides were then electrophoresed at 23 V for 20 min in either a neutral (TBE pH 7.4) or an alkaline buffer (50 mM NaOH, 1 mM EDTA). Slides were washed twice in water (alkaline treated slides were neutralized in TBE for 5 min before washing), fixed in 70% ethanol for 10 min, and dried. Slides were rehydrated in water, incubated in 2.5 μg/ml propidium iodide for 15 min to stain DNA, and washed twice in water for 10 min each, then mounted with Vectashield mounting media (Vector Lab H-1000) before imaging. Images were obtained using a Nikon TE2000 inverted microscope with a 20x oil objective and a Nikon DS-Qi2 camera, and quantified using the public domain CaspLab software (casplab.com) [90]. The DNA in the comet tail, as a percentage of the total DNA in the comet, was quantified. This value represents the amount of total DNA damage and is not affected by the length of the tail which may be influenced by slight changes in buffer composition, electrophoresis conditions, and DNA fragment size.

To quantify 8-OHdG levels, ~22,500 nuclei in 45 μl 0.9% low-melt agarose were plated onto agarose-coated slides, covered with a 22 mm x 22 mm coverslip, and then allowed to solidify for 30 min at 4°C. Coverslips were removed and the slides were then lysed in an alkaline (pH 10) buffer, neutralized, fixed, and dried as described above. Slides were then rehydrated in water and immunostaining with anti-8-OHdG antibody (Millipore AB5830, 1:200) following standard procedures. Secondary antibody was obtained from Jackson ImmunoResearch Laboratories (705-165-147), and DNA was stained with DAPI. Images of isolated nuclei were obtained using a Nikon TE2000 inverted microscope with a 20x oil objective and a Nikon DS-Qi2 camera.

Image and statistical analyses

Analysis of immunohistochemistry and nuclear immunostaining images was performed with Nikon NIS-Elements AR Analysis software (5.02.01). For γH2AX, 53bp1, LC3, p62, and PSD95 quantification, puncta under 2 pixels were excluded. For Vglut2 and Vglut1 quantification, puncta under 3 pixels were excluded. For DAPI quantification in brain sections, nuclei under 15 pixels were excluded. To determine the calbindin$^+$ cell density, the number of calbindin$^+$ cells along the entire length of the Purkinje cell layer were counted and divided by the total length of the layer. Numerical data were analyzed using GraphPad Prism 9. Statistical significance in the χ^2 test, unpaired t-test, paired t-test, 1-way ANOVA, or 2-way ANOVA was set at $p < 0.05$. Tukey's multiple comparison test was used for post-hoc analysis of ANOVA tests.

Chapter III: Characterization of *Htt*$^{\Delta E1/\Delta E1}$, *Htt*$^{\Delta E1/+}$, and *Htt*$^{\Delta E1/-}$ mice

Chapters II and III are modified and expanded from the following manuscript: Braatz EM, André EA, Liu JP, Zeitlin SO. Characterization of a Knock-In Mouse Model with a Huntingtin Exon 1 Deletion. J Huntingtons Dis. 2021 Aug 25. doi: 10.3233/JHD-210494. Epub ahead of print. PMID: 34459410.

Introduction

The protein product of the *Huntingtin* (*HTT*) gene, Huntingtin (HTT), is a large 3144 amino acid protein (~350 kD) containing a polyglutamine (polyQ) stretch encoded by a CAG repeat within *HTT* exon 1 that when expanded, causes Huntington's disease (HD) [9]. The polyQ stretch is flanked by the first 17 amino acids of HTT (N17 domain), forming an amphipathic helix capable of interacting with membranes [30], and a proline-rich region (PRR), acting as a structural spacer with the potential to interact with SH3 and WW domain-containing proteins [91, 92]. Mice with single- or double-domain deletions within Htt's exon 1 are born at the expected Mendelian frequency, survive into adulthood, and are fertile, suggesting that Htt's N-terminal domains are not required for its critical functions during embryogenesis or postnatal survival [4-7, 43]. HTT has been proposed to participate in selective macroautophagy, and the N-terminal, middle, and C-terminal portions of HTT have sequence and structural similarity to the yeast autophagy proteins Atg23, Vac8, and Atg11 [21, 22]. Overexpressing a version of *Htt* with a CAG repeat deletion (*Htt*$^{\Delta Q}$) in vitro leads to an increase in autophagosome formation, and the autophagosome marker microtubule-associated protein 1A/1B-light chain 3-II (LC3-II) is elevated in aged *Htt*$^{\Delta Q/+}$ mice [8]. In primary neuronal cultures, however, neither *Htt*$^{\Delta Q/\Delta Q}$ neurons nor neurons with both a polyQ and PRR deletion (*Htt*$^{\Delta QP/\Delta QP}$) exhibit changes in

autophagic flux [4]. Atg23 and Atg11 coordinate autophagosome formation in yeast, and HTT aa1-568 interacts in vitro with an HTT C-terminal aa 2416-3144 fragment [22, 93]. However, HTT aa1-90 encoded by exon 1 are not required for this interaction [22]. Based on these findings, the extent to which the Htt N-terminus functions in basal neuronal autophagy is not clear.

In vitro studies of the HTT N-terminus have also demonstrated a role for the N17 domain in both the cell stress response and as sensor for oxidative stress [1, 23, 30]. Elevated reactive oxygen species (ROS) can oxidize methionine residues 1 and 8 within the N17 domain, resulting in HTT's translocation into the nucleus where it colocalizes with the ataxia-telangiectasia mutated protein (ATM) at sites of DNA damage [23]. Huntingtin is proposed to be involved in base excision repair [23, 94], transcription coupled DNA repair [85], and possibly also in double strand DNA break repair due to a functional interaction between HTT and ATM [23, 89], but how different HTT domains contribute to HTT's involvement in DNA repair pathways is still unclear.

Aged mice homozygous for a deletion of the exon 1 sequences encoding the N17 domain (*Htt*$^{\Delta N17}$) have reduced numbers of thalamostriatal glutamatergic synapses [4], although whether this is the result of a deficit in synaptic development or maintenance is not known. The phenotypic effects of deleting the Htt polyQ and PRR domains individually are not additive when both domains are deleted in mice [4-6, 8], suggesting that the function of the Htt N-terminus may not be fully understood by characterizing its domains in isolation. Using a mouse model with a deletion of all three functional domains of the Htt N-terminus (*Htt*$^{\Delta E1}$), I performed longitudinal behavioral characterization and investigated several aging-related cellular processes in the brain

including DNA damage repair, autophagy, and synaptic maintenance to address these points.

Htt$^{\Delta E1/\Delta E1}$ and *Htt*$^{\Delta E1/-}$ mice are born at the expected Mendelian frequency, can survive through 24 months of age, and are fertile. However, *Htt*$^{+/+}$ and *Htt*$^{\Delta E1/\Delta E1}$ progeny from *Htt*$^{\Delta E1/+}$ intercrosses were born at a distorted male/female ratio. *Htt*$^{\Delta E1/\Delta E1}$ mice exhibit a modest deficit in accelerating rotarod performance, and an increase in cortical and striatal DNA double-strand breaks (DSBs) at 3 months of age with elevated levels of pan-nuclear p53-binding protein 1 (53bp1, a protein functioning in double-strand DNA break repair [95]). However, no changes in Htt's subcellular localization, the basal levels of autophagy markers or in glutamatergic corticocortical, corticostriatal, thalamocortical, or thalamostriatal synapse numbers were observed.

Results

Confirmation of the Htt$^{\Delta E1}$ mouse allele

The *Htt*$^{\Delta E1}$ knock-in mice contain a synthetic sequence lacking amino acids (aa) 2-17 of the N17 domain, the polyQ, and the PRR domains of Htt, which replaces the wild type *Htt* exon 1 sequence (Fig. 3-1). To confirm expression of ΔE1-Htt in brain tissue, cytosolic, microsomal, and nuclear protein fractions from 6-month-old *Htt*$^{+/+}$, *Htt*$^{\Delta E1/+}$, and *Htt*$^{\Delta E1/\Delta E1}$ mouse brains were analyzed by western blotting with the MAB2166 antibody (Millipore), which recognizes an epitope present in both WT-Htt and ΔE1-Htt (aa181-810), and microsomal fractions were also analyzed with the H7540 antibody (Sigma-Aldrich), recognizing the first 17 aa of Htt that are deleted in ΔE1-Htt. ΔE1-Htt migrates faster through the gel than WT-Htt, resulting in a doublet in the *Htt*$^{\Delta E1/+}$ sample detected

by the MAB2166 antibody and a single band corresponding to WT-Htt detected by the H7540 antibody (Fig. 3-2C).

The Htt N-terminus encoded by exon 1 is not essential for embryonic survival

Htt knockout mice die early during embryogenesis [40-42]. To determine if the Htt N-terminus is required for embryonic development, progeny from $Htt^{\Delta E1/+}$ intercrosses (124 litters, average litter size 5.94) were sexed and genotyped, and the ratio of $Htt^{+/+}$, $Htt^{\Delta E1/+}$, and $Htt^{\Delta E1/\Delta E1}$ pups was compared to the expected Mendelian ratio (Table 3-1). Female and male pups were born at 1:1 ratio, and the ratio of total (male + female) $Htt^{+/+}$, $Htt^{\Delta E1/+}$, and $Htt^{\Delta E1/\Delta E1}$ progeny was not significantly different from the Mendelian ratio, suggesting that the *Htt* exon 1-encoded N-terminal domains are not required for its critical functions during early embryogenesis. When separated by sex, however, the percentage of male $Htt^{\Delta E1/\Delta E1}$ progeny (30.7%) was increased and $Htt^{+/+}$ progeny (18.6%) was decreased (Table 3-1, χ^2=10.677, p=0.0048) compared to the Mendelian ratio. Conversely, the percentage of female $Htt^{+/+}$ progeny (29.4%) was increased, while the $Htt^{\Delta E1/\Delta E1}$ progeny (19.7%) was decreased (χ^2=7.119, p=0.0285). Both male and female $Htt^{\Delta E1/\Delta E1}$ mice are fertile and the litter sizes obtained from $Htt^{\Delta E1/\Delta E1}$ intercrosses are within normal range (8 litters, average litter size 5.11) without a significant change in the male to female ratio of their progeny (males: 41.3%, females: 58.7%, χ^2=1.391, p=0.2382). Progeny obtained from $Htt^{\Delta E1/+}$ (male) x $Htt^{+/-}$ (female) and $Htt^{\Delta E1/+}$ (female) x $Htt^{+/-}$ (male) intercrosses were both born at the expected Mendelian ratio, with no sex ratio distortion observed (Tables 3-2 and 3-3).

Deletion of Htt's N-terminal domains has no apparent effect on ΔE1-Htt's subcellular localization

In vitro studies have identified HTT N17 as both a membrane association and a nuclear export domain, suggesting that HTT's N-terminus may regulate its subcellular localization [29, 30, 96]. To examine if the combined deletion of the three N-terminal domains of Htt affects its subcellular localization, Htt levels were first quantified in whole brain cytosolic, microsomal, and nuclear protein fractions obtained from 6-month-old $Htt^{+/+}$, $Htt^{\Delta E1/+}$, $Htt^{\Delta E1/\Delta E1}$, $Htt^{+/-}$, and $Htt^{\Delta E1/-}$ mice by western blotting. There was no significant difference in the levels of cytosolic, total microsomal, or nuclear WT-Htt and ΔE1-Htt between $Htt^{+/+}$ and $Htt^{\Delta E1/\Delta E1}$ fractions, between $Htt^{+/-}$ and $Htt^{\Delta E1/-}$ fractions, or within $Htt^{\Delta E1/+}$ fractions (Fig 3-2A, 3-2B). To circumvent the confounding factor of comparing Htt levels between different animals, whole brain lysates from 6-month-old $Htt^{\Delta E1/+}$ mice were prepared and separated into cytosolic (C), nuclear (N), 9k xg pellet (P1, heavy microsomal), and 100k xg pellet (P2, light microsomal) fractions. WT-Htt and ΔE1-Htt levels in each fraction were analyzed by western blotting (Fig. 3-2D). There were no significant differences in the ratio of the fluorescence intensity of the ΔE1-Htt to WT-Htt bands between any of the fractions (Fig. 3-2E), indicating that ΔE1-Htt subcellular localization is not significantly altered under homeostatic conditions in vivo.

Characterization of motor phenotypes in N-terminus deletion mice.

$Htt^{+/+}$, $Htt^{\Delta E1/+}$, $Htt^{\Delta E1/\Delta E1}$, $Htt^{+/-}$, and $Htt^{\Delta E1/-}$ mice were weighed and subjected to a panel of behavioral tests at 3, 6, 12, and 18 months of age (see Table 3-4 for the number of mice tested at each experimental time point) to examine whether the HTT N-terminus has an effect on body weight (Fig. 3-3), rotarod performance (Fig. 3-4, Table 3-

5), forelimb grip strength (Fig. 3-5), or activity levels (Figs. 3-6, 3-7, 3-8). $Htt^{\Delta E1/-}$ mice exhibit a reduced body weight compared to $Htt^{\Delta E1/+}$ and $Htt^{\Delta E1/\Delta E1}$ mice at 3 ($Htt^{\Delta E1/+}$: p=0.0183, $Htt^{\Delta E1/\Delta E1}$: p=0.0047, Tukey's multiple comparison test), 6 ($Htt^{\Delta E1/+}$: p=0.0117, $Htt^{\Delta E1/\Delta E1}$: p=0.0037, Tukey's multiple comparison test), 12 ($Htt^{\Delta E1/+}$: p=0.0023, $Htt^{\Delta E1/\Delta E1}$: p=0.0004, Tukey's multiple comparison test), and 18 months of age ($Htt^{\Delta E1/+}$: p=0.0423, $Htt^{\Delta E1/\Delta E1}$: p=0.0104, Tukey's multiple comparison test), and compared to $Htt^{+/+}$ mice at 3 months of age (p=0.0020, Tukey's multiple comparison test). Additionally, $Htt^{+/-}$ mice exhibit significantly reduced body weight compared to $Htt^{\Delta E1/\Delta E1}$ mice at 12 months of age (p=0.0178, Tukey's multiple comparison test).

$Htt^{\Delta E1/\Delta E1}$ mice display rotarod deficits compared to $Htt^{+/+}$ mice (Fig. 3-4, Table 3-5) at 3 (p=0.0455, F=4.276, D_F =1, 2-way ANOVA), 12 (p=0.0231, F=5.614, D_F =1, 2-way ANOVA), and 18 months of age (p=0.0327, F=4.945, D_F=1, 2-way ANOVA). Although there was no significant difference in accelerating rotarod performance between $Htt^{\Delta E1/\Delta E1}$ and $Htt^{+/+}$ mice at 6 months of age, there was a trend toward a rotarod deficit in $Htt^{\Delta E1/\Delta E1}$ mice (p=0.0627, F=3.677, D_F=1, 2-way ANOVA). $Htt^{\Delta E1/+}$, $Htt^{\Delta E1/-}$, and $Htt^{+/-}$ mice displayed no significant differences in accelerating rotarod performance compared to $Htt^{+/+}$ mice at 3, 6, 12, or 18 months of age, however, $Htt^{\Delta E1/\Delta E1}$ mice performed significantly worse on the rotarod compared to $Htt^{\Delta E1/-}$ mice at 3 (p=0.0393, F=4.558, D_F=1, 2-way ANOVA), 6 (p=0.0071, F=8.097, D=1, 2-way ANOVA), 12 (p=0.0104, F=7.280, D_F=1, 2-way ANOVA), and 18 months of age (p=0.0135, F=6.747, D_F=1, 2-way ANOVA) and compared to $Htt^{+/-}$ mice at 6 (p=0.0028, F=10.22, D_F=1, 2-way ANOVA), 12 (p=0.0088, F=7.654, D_F=1, 2-way ANOVA), and 18 months of age (p=0.0042, F=9.343, D_F=1, 2-way ANOVA). Additionally, $Htt^{\Delta E1/+}$ mice performed significantly worse on rotarod compared to $Htt^{+/-}$ mice at 12 (p=0.0476, F=4.193, D_F=1, 2-way ANOVA) and 18

months of age (p=0.0132, F=6.795, D_F=1, 2-way ANOVA), and compared to $Htt^{\Delta E1/-}$ mice at 12 (p=0.0456, F=4.271, D_F=1, 2-way ANOVA) and 18 months of age (p=0.0315, F=5.009, D_F=1, 2-way ANOVA).

There were no differences in forelimb grip strength at 3, 6, or 12 months of age (Fig 3-5). At 18 months of age, $Htt^{\Delta E1/-}$ (p=0.0002, Tukey's multiple comparison test) and $Htt^{+/-}$ (p=0.0165, Tukey's multiple comparison test) mice both exhibited reduced forelimb grip strength compared to $Htt^{+/+}$ mice, and $Htt^{\Delta E1/-}$ mice exhibited reduced grip strength compared to $Htt^{\Delta E1/+}$ (p=0.0203, Tukey's multiple comparison test) and $Htt^{\Delta E1/\Delta E1}$ mice (p=0.0217, Tukey's multiple comparison test) as well.

Mice were subjected to activity monitoring for 5 minutes at each experimental time point, and the total distance moved (Fig. 3-6), horizontal activity (Fig. 3-7), and vertical activity (Fig. 3-8) were recorded. There were no differences in the total distance moved at 3, 12, or 18 months of age. At 6 months of age, $Htt^{\Delta E1/+}$ mice moved less $Htt^{+/-}$ mice (p=0.0400, Tukey's multiple comparison test). There were no differences in horizontal activity levels at 3, 12, or 18 months of age. At 6 months of age $Htt^{+/-}$ mice exhibited more horizontal activity compared to $Htt^{+/+}$ mice (p=0.0375, Tukey's multiple comparison test) and $Htt^{\Delta E1/+}$ mice (p =0.0018, Tukey's multiple comparison test). At 3 months of age, $Htt^{+/-}$ mice exhibited reduced levels of vertical activity compared to $Htt^{+/+}$ mice (p=0.0169, Tukey's multiple comparison test). There were no differences in vertical activity levels at 6, 12, or 18 months of age.

Deletion of the Htt N-terminus does not affect spatial learning and memory.

$Htt^{+/+}$, $Htt^{\Delta E1/+}$, $Htt^{\Delta E1/\Delta E1}$, $Htt^{+/-}$, and $Htt^{\Delta E1/-}$ mice were subjected to Morris water maze testing (Fig. 3-9, Table 3-6) at 14 and 19 months of age to examine the effects of the HTT N-terminus on spatial learning and memory. There were no differences in Morris water maze performance between $Htt^{+/+}$ mice and $Htt^{\Delta E1/+}$, $Htt^{\Delta E1/\Delta E1}$, $Htt^{+/-}$, or $Htt^{\Delta E1/-}$ mice in the latency to the platform for the acquisition phase, reversal phase, or visible platform trial, in the time spent in the platform quadrant during the probe trial, or in the swim velocity during the probe trial.

Double-strand DNA breaks are increased in the cortex and striatum of 3-month-old $Htt^{\Delta E1/\Delta E1}$ mice

In vitro studies have shown that HTT localizes to sites of DNA damage upon oxidative stress or following UV laser micro-irradiation [23]. To examine if the deletion of Htt's N-terminal domains results in any change in the DNA damage response, the single-nucleus gel electrophoresis comet assay [97] was used to quantify DNA breaks in young (3-month-old) and older (13- to 16-month-old) $Htt^{\Delta E1/\Delta E1}$ and $Htt^{+/+}$ mice. Nuclei from dissected cortex, striatum, thalamus, and cerebellum were isolated using an iodixanol gradient, embedded in low-melting point agarose, and then lysed and electrophoresed at alkaline pH to detect both DNA single strand breaks (SSBs) and double strand breaks (DSBs) or under neutral pH to detect only DSBs. A small but significant increase in the percentage of DNA detected in the tail of the comet was observed in the cortex and striatum of 3-month-old $Htt^{\Delta E1/\Delta E1}$ mice compared to controls under neutral pH conditions (Fig. 3-10A, 3-10B, cortex: $Htt^{+/+}$: 15.00±1.43%, $Htt^{\Delta E1/\Delta E1}$: 18.00±1.35%, p=0.0053; striatum: $Htt^{+/+}$: 17.33±1.57%, $Htt^{\Delta E1/\Delta E1}$: 22.62±1.78%, p=0.0289, mean±SEM, paired t-test, 104-202 nuclei/mouse, 6 mice/genotype), indicating that there is an elevated level

of DSBs in the *Htt*$^{\Delta E1/\Delta E1}$ cortex and striatum at 3 months of age. However, no difference in the levels of DSBs were observed in the thalamus or cerebellum between 3-month-old *Htt*$^{\Delta E1/\Delta E1}$ and control mice (Fig 3-10A), suggesting that the increased DSBs in the *Htt*$^{\Delta E1/\Delta E1}$ brain is region-specific. In contrast, no differences in the level of SSBs were observed in the cortex, striatum, thalamus, and cerebellum in a comparison between *Htt*$^{\Delta E1/\Delta E1}$ and controls at 3 months of age (Fig. 3-10A), and no differences in either DNA SSBs or DSBs were observed in these brain regions obtained from 13-16-month-old *Htt*$^{\Delta E1/\Delta E1}$ and *Htt*$^{+/+}$ mice (Fig. 3-10A).

Although the comet assay can provide a direct assessment of the level of DNA breaks in a single cell, slight differences during nuclear isolation, lysis, and electrophoresis made it difficult to compare results between different sets of experiments. Therefore, the expression of DSB markers were examined by immunohistochemistry in the cortex and striatum of 3- and 12-month-old *Htt*$^{+/+}$ and *Htt*$^{\Delta E1/\Delta E1}$ mice. The histone H2A variant H2AX is phosphorylated by ATM at the sites of DSBs to form γH2AX [98], which then helps to recruit DNA repair proteins into the DNA repair complex. The presence of nuclear γH2AX puncta has been widely used to visualize DSBs in vitro and in vivo [99]. A greater percentage of nuclei with γH2AX^{+} puncta was observed in both the cortex and striatum of *Htt*$^{\Delta E1/\Delta E1}$ mice in comparison to *Htt*$^{+/+}$ controls at 3 months of age (Fig. 3-11A, 3-11B, cortex: *Htt*$^{+/+}$: 17.66±3.18%, *Htt*$^{\Delta E1/\Delta E1}$: 49.50±8.76%, p=0.0142; striatum: *Htt*$^{+/+}$: 6.47±1.79%, *Htt*$^{\Delta E1/\Delta E1}$: 31.35±9.12%, p=0.0368; mean±SEM, unpaired t-test, 8-9 images/mouse, 4 mice/genotype). In contrast, no difference between genotypes was detected at 12 months of age (Fig. 3-11A, 3-11B).

Increased levels of DSBs could result from either an increase in DSB formation or from a deficit in DSB repair. To determine whether DNA repair is altered in the *Htt*$^{\Delta E1/\Delta E1}$ cortex and striatum, a large amount of DNA damage was induced and the mice were examined to determine if repair occurs in the *Htt*$^{\Delta E1/\Delta E1}$ mice at a comparable level to the *Htt*$^{+/+}$ controls. 3-month-old *Htt*$^{+/+}$ and *Htt*$^{\Delta E1/\Delta E1}$ mice were exposed to a single 7Gy dose of γ-irradiation, and their brains were collected at 3- or 24-hours following irradiation. In cortex and striatum of the 3-month-old *Htt*$^{+/+}$ mice, the percentage of nuclei with γH2AX^{+} puncta increased by 3 hours after irradiation, then returned to near basal levels by 24 hours after irradiation (Fig. 3-11A, 3-11C). A similar pattern was observed in the striatum of 3-month-old *Htt*$^{\Delta E1/\Delta E1}$ mice (Fig. 3-11A, 3-11C). However, there is no significant increase in the percentage of nuclei with γH2AX^{+} puncta in the cortex of 3-month-old *Htt*$^{\Delta E1/\Delta E1}$ mice 3 hours after γ-irradiation, probably due to a *Htt*$^{\Delta E1/\Delta E1}$ mouse with high levels of γH2AX^{+} without irradiation (Fig. 3-11A, 3-11C). Nevertheless, in contrast to the higher percentage of nuclei with γH2AX^{+} puncta present in the *Htt*$^{\Delta E1/\Delta E1}$ mice prior to γ-irradiation, there is no significant difference in the percentage of nuclei with γH2AX^{+} puncta between genotypes at either 3 or 24 hours after γ-irradiation (Fig. 3-11A, 3-11C, 3 hour post-irradiation cortex: *Htt*$^{+/+}$: 59.81±4.67%, *Htt*$^{\Delta E1/\Delta E1}$: 64.52±3.86%, p=0.4590; striatum: *Htt*$^{+/+}$: 48.96±4.57%, *Htt*$^{\Delta E1/\Delta E1}$: 55.83±3.52%, p=0.2678; 24 hour post-irradiation cortex: *Htt*$^{+/+}$: 29.54±3.67%, *Htt*$^{\Delta E1/\Delta E1}$: 24.91±4.66%, p=0.4788; striatum: *Htt*$^{+/+}$: 26.35±2.84%, *Htt*$^{\Delta E1/\Delta E1}$: 33.08±4.74%, p=0.2902; mean±SEM, unpaired t-test, 8-9 images/mouse, 3-5 mice/genotype). These results suggest that DNA repair after acute damage is not significantly impaired in the *Htt*$^{\Delta E1/\Delta E1}$ mice compared to the controls.

Pan-nuclear 53bp1 levels are elevated in the cortex and striatum of 3-month-old $Htt^{\Delta E1/\Delta E1}$ mice

Next, the expression of 53bp1, a protein involved in the non-homologous end-joining (NHEJ) repair pathway for DNA DSBs, was examined by immunohistochemistry (for review of 53bp1 functions, see [95]). Although an increase in 53bp1$^+$ puncta at the sites of DNA DSBs in the $Htt^{\Delta E1/\Delta E1}$ brains where elevated γH2AX$^+$ puncta were present were expected, instead pan-nuclear 53bp1 staining in both the cortex and striatum of $Htt^{\Delta E1/\Delta E1}$ mice was observed at 3 months of age that was absent in the $Htt^{+/+}$ mice (Fig. 3-12A). By 12 months of age, pan-nuclear 53bp1 can be detected in the cortex and striatum of both the $Htt^{+/+}$ and $Htt^{\Delta E1/\Delta E1}$ mice (Fig 3-12A).

To determine the age at which pan-nuclear 53bp1 is first elevated, additional brains from $Htt^{+/+}$ and $Htt^{\Delta E1/\Delta E1}$ mice at 2 and 4 months of age were collected and examined. In both cortex and striatum of $Htt^{+/+}$ mice, pan-nuclear 53bp1 levels are low at 2 and 3 months of age but are increased to a level comparable to that observed in $Htt^{\Delta E1/\Delta E1}$ mice at 4 months of age (Fig 3-12A). At 4 months of age, there is also no difference between genotypes in the percentage of nuclei with γH2AX staining (cortex: $Htt^{+/+}$: 45.72±3.79%, $Htt^{\Delta E1/\Delta E1}$: 30.95±3.97%, p=0.0545; striatum: $Htt^{+/+}$: 26.40±2.88%, $Htt^{\Delta E1/\Delta E1}$: 17.69±2.43%, p=0.0821; mean±SEM, unpaired t-test, 9 images/mouse, 3 mice/genotype). Higher levels of pan-nuclear 53bp1 staining can be detected in the $Htt^{\Delta E1/\Delta E1}$ striatum at 2 and 3 months of age in comparison to the controls (Fig. 3-12A, 3-12B, 2 months: $Htt^{+/+}$: 8.08±5.37%, $Htt^{\Delta E1/\Delta E1}$: 27.77±3.17%, p=0.0344; 3 months: $Htt^{+/+}$: 0.26±0.16%, $Htt^{\Delta E1/\Delta E1}$: 23.02±4.14%, p=0.0015. mean±SEM, unpaired t-test, 9 images/mouse, 3-4 mice/genotype). An increase in the pan-nuclear 53bp1 staining can

also be detected in the $Htt^{\Delta E1/\Delta E1}$ cortex at 3 months of age (Fig 3-12A, 3-10B. $Htt^{+/+}$: 3.73±2.61%, $Htt^{\Delta E1/\Delta E1}$: 44.29±9.69%, p=0.0068. mean±SEM, unpaired t-test, 9 images/mouse, 4 mice/genotype).

To investigate if the pan-nuclear 53bp1 is present in neurons or glia, brain sections from 3-month-old $Htt^{+/+}$ and $Htt^{\Delta E1/\Delta E1}$ mice were co-immunostained with 53bp1 and NeuN (a protein present in many but not all neurons, for review, see [100]) antibodies (Fig. 3-12C). The percentage of $NeuN^+$ cells was not significantly different between genotypes (Fig. 3-12D), but the percentage of $NeuN^+$ cells with elevated 53bp1 levels was ~72% higher in the $Htt^{\Delta E1/\Delta E1}$ cortex and ~ 83% higher in the $Htt^{\Delta E1/\Delta E1}$ striatum compared to the controls. (Fig. 3-12E, cortex: $Htt^{+/+}$: 21.58±11.62%, $Htt^{\Delta E1/\Delta E1}$: 93.90±3.44%, p=0.0010; striatum: $Htt^{+/+}$: 0.77±0.45%, $Htt^{\Delta E1/\Delta E1}$: 83.90±8.25%, p<0.0001. mean±SEM, unpaired t-test, 9 images/mouse, 4 mice/genotype). A higher percentage of $NeuN^-$ cells in the $Htt^{\Delta E1/\Delta E1}$ cortex also exhibited elevated nuclear 53bp1 levels in comparison to the controls (Fig. 3-12F, $Htt^{+/+}$: 0.89±0.52%, $Htt^{\Delta E1/\Delta E1}$: 20.04±5.01%, p=0.0090, mean±SEM, unpaired t-test, 9 images/mouse, 4 mice/genotype). These $NeuN^-53bp1^+$ cells (~8% of the total cells) could be either $NeuN^-$ neurons or glial cells. In contrast, very few $NeuN^-$ cells in the striatum exhibited elevated levels of 53bp1 in both genotypes (Fig. 3-12F). These results suggest that the elevated levels of pan-nuclear 53bp1 occur predominantly in neurons.

To confirm the elevated 53bp1 levels observed by immunohistochemistry in the $Htt^{\Delta E1/\Delta E1}$ mice, 53bp1 levels in cortical tissue from 3-month-old $Htt^{\Delta E1/\Delta E1}$ and $Htt^{+/+}$ mice were analyzed by western blotting. A higher level of 53bp1 was detected in $Htt^{\Delta E1/\Delta E1}$ cortical protein lysates in comparison to the controls (Fig. 3-13A. 3-13B, $Htt^{+/+}$:

0.14±0.01, *Htt*$^{\Delta E1/\Delta E1}$: 0.17±0.01; p=0.0257. mean±SEM, unpaired t-test, 3 mice/genotype).

Purkinje cell density and DNA damage marker levels are not altered in 3- month-old *Htt*$^{\Delta E1/\Delta E1}$ *mice*

Purkinje cell loss affects motor function [101, 102], and has been reported in mouse models of HD [103] and in post-mortem brains of HD patients with primarily motor symptoms [104]. To determine if Purkinje cell loss could contribute to the rotarod deficit observed in the *Htt*$^{\Delta E1/\Delta E1}$ mice, Purkinje cell density was examined in 3-month-old *Htt*$^{+/+}$ and *Htt*$^{\Delta E1/\Delta E1}$ mice by immunohistochemistry using a calbindin antibody. There were no differences in Purkinje cell density between genotypes (Fig. 3-14A, 3-14B, *Htt*$^{+/+}$: 24.40±1.05 cells/mm, *Htt*$^{\Delta E1/\Delta E1}$: 23.27±1.26 cells/mm, p=0.5156. mean±SEM, unpaired t-test, 4 images/mouse, 4 mice/genotype).

No difference between genotypes in either DNA SSB or DSB damage were observed in the cerebellum by comet assay (Fig. 3-10A), however, Purkinje cells represent a small percentage of the total neurons in the mouse cerebellum (~1 Purkinje cell per 175 granule cells, [105]). Therefore, γH2AX and 53bp1 levels in Purkinje cells were also analyzed by immunohistochemistry. Interestingly, in contrast to the cortex and striatum, pan-nuclear 53bp1 staining was present in the majority of Purkinje cells in the *Htt*$^{+/+}$ mice at 3 months of age at a level similar to that observed in the *Htt*$^{\Delta E1/\Delta E1}$ cerebellum (Fig. 3-14C, 3-14D, *Htt*$^{+/+}$: 89.73±4.48%, *Htt*$^{\Delta E1/\Delta E1}$: 97.56±1.01%, p=0.1390. Mean±SEM, unpaired t-test, 157-224 cells/mouse, 4 mice/genotype). No differences in the percentage of Purkinje cells with γH2AX puncta were observed between genotypes

(Fig. 3-14E). These data suggest that loss of the Htt N-terminus does not affect cell density or the levels of DNA damage repair markers in Purkinje cells.

DNA and protein oxidation products are not altered in 3-month-old $Htt^{\Delta E1/\Delta E1}$ brains

In a cell culture model, the N17 domain was shown to act as a sensor for oxidative stress [1], suggesting that without exon 1-encoded domains, oxidative damage could be altered in the $Htt^{\Delta E1/\Delta E1}$ mice. To determine whether DNA oxidation levels are altered in the cortex and striatum of 3-month-old $Htt^{\Delta E1/\Delta E1}$ mice in comparison to controls, isolated nuclei were embedded in agarose and lysed under alkaline conditions to expose 8-hydroxy-2´-deoxyguanosine (8-OHdG), a common product of DNA oxidation [106]. Alkaline treatment denatures DNA and increases nuclear volume that together helps to expose the 8-OHdG epitopes, but the treatment also results in a more diffuse DAPI staining (Fig 3-15A). No differences in 8-OHdG levels between genotypes were observed in either the cortical or the striatal nuclei, but the amount of 8-OHdG detected in both $Htt^{+/+}$ and $Htt^{\Delta E1/\Delta E1}$ nuclei was low (Fig.3-15A, 3-15B). To determine whether increased oxidative stress would differentially affect 8-OHdG levels in the $Htt^{\Delta E1/\Delta E1}$ and $Htt^{+/+}$ cortex and striatum, $KBrO_3$ was administered to 3-month-old $Htt^{+/+}$ and $Htt^{\Delta E1/\Delta E1}$ mice in their drinking water at 2 g/L for 7 days to induce oxidative DNA damage. Administration of $KBrO_3$, which is a renal carcinogen that preferentially produces 8-OHdG lesions [107], also elevates reactive oxygen species in the brain [108]. Although 8-OHdG levels were elevated in cortical and striatal nuclei isolated from both $Htt^{+/+}$ and $Htt^{\Delta E1/\Delta E1}$ mice after $KBrO_3$ treatment, no significant differences between genotypes were observed (Fig. 3-15A, 3-15B).

To examine protein oxidation levels, total proteins from the cortex and striatum of 3-month-old *Htt*$^{+/+}$ and *Htt*$^{\Delta E1/\Delta E1}$ mice were used to assess the level of protein carbonyls, a product of protein oxidation [109], by western blotting. No differences in the levels of protein carbonyls were observed between genotypes (Fig. 3-15C, 3-15D). The absence of altered DNA and protein oxidation product levels in the *Htt*$^{\Delta E1/\Delta E1}$ cortex and striatum in comparison to *Htt*$^{+/+}$ controls suggests that deletion of the Htt N-terminal domains does not significantly affect the levels of oxidative damage.

Autophagy markers are not altered under basal conditions in Htt$^{\Delta E1/\Delta E1}$ *mice*

To determine whether the steady-state autophagy is affected by ΔE1-Htt, the levels of autophagy markers LC3 and p62 in 3-month-old *Htt*$^{\Delta E1/\Delta E1}$ and *Htt*$^{+/+}$ mice were compared. During autophagosome assembly, phosphatidylethanolamine is conjugated to cytosolic LC3 (LC3-I), that is then incorporated into the autophagosome membrane as LC3-II [80, 110, 111]. LC3-II is subsequently linked to ubiquitinated cargo though the adaptor protein p62 [81, 110]. Therefore, LC3-II and p62 levels in the microsomal protein fractions obtained from dissected cortex and striatum of 3-month-old *Htt*$^{+/+}$ and *Htt*$^{\Delta E1/\Delta E1}$ mice were examined (Fig. 3-16A-C). There were no significant differences in the levels of LC3-II or p62 between genotypes. The co-localization of LC3 and p62 in the cortex and striatum of 3-month-old *Htt*$^{+/+}$ and *Htt*$^{\Delta E1/\Delta E1}$ mice was also examined by immunohistochemistry, where there was no difference between genotypes (Fig. 3-16D, 3-16E).

To ascertain that autophagy is not affected in aged animals, LC3 western blotting using whole brain microsomal fractions from 24-month-old *Htt*$^{+/+}$ and *Htt*$^{\Delta E1/\Delta E1}$ mice was performed, and no difference in the LC3-II to LC3-I ratio was detected between

genotypes (Fig. 3-16F, 3-16G). These data suggest that basal autophagy levels are not altered in the *Htt*$^{\Delta E1/\Delta E1}$ mouse brains in vivo.

Glutamatergic corticocortical, corticostriatal, thalamocortical, and thalamostriatal synapse numbers are not altered in Htt$^{\Delta E1/\Delta E1}$ *mice at 18 months of age*

Mice with a conditional knockout of cortical *Htt* exhibit altered numbers of glutamatergic synapses in the cortex and striatum, and mice with a conditional knockout of *Htt* in striatal projection neurons exhibit altered numbers of inhibitory synapses in the external globus pallidus [76, 77]. Additionally, *Htt*$^{\Delta N17/\Delta N17}$ mice exhibit a reduction in glutamatergic thalamostriatal synapses at 24 months of age. To determine whether *Htt*$^{\Delta E1/\Delta E1}$ mice exhibit a phenotype similar to the *Htt*$^{\Delta N17/\Delta N17}$ mice, colocalization of the presynaptic markers Vglut1 (expressed in cortical projection neurons) or Vglut2 (expressed in thalamic projection neurons) with the post-synaptic marker PSD95 was quantified in the cortex and striatum of 18-month-old *Htt*$^{\Delta E1/\Delta E1}$ and *Htt*$^{+/+}$ mice. There were no significant differences in the numbers of glutamatergic corticocortical, corticostriatal, thalamocortical, or thalamostriatal synapses between genotypes (Fig. 3-17A-D). In addition, no significant differences in the levels of Vglut1, Vglut2, and PSD95 expression were detected in whole brain microsomal fractions from 24-month-old *Htt*$^{\Delta E1/\Delta E1}$ and *Htt*$^{+/+}$ mice (Fig. 3-17E-H).

Discussion

Htt$^{\Delta E1/\Delta E1}$ progeny from *Htt*$^{\Delta E1/+}$ x *Htt*$^{\Delta E1/+}$ intercrosses and *Htt*$^{\Delta E1/-}$ progeny from *Htt*$^{\Delta E1/+}$ x *Htt*$^{+/-}$ intercrosses were born at the expected Mendelian frequency and survive up to 24 months of age, suggesting that the domains encoded by exon 1 are not required for Htt's critical role during embryogenesis or for survival in adulthood. This is

consistent with prior work showing that transgenic expression of an N-terminal truncated fragment of HTT lacking the first 169 aa can support survival in adult mice that lack normal *Htt* expression [43].

The cause of the sex-specific non-Mendelian genotype frequency observed in the progeny from $Htt^{\Delta E1/+}$ intercrosses is not known. Two independent $Htt^{\Delta E1}$ knock-in lines were included in this study, and therefore off-target effects are not likely to contribute to our observation. This difference could be explained by an increase in $Htt^{\Delta E1}$ Y and Htt^{+} X sperm with a similar decrease in Htt^{+} Y and $Htt^{\Delta E1}$ X sperm, indicating that non-random meiotic chromosomal segregation could be a possible cause of this effect. Although no meiotic deficits were noted in mice with a conditional knockout of *Htt* in the testes [112], a small change in the segregation frequency might not be detected. Alternatively, a change in sperm swim rate or ability to fertilize an egg could skew the ratio of the expected progeny. A thorough characterization of sperm from $Htt^{\Delta E1/+}$ mice will be required to understand the sex-specific non-Mendelian transmission of the $Htt^{\Delta E1}$ allele. Although no sex specific allelic distortion was observed in progeny from $Htt^{\Delta E1/+}$ x $Htt^{+/-}$ intercrosses, the limited numbers of litters produced may not be enough to uncover subtle differences in allelic frequency.

Under basal conditions, there was no alteration in the subcellular localization of $Htt^{\Delta E1}$ compared to Htt^{+}. This result is consistent with prior observations showing that deletion of the Htt N17 domain does not affect the subcellular localization of ΔN17-Htt in vivo [4]. A second HTT membrane-association domain (aa 172-372) is retained in ΔE1-Htt, as well as a nuclear export signal in the C-terminus [113, 114]. Our data does not exclude the possibility that differences in Htt localization exist in different brain regions or

cell types that cannot be detected in whole brain lysate, or that there may be subtle differences in Htt localization that cannot be detected by western blotting. A brain region-specific study with a more sensitive detection method will be required to reveal subtle differences in Htt localization in vivo.

Previous evaluations of the role of Htt's N-terminal domains in motor performance and spatial learning and memory have reported differential effects from the deletion of individual N-terminal Htt domains. $Htt^{\Delta Q/\Delta Q}$ and $Htt^{\Delta QP/\Delta QP}$ mice exhibited improved rotarod performance while rotarod performance was mostly unaffected in $Htt^{\Delta N17/\Delta N17}$ and $Htt^{\Delta P/\Delta P}$ mice [4, 5]. In contrast, a modest deficit in rotarod performance was observed in the $Htt^{\Delta E1/\Delta E1}$ mice. At 18-19 months of age, $Htt^{\Delta P/\Delta P}$ mice exhibited impaired Morris water maze performance, while no differences were observed in $Htt^{\Delta N17/\Delta N17}$, $Htt^{\Delta QP/\Delta QP}$, or $Htt^{\Delta E1/\Delta E1}$ mice compared to controls [4-6]. However, a direct comparison of behavioral phenotypes between the $Htt^{\Delta E1/\Delta E1}$ mice and the previously characterized domain-deletion mice is difficult, as the $Htt^{\Delta E1/\Delta E1}$ mice are congenic in the C57BL/6J background while the $Htt^{\Delta N17/\Delta N17}$, $Htt^{\Delta Q/\Delta Q}$, $Htt^{\Delta P/\Delta P}$, and $Htt^{\Delta QP/\Delta QP}$ mice were in a mixed 129Sv x C57BL/6J genetic background. Nonetheless, the differential motor and cognitive performances observed between $Htt^{\Delta N17/\Delta N17}$, $Htt^{\Delta Q/\Delta Q}$, $Htt^{\Delta P/\Delta P}$, $Htt^{\Delta QP/\Delta QP}$, and $Htt^{\Delta E1/\Delta E1}$ mice suggest that the N17, polyQ, and PRR domains do not function independently of each other, consistent with the hypothesis that polyQ domain flexibility allows for interactions between the N17 and PRR domains [28]. Unlike the $Htt^{\Delta E1/\Delta E1}$ mice, $Htt^{\Delta E1/-}$ mice do not exhibit a rotarod deficit compared to $Htt^{+/+}$ mice. In fact, $Htt^{\Delta E1/-}$ mice outperform $Htt^{\Delta E1/\Delta E1}$ mice on the rotarod at 3, 6, 12, and 18 months of age. However, *Htt* levels correlate with body weight in mice [60] and $Htt^{\Delta E1/-}$ mice exhibit reduced body weight compared to $Htt^{\Delta E1/\Delta E1}$ mice at 3, 6, 12, and 18 months of age.

Because body weight can affect rotarod performance [115], the effect of reducing Htt levels on rotarod performance may be dominant over the effect of deleting the Htt N-terminus.

Elevated pan-nuclear 53bp1 levels and increased neuronal γH2AX puncta have been reported in post-mortem Alzheimer's disease brain tissue and from individuals with mild cognitive impairment in comparison to age-matched control tissue [116]. Elevated pan-nuclear 53bp1 has also been reported in fibroblasts collected from centenarians (aged 95-105) compared to fibroblasts from younger subjects (aged 65-80) [117]. The centenarian fibroblasts were able to resolve induced oxidative DNA damage more quickly than the fibroblasts obtained from younger subjects (aged 65-80) [117], suggesting that increased pan-nuclear 53bp1 levels may be a compensatory response to genotoxic stress. The increase in pan-nuclear 53bp1 levels observed in the $Htt^{\Delta E1/\Delta E1}$ cortex and striatum may therefore be a compensatory response to the elevated DSBs caused by either an early elevation in genotoxic stress or a subtle deficit in DSB repair. A similar elevation in pan-nuclear 53bp1 levels that occurs slightly later in the cortex and striatum of wild type mice could be due to normal aging. The brain regional differences in the timing of 53bp1 elevation may correlate with potential brain-regional susceptibilities to DNA damage.

ROS is a possible source of genotoxic stress, and the Htt N-terminus is able to respond to the presence of ROS in vitro [1]. DNA oxidation, however, results in the formation of multiple forms of DNA damage, including SSBs and DSBs [118]. The lack of elevated 8-OHdG in nuclei isolated from $Htt^{\Delta E1/\Delta E1}$ cortex and striatum is consistent with the lack of elevated SSBs detected by the comet assay in 3-month-old $Htt^{\Delta E1/\Delta E1}$ mice in

comparison to *Htt*$^{+/+}$ mice and suggests that SSB repair is functioning normally in the *Htt*$^{\Delta E1/\Delta E1}$ mice. However, nuclei with relatively high levels of DNA damage could possibly be preferentially lost during the isolation process and therefore be excluded from the comet assay or 8-OHdG immunostaining analyses. In addition to oxidative damage, other mechanisms could also cause increased DSBs in the brain, including neuronal activity [119]. Additionally, DNA repair in the cortex and striatum following γ-irradiation appeared to function normally in *Htt*$^{\Delta E1/\Delta E1}$ mice at 3 months of age, suggesting that DNA damage caused by γ-irradiation may recruit compensatory repair pathways that do not require participation of Htt's N-terminal domains. Based on our data, a small increase in genotoxicity, a subtle deficit in DNA repair, or a combination of both could potentially contribute to the elevated DSBs observed in the *Htt*$^{\Delta E1/\Delta E1}$ mice at 3 months of age.

Our results are consistent with prior studies demonstrating that deletion of the N17 domain or the polyQ and PRR domains together do not affect basal autophagy levels [4]. *Htt*$^{\Delta N17/\Delta N17}$ mice exhibit a slight reduction in glutamatergic thalamostriatal synapses at 24 months of age [4], however, the numbers of glutamatergic corticocortical, corticostriatal, thalamocortical, and thalamostriatal synapses in 18-month-old *Htt*$^{\Delta E1/\Delta E1}$ mice are not significantly different from the numbers in *Htt*$^{+/+}$ mice. Both age and genetic background differences in the mice may contribute to this discrepancy.

Similar to the phenotypes exhibited by *Htt*$^{\Delta N17/\Delta N17}$, *Htt*$^{\Delta Q/\Delta Q}$, *Htt*$^{\Delta P/\Delta P}$, and *Htt*$^{\Delta QP/\Delta QP}$ mouse models, the behavioral and cellular phenotypes exhibited by adult *Htt*$^{\Delta E1/\Delta E1}$ mice are subtle and suggest that deletion off all three domains encoded by *Htt* exon 1 only modestly impact the efficiency of normal homeostatic Htt functions in mice.

Fig. 3-1: Diagram of wild-type (*Htt*$^{+}$) and N-terminal deletion (*Htt*$^{\Delta E1}$) versions of *Htt*'s exon 1. The amino acid sequence of the Htt N-terminus includes the N17 domain (bolded), the polyQ domain (italicized), and PRR domain (underlined).

***Htt*$^{\Delta E1/+}$ x *Htt*$^{\Delta E1/+}$**

	***Htt*$^{+/+}$ (%)**	***Htt*$^{\Delta E1/+}$ (%)**	***Htt*$^{\Delta E1/\Delta E1}$ (%)**	**Total**	**χ^2**	**p-value**
Total	177 (24.1%)	374 (50.8%)	185 (25.1%)	736	0.37	0.8313
Male	68 (18.6%)	185 (50.7%)	112 (30.7%)	365	10.677	0.0048
Female	109 (29.4%)	189 (50.9%)	73 (19.7%)	371	7.119	0.0285

Table 3-1: The number (percentage) of *Htt*$^{+/+}$, *Htt*$^{\Delta E1/+}$, and *Htt*$^{\Delta E1/\Delta E1}$ progeny from *Htt*$^{\Delta E1/+}$ intercrosses compared to the expected Mendelian ratio.

***Htt*$^{\Delta E1/+}$ (M) x *Htt*$^{+/-}$ (F)**

	***Htt*$^{+/+}$ (%)**	***Htt*$^{+/-}$ (%)**	***Htt*$^{\Delta E1/+}$ (%)**	***Htt*$^{\Delta E1/-}$ (%)**	**Total**	**χ^2**	**p-value**
Total	22 (26.8%)	16 (19.5%)	25 (30.5%)	19 (23.2%)	82	2.195	0.5329
Male	14 (31.1%)	8 (17.8%)	14 (31.1%)	9 (20.0%)	45	2.733	0.4346
Female	8 (21.6%)	8 (21.6%)	11 (29.7%)	10 (27.0%)	37	0.730	0.8662

Table 3-2: The number (percentage) of *Htt*$^{+/+}$, *Htt*$^{+/-}$, *Htt*$^{\Delta E1/+}$, and *Htt*$^{\Delta E1/-}$ progeny from *Htt*$^{\Delta E1/+}$ (M) x *Htt*$^{+/-}$ (F) intercrosses compared to the expected Mendelian ratio.

***Htt*$^{\Delta E1/+}$ (F) x *Htt*$^{+/-}$ (M)**

	***Htt*$^{+/+}$ (%)**	***Htt*$^{+/-}$ (%)**	***Htt*$^{\Delta E1/+}$ (%)**	***Htt*$^{\Delta E1/-}$ (%)**	**Total**	**χ^2**	**p-value**
Total	35 (21.5%)	39 (23.9%)	49 (30.1%)	40 (24.5%)	163	2.571	0.4627
Male	18 (23.4%)	17 (22.1%)	26 (33.8%)	16 (20.1%)	77	3.260	0.3533
Female	17 (19.8%)	22 (25.6%)	23 (26.7%)	24 (27.9%)	86	1.349	0.7176

Table 3-3: The number (percentage) of *Htt*$^{+/+}$, *Htt*$^{+/-}$, *Htt*$^{\Delta E1/+}$, and *Htt*$^{\Delta E1/-}$ progeny from *Htt*$^{\Delta E1/+}$ (F) x *Htt*$^{+/-}$ (M) intercrosses compared to the expected Mendelian ratio.

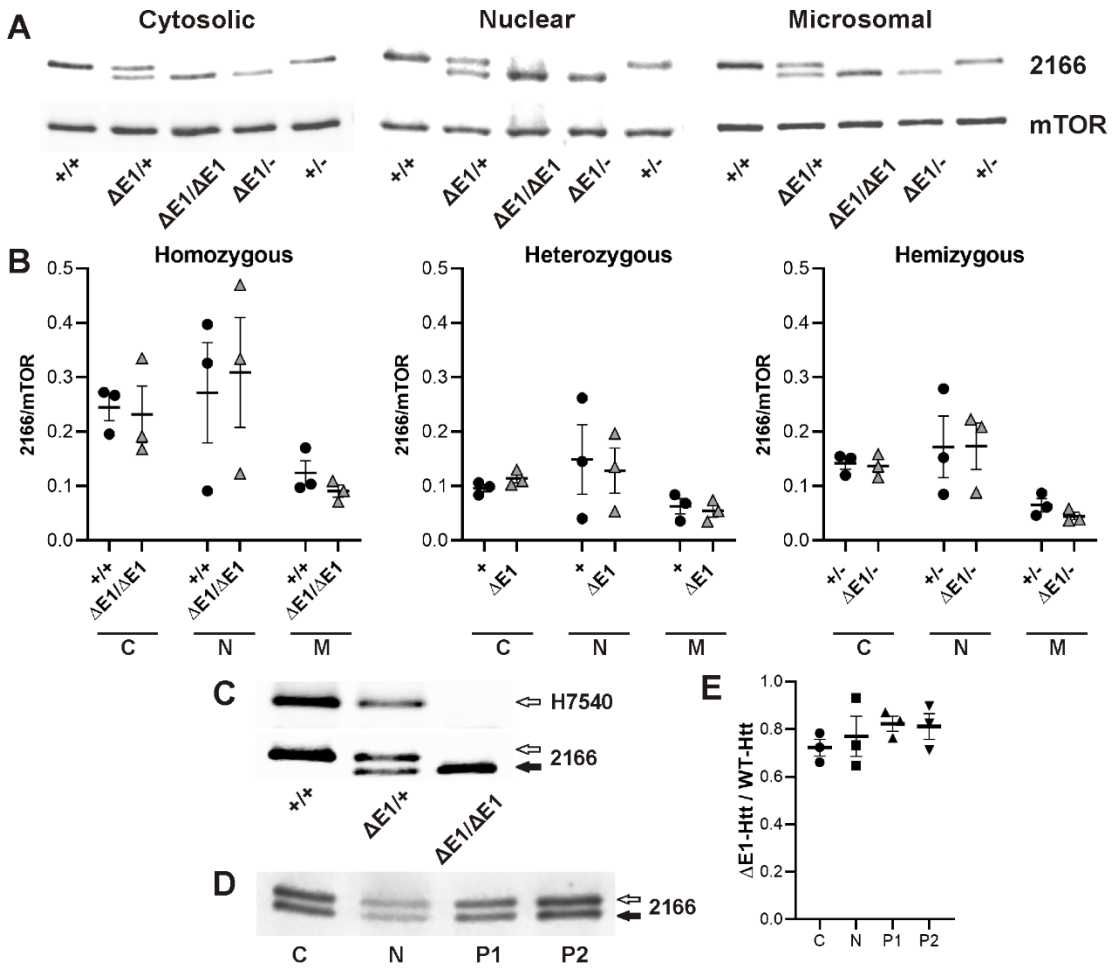

Fig. 3-2: Deletion of the 3 N-terminal domains of Htt does not affect its subcellular distribution. (A) Western blot of whole brain cytosolic, nuclear, and total microsomal fractions from 6-month-old *Htt*$^{+/+}$ (+/+), *Htt*$^{\Delta E1/+}$ (ΔE1/+), *Htt*$^{\Delta E1/\Delta E1}$ (ΔE1/ΔE1), *Htt*$^{\Delta E1/-}$ (ΔE1/-), and *Htt*$^{+/-}$ (+/-) mice probed with the 2166 antibody (Millipore MAB2166), which recognizes an epitope present in both wild type (WT-Htt, upper band) and N-terminal deleted Htt (ΔE1-Htt, lower band) and an mTOR antibody as a loading control.
(B) Quantification of Htt's subcellular localization in 6-month-old mice. The ratios of the relative fluorescence of WT-Htt or ΔE1-Htt to mTOR were calculated and compared

between homozygous, heterozygous, and hemizygous fractions. Mean±SEM, unpaired t-test, 3 mice/genotype.

Cytosolic: $Htt^{+/+}$: 0.24±0.02, $Htt^{\Delta E1/+}$: WT-Htt: 0.10±0.01, ΔE1-Htt: 0.11±0.01, $Htt^{\Delta E1/\Delta E1}$: 0.23±0.05, $Htt^{\Delta E1/-}$: 0.14±0.01, $Htt^{+/-}$: 0.14±0.01, $Htt^{+/+}$ compared to $Htt^{\Delta E1/\Delta E1}$: p=0.8287, $Htt^{+/-}$ compared to $Htt^{\Delta E1/-}$: p=0.7717, $Htt^{\Delta E1/+}$: WT-Htt compared to ΔE1-Htt: p=0.01644.

Nuclear: $Htt^{+/+}$: 0.27±0.09, $Htt^{\Delta E1/+}$: WT-Htt: 0.15±0.06, ΔE1-Htt: 0.13±0.04, $Htt^{\Delta E1/\Delta E1}$: 0.31±0.10, $Htt^{\Delta E1/-}$: 0.17±0.04, $Htt^{+/-}$: 0.17±0.06, $Htt^{+/+}$ compared to $Htt^{\Delta E1/\Delta E1}$: p=0.7989, $Htt^{+/-}$ compared to $Htt^{\Delta E1/-}$: p=0.9887, $Htt^{\Delta E1/+}$: WT-Htt compared to ΔE1-Htt: p=0.7983.

Total microsomal: $Htt^{+/+}$: 0.12±0.02, $Htt^{\Delta E1/+}$: WT-Htt: 0.06±0.01, ΔE1-Htt: 0.05±0.01, $Htt^{\Delta E1/\Delta E1}$: 0.09±0.01, $Htt^{\Delta E1/-}$: 0.04±0.01, $Htt^{+/-}$: 0.06±0.01, $Htt^{+/+}$ compared to $Htt^{\Delta E1/\Delta E1}$: p=0.2678, $Htt^{+/-}$ compared to $Htt^{\Delta E1/-}$: p=0.2146, $Htt^{\Delta E1/+}$: WT-Htt compared to ΔE1-Htt: p=0.6708.

(C) Western blot of whole brain total microsomal fractions from 6-month-old $Htt^{+/+}$, $Htt^{\Delta E1/+}$, and $Htt^{\Delta E1/\Delta E1}$ mice probed with the 2166 antibody, which recognizes an epitope present in both WT-Htt (white arrow) and ΔE1-Htt (black arrow), and probed with the H7540 antibody (Sigma-Aldrich), which recognizes the first 17 amino acids of Htt.

(D) Western blot with 2166 of whole brain lysates from 6-month-old $Htt^{\Delta E1/+}$ mice that were separated into cytosolic (C), nuclear (N), 9k xg heavy microsomal (P1), and 100k xg light microsomal (P2) fractions.

(E) Quantification of Htt's subcellular localization in 6-month-old mice. The ratios of the relative fluorescence of ΔE1-Htt to WT-Htt were calculated in each fraction. No differences were observed in the ΔE1-Htt to WT-Htt ratio between fractions. Mean±SEM, 1-way ANOVA, n=3 mice. C: 0.72±0.04, N: 0.77±0.08, P1: 0.82±0.03, P2: 0.81±0.05, p=0.5921 F=0.6627, D_F=3.

Age	*Htt*$^{+/+}$	*Htt*$^{\Delta E1/+}$	*Htt*$^{\Delta E1/\Delta E1}$	*Htt*$^{+/-}$	*Htt*$^{\Delta E1/-}$
3 Months	20	20	20	20	20
6 Months	20	20	20	20	20
12 Months	20	20	19	20	20
14 Months	19	19	19	20	20
18 Months	19	18	18	20	20
19 Months	19	18	18	20	19

Table 3-4: Number of animals used at each experimental time point for behavioral testing.

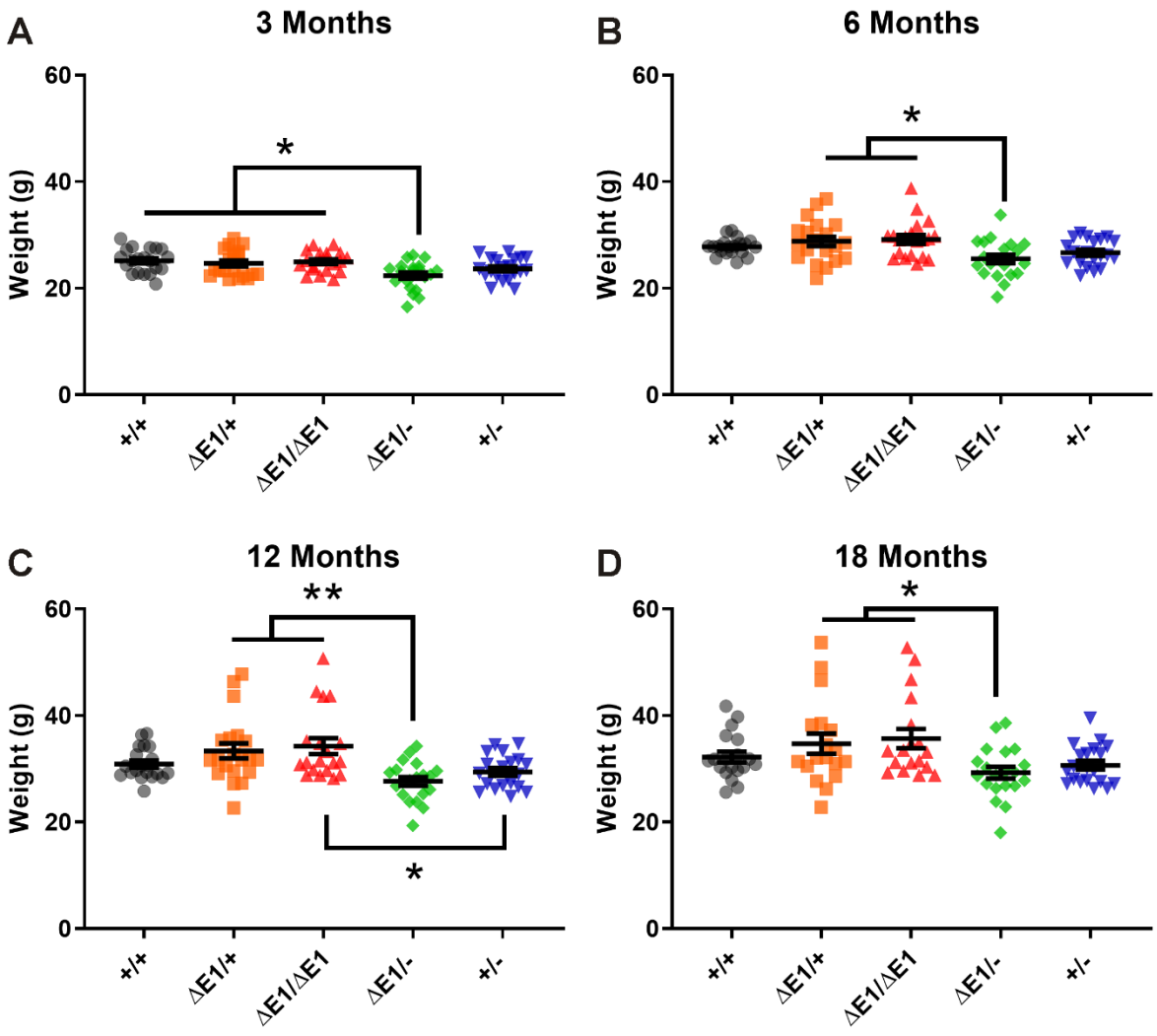

Figure 3-3: Body weight of *Htt*$^{+/+}$, *Htt*$^{\Delta E1/+}$, *Htt*$^{\Delta E1/\Delta E1}$, *Htt*$^{+/-}$, and *Htt*$^{\Delta E1/-}$ mice. *Htt*$^{+/+}$ (+/+), *Htt*$^{\Delta E1/+}$ (ΔE1/+), *Htt*$^{\Delta E1/\Delta E1}$ (ΔE1/ΔE1), *Htt*$^{\Delta E1/-}$ (ΔE1/-), and *Htt*$^{+/-}$ (+/-) mice were weighed at (A) 3, (B) 6, (C) 12, and (D) 18 months of age. 1-way ANOVA with Tukey's multiple comparison test. *p<0.05, **p<0.01, mean ± SEM.

3 months: *Htt*$^{+/+}$: 25.18±0.50 g, *Htt*$^{\Delta E1/+}$: 24.67±0.57 g, *Htt*$^{\Delta E1/\Delta E1}$: 24.99±0.43 g, *Htt*$^{+/-}$: 23.67±0.46 g, *Htt*$^{\Delta E1/-}$: 22.40±0.59 g, p=0.0009, F=5.108, D_F=4; 6 months: *Htt*$^{+/+}$: 27.78±0.34 g, *Htt*$^{\Delta E1/+}$: 28.80±0.87 g, *Htt*$^{\Delta E1/\Delta E1}$: 29.16±0.79 g, *Htt*$^{+/-}$: 26.68±0.55 g, *Htt*$^{\Delta E1/-}$

: 25.54±0.79 g*, p*=0.0019, F=4.604, D_F=4; 12 months: $Htt^{+/+}$*:* 30.94±0.65 g*,* $Htt^{\Delta E1/+}$*:* 33.38±1.15 g*,* $Htt^{\Delta E1/\Delta E1}$*:* 34.25±1.50 g*,* $Htt^{+/-}$*:* 29.44±0.69 g*,* $Htt^{\Delta E1/-}$*:* 27.66±0.82 g*, p*=0.0001, F=6.471, D_F=4; 18 months: $Htt^{+/+}$*:* 32.21±0.99 g*,* $Htt^{\Delta E1/+}$*:* 34.73±1.90 g*,* $Htt^{\Delta E1/\Delta E1}$*:* 35.67±1.79 g*,* $Htt^{+/-}$*:* 30.70±0.81 g*,* $Htt^{\Delta E1/-}$*:* 29.28±1.08 g*, p*=0.0056, F=3.923, D_F=4.

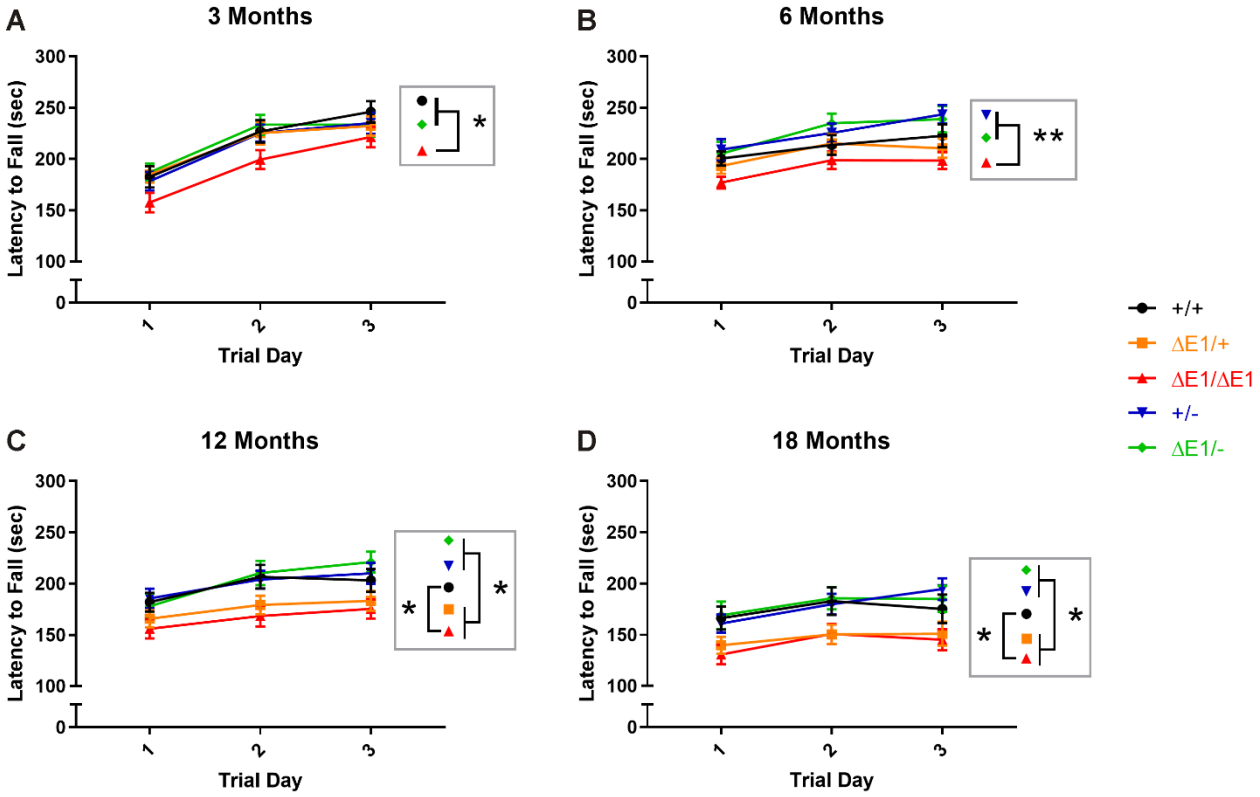

Figure 3-4: *Htt*$^{\Delta E1/\Delta E1}$ mice exhibit a deficit in the accelerating rotarod test. *Htt*$^{+/+}$ (+/+), *Htt*$^{\Delta E1/+}$ (ΔE1/+), *Htt*$^{\Delta E1/\Delta E1}$ (ΔE1/ΔE1), *Htt*$^{\Delta E1/-}$ (ΔE1/-), and *Htt*$^{+/-}$ (+/-) mice were subjected to three trials per day of rotarod testing over three consecutive days at (A) 3, (B) 6, (C) 12, and (D) 18 months of age. See Table 3-3 for detailed statistical values. 2-way ANOVA. *p<0.05, mean ± SEM.

3 months: *Htt*$^{+/+}$*:* 218.5±6.9 sec, *Htt*$^{\Delta E1/+}$*:* 214.1±6.1 sec, *Htt*$^{\Delta E1/\Delta E1}$*:* 192.8±6.4 sec, *Htt*$^{+/-}$*:* 212.9±6.1 sec, *Htt*$^{\Delta E1/-}$*:* 218.0±6.4 sec; 6 months: *Htt*$^{+/+}$*:* 212.2±5.5 sec, *Htt*$^{\Delta E1/+}$*:* 206.3±5.1 sec, *Htt*$^{\Delta E1/\Delta E1}$*:* 191.4±4.6 sec, *Htt*$^{+/-}$*:* 226.1±5.7 sec, *Htt*$^{\Delta E1/-}$*:* 226.3±6.7 sec; 12 months: *Htt*$^{+/+}$*:* 197.2±6.2 sec, *Htt*$^{\Delta E1/+}$*:* 176.0±5.2 sec, *Htt*$^{\Delta E1/\Delta E1}$*:* 166.5±5.6 sec, *Htt*$^{+/-}$*:* 199.8±5.6 sec, *Htt*$^{\Delta E1/-}$*:* 203.2±6.9 sec; 18 months: *Htt*$^{+/+}$*:* 174.8±7.4 sec, *Htt*$^{\Delta E1/+}$*:* 147.1±5.6 sec, *Htt*$^{\Delta E1/\Delta E1}$*:* 142.2±5.7 sec, *Htt*$^{+/-}$*:* 178.4±5.9 sec, *Htt*$^{\Delta E1/-}$*:* 179.8±7.1 sec.

Genotype 1	Genotype 2	3 Months	6 Months	12 Months	18 Months
***Htt*$^{+/+}$**	***Htt*$^{\Delta E1/+}$**	*p*=0.7360 F=0.1154 D_F=1	*p*=0.6178 F=0.2531 D_F=1	*p*=0.0985 F=2.868 D_F=1	*p*=0.0697 F=3.501 D_F=1
***Htt*$^{+/+}$**	***Htt*$^{\Delta E1/\Delta E1}$**	***p*=0.0455** **F=4.276** **D_F=1**	*p*=0.0627 F=3.677 D_F=1	***p*=0.0231** **F=5.614** **D_F=1**	***p*=0.0327** **F=4.945** **D_F=1**
***Htt*$^{+/+}$**	***Htt*$^{+/-}$**	*p*=0.6349 F=0.2292 D_F=1	*p*=0.2597 F=1.309 D_F=1	*p*=0.8389 F=0.04192 D_F=1	*p*=0.7980 F=0.06648 D_F=1
***Htt*$^{+/+}$**	***Htt*$^{\Delta E1/-}$**	*p*=0.9669 F=0.001746 D_F=1	*p*=0.2999 F=1.105 D_F=1	*p*=0.6731 F=0.1807 D_F=1	*p*=0.7585 F=0.09594 D_F=1
***Htt*$^{\Delta E1/+}$**	***Htt*$^{\Delta E1/\Delta E1}$**	*p*=0.0846 F=3.136 D_F=1	*p*=0.1627 F=2.026 D_F=1	*p*=0.4364 F=0.6190 D_F=1	*p*=0.6932 F=0.1583 D_F=1
***Htt*$^{\Delta E1/+}$**	***Htt*$^{+/-}$**	*p*=0.9155 F=0.01141 D_F=1	*p*=0.1008 F=2.828 D_F=1	***p*=0.0476** **F=4.193** **D_F=1**	***p*=0.0132** **F=6.795** **D_F=1**
***Htt*$^{\Delta E1/+}$**	***Htt*$^{\Delta E1/-}$**	*p*=0.7558 F=0.09816 D_F=1	*p*=0.1345 F=2.338 D_F=1	***p*=0.0456** **F=4.271** **D_F=1**	***p*=0.0315** **F=5.009** **D_F=1**
***Htt*$^{\Delta E1/\Delta E1}$**	***Htt*$^{+/-}$**	*p*=0.0672 F=3.550 D_F=1	***p*=0.0028** **F=10.22** **D_F=1**	***p*=0.0088** **F=7.654** **D_F=1**	***p*=0.0042** **F=9.343** **D_F=1**
***Htt*$^{\Delta E1/\Delta E1}$**	***Htt*$^{\Delta E1/-}$**	***p*=0.0393** **F=4.558** **D_F=1**	***p*=0.0071** **F=8.097** **D_F=1**	***p*=0.0104** **F=7.280** **D_F=1**	***p*=0.0135** **F=6.747** **D_F=1**
***Htt*$^{+/-}$**	***Htt*$^{\Delta E1/-}$**	*p*=0.6482 F=0.2115 D_F=1	*p*=0.9867 F=0.0002834 D_F=1	*p*=0.7991 F=0.06566 D_F=1	*p*=0.9206 F=0.01006 D_F=1

Table 3-5: Statistical values for the accelerating rotarod results (Fig. 3-4) calculated using 2-way ANOVA. Statistically significant values ($p<0.05$) are bolded.

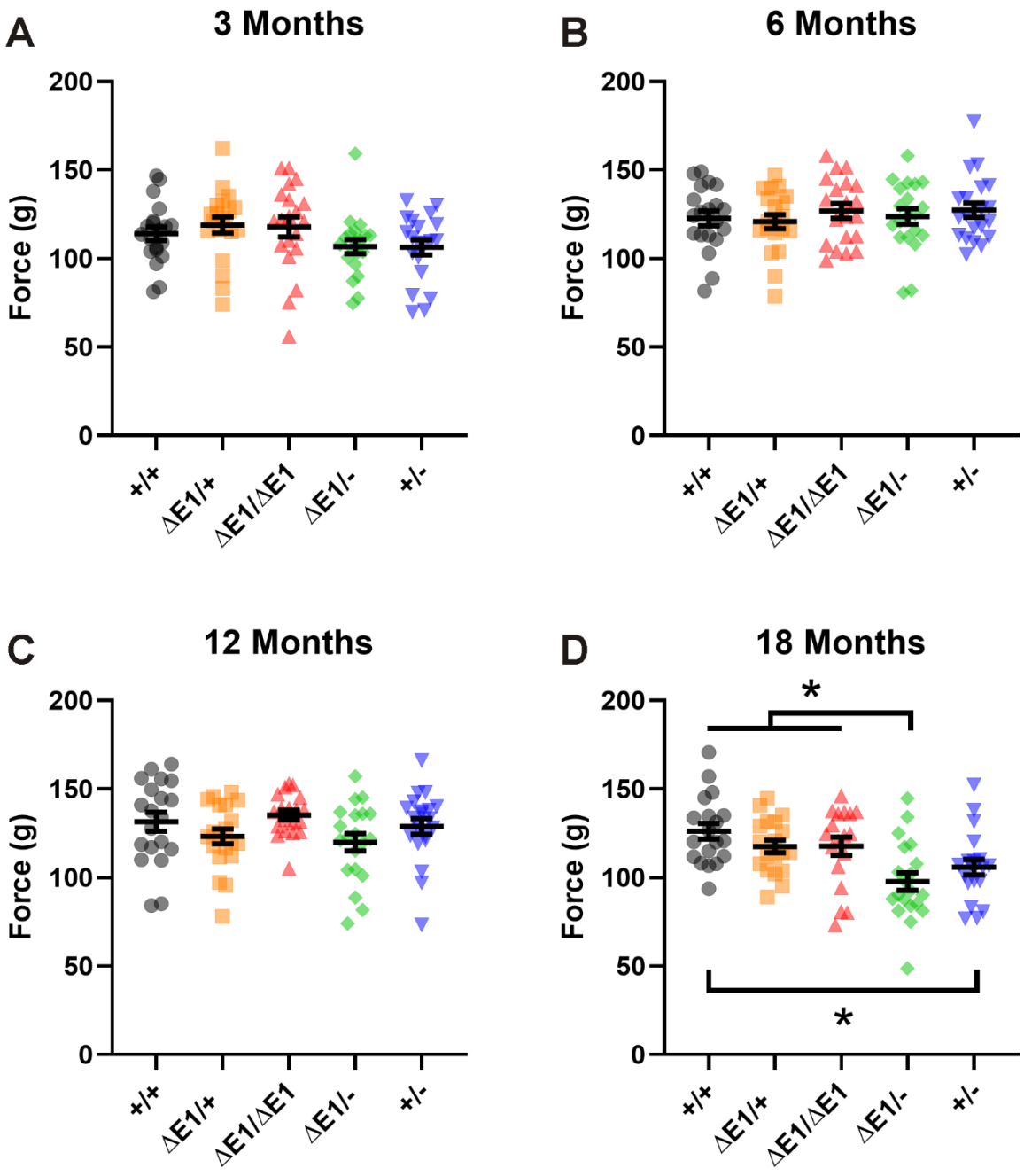

Figure 3-5: Forelimb grip strength is not changed in *Htt*$^{\Delta E1/+}$ or *Htt*$^{\Delta E1/\Delta E1}$ mice, but is reduced in aged *Htt*$^{+/-}$ and *Htt*$^{\Delta E1/-}$ mice. *Htt*$^{+/+}$ (+/+), *Htt*$^{\Delta E1/+}$ (ΔE1/+), *Htt*$^{\Delta E1/\Delta E1}$ (ΔE1/ΔE1), *Htt*$^{\Delta E1/-}$ (ΔE1/-), and *Htt*$^{+/-}$ (+/-) mice were subjected to forelimb grip strength

testing at (A) 3, (B) 6, (C) 12, and (D) 18 months of age. 1-way ANOVA with Tukey's multiple comparison test. *p<0.05, mean ± SEM.

3 months: $Htt^{+/+}$: 114.1±3.9 g, $Htt^{\Delta E1/+}$: 118.9±4.5 g, $Htt^{\Delta E1/\Delta E1}$: 117.8±5.6 g, $Htt^{+/-}$: 106.3±4.3 g, $Htt^{\Delta E1/-}$: 106.7±4.0 g, p=0.1417, F=1.768, D_F=4; 6 months: $Htt^{+/+}$: 122.8±4.1 g, $Htt^{\Delta E1/+}$: 120.9±3.9 g, $Htt^{\Delta E1/\Delta E1}$: 126.9±4.1 g, $Htt^{+/-}$: 127.3±4.1 g, $Htt^{\Delta E1/-}$: 123.8±4.4 g, p=0.7751, F=0.4459, D_F=4; 12 months: $Htt^{+/+}$: 131.6±5.3 g, $Htt^{\Delta E1/+}$: 123.2±4.1 g, $Htt^{\Delta E1/\Delta E1}$: 135.3±2.7 g, $Htt^{+/-}$: 128.9±4.5 g, $Htt^{\Delta E1/-}$: 120.0±4.9 g, p=0.1093, F=1.945, D_F=4; 18 months: $Htt^{+/+}$: 126.2±4.4 g, $Htt^{\Delta E1/+}$: 117.6±3.5 g, $Htt^{\Delta E1/\Delta E1}$: 117.7±5.2 g, $Htt^{+/-}$: 105.9±4.3 g, $Htt^{\Delta E1/-}$: 97.78±5.0 g, p=0.0002, F=6.174, D_F=4.

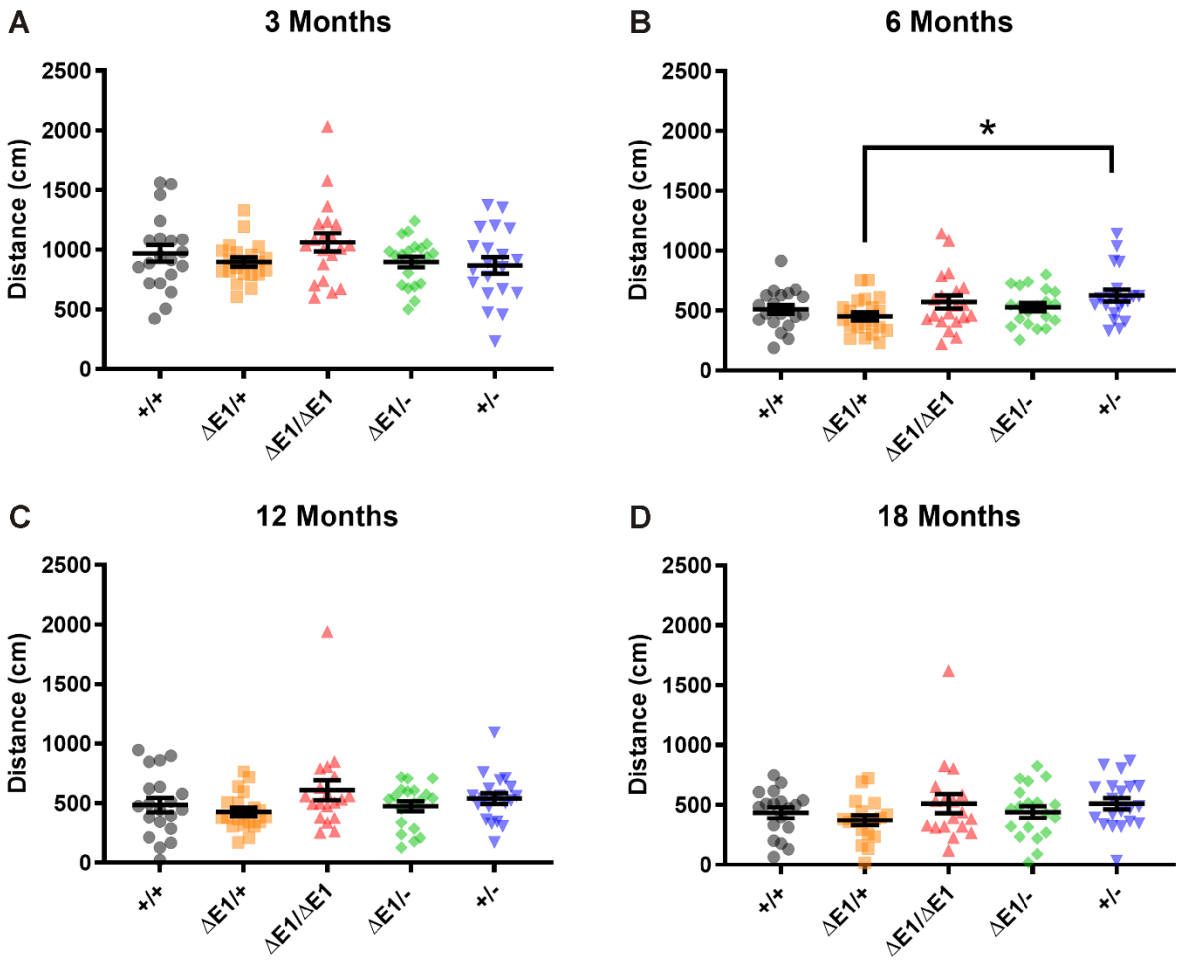

Figure 3-6: Deletion of the Htt N-terminus does not affect total distance traveled during activity monitoring. *Htt*$^{+/+}$ (+/+), *Htt*$^{\Delta E1/+}$ (ΔE1/+), *Htt*$^{\Delta E1/\Delta E1}$ (ΔE1/ΔE1), *Htt*$^{\Delta E1/-}$ (ΔE1/-), and *Htt*$^{+/-}$ (+/-) mice were placed in an activity monitoring apparatus for one 5 min trial at (A) 3, (B) 6, (C) 12, and (D) 18 months of age. The total distance traveled was recorded. 1-way ANOVA with Tukey's multiple comparison test. *p<0.05, mean ± SEM.

3 months: $Htt^{+/+}$: 970.7±70.1 cm, $Htt^{\Delta E1/+}$: 898.3±38.1 cm, $Htt^{\Delta E1/\Delta E1}$: 1062±76 cm, $Htt^{+/-}$: 869.6±68.1 cm, $Htt^{\Delta E1/-}$: 898.8±44.6 cm, p=0.1781, F=1.610, D_F=4; 6 months: $Htt^{+/+}$: 510.7±37.1 cm, $Htt^{\Delta E1/+}$: 453.1±*34.2* cm, $Htt^{\Delta E1/\Delta E1}$: 571.0±54.1 cm, $Htt^{+/-}$: 625.2±48.7 cm, $Htt^{\Delta E1/-}$: 528.5±34.4 cm, p=0.0624, F=2.321, D_F=4; 12 months: $Htt^{+/+}$: 485.7±58.7 cm, $Htt^{\Delta E1/+}$: 428.2±35.1 cm, $Htt^{\Delta E1/\Delta E1}$: 608.9±83.9 cm, $Htt^{+/-}$: 539.8±44.1 cm, $Htt^{\Delta E1/-}$: 475.7±41.0 cm, p=0.1884, F=1.571, D_F=4; 18 months: $Htt^{+/+}$: 433.9±45.7 cm, $Htt^{\Delta E1/+}$: 371.8±42.2 cm, $Htt^{\Delta E1/\Delta E1}$: 511.6±79.3 cm, $Htt^{+/-}$: 510.6±46.5 cm, $Htt^{\Delta E1/-}$: 440.6±50.8 cm, p=0.3289, F=1.172, D_F=4.

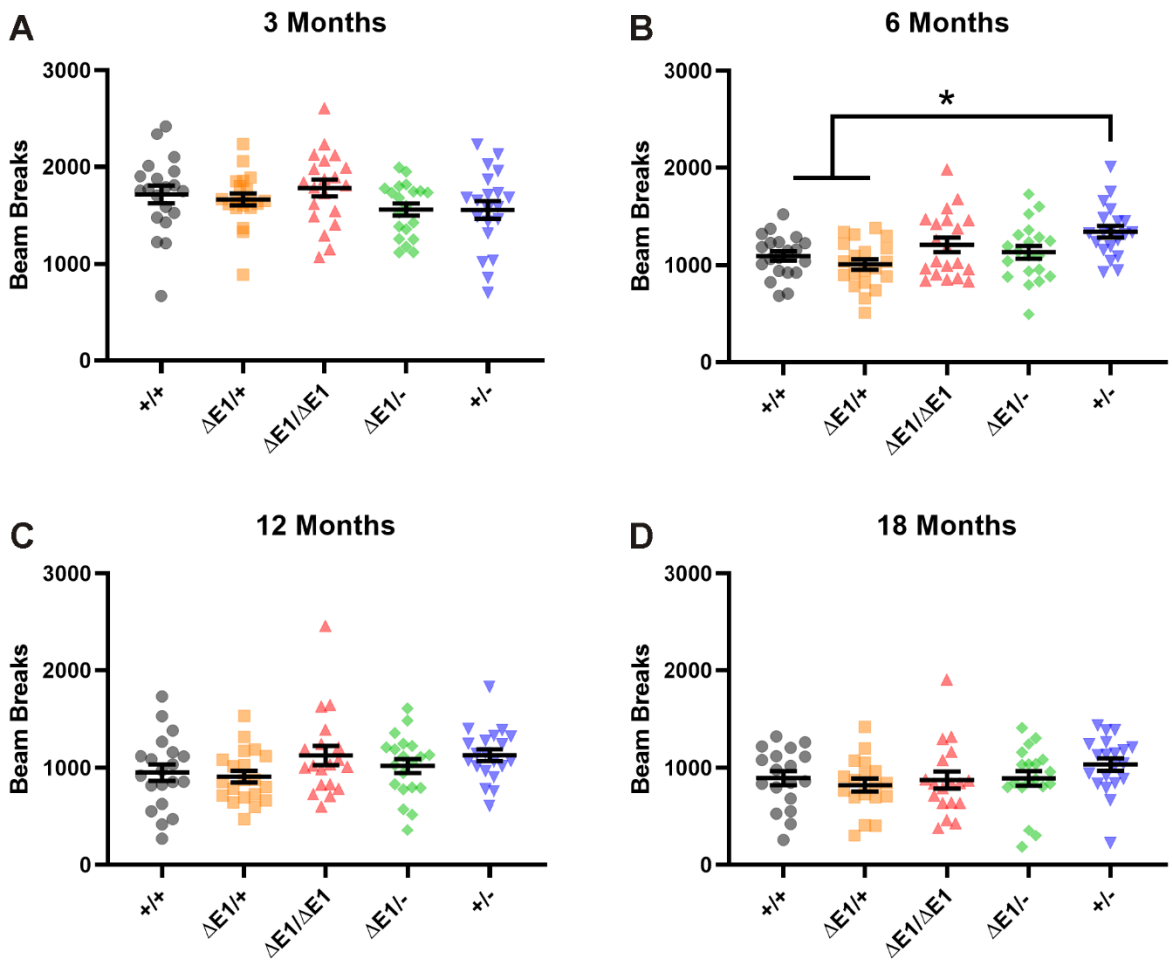

Figure 3-7: Deletion of the Htt N-terminus does not affect horizontal activity levels.

$Htt^{+/+}$ (+/+), $Htt^{\Delta E1/+}$ (ΔE1/+), $Htt^{\Delta E1/\Delta E1}$ (ΔE1/ΔE1), $Htt^{\Delta E1/-}$ (ΔE1/-), and $Htt^{+/-}$ (+/-) mice were placed in an activity monitoring apparatus for one 5 min trial at (A) 3, (B) 6, (C) 12, and (D) 18 months of age. Horizontal activity measurements were recorded. 1-way ANOVA with Tukey's multiple comparison test. *p<0.05, mean ± SEM.

3 months: $Htt^{+/+}$: 1716±89, $Htt^{\Delta E1/+}$: 1665±62, $Htt^{\Delta E1/\Delta E1}$: 1782±85, $Htt^{+/-}$: 1557±92, $Htt^{\Delta E1/-}$: 1561±62, p=0.1998, F=1.530, D_F=4; 6 months: $Htt^{+/+}$: 1094±49, $Htt^{\Delta E1/+}$: 1008±54,

$Htt^{\Delta E1/\Delta E1}$: 1209±74*, $Htt^{+/-}$:* 1345±60*, $Htt^{\Delta E1/-}$:* 1133±67*, p*=0.0031, F=4.296, D_F=4; 12 months: *$Htt^{+/+}$:* 953±83*, $Htt^{\Delta E1/+}$:* 910±60*, $Htt^{\Delta E1/\Delta E1}$:* 1128±99*, $Htt^{+/-}$:* 1131±61*, $Htt^{\Delta E1/-}$:* 1020±72*, p*=0.1485, F=1.736, D_F=4; 18 months: *$Htt^{+/+}$:* 897±73*, $Htt^{\Delta E1/+}$:* 825±66*, $Htt^{\Delta E1/\Delta E1}$:* 877±88*, $Htt^{+/-}$:* 1036±64*, $Htt^{\Delta E1/-}$:* 894±75*, p*=0.3217, F=1.188, D_F=4.

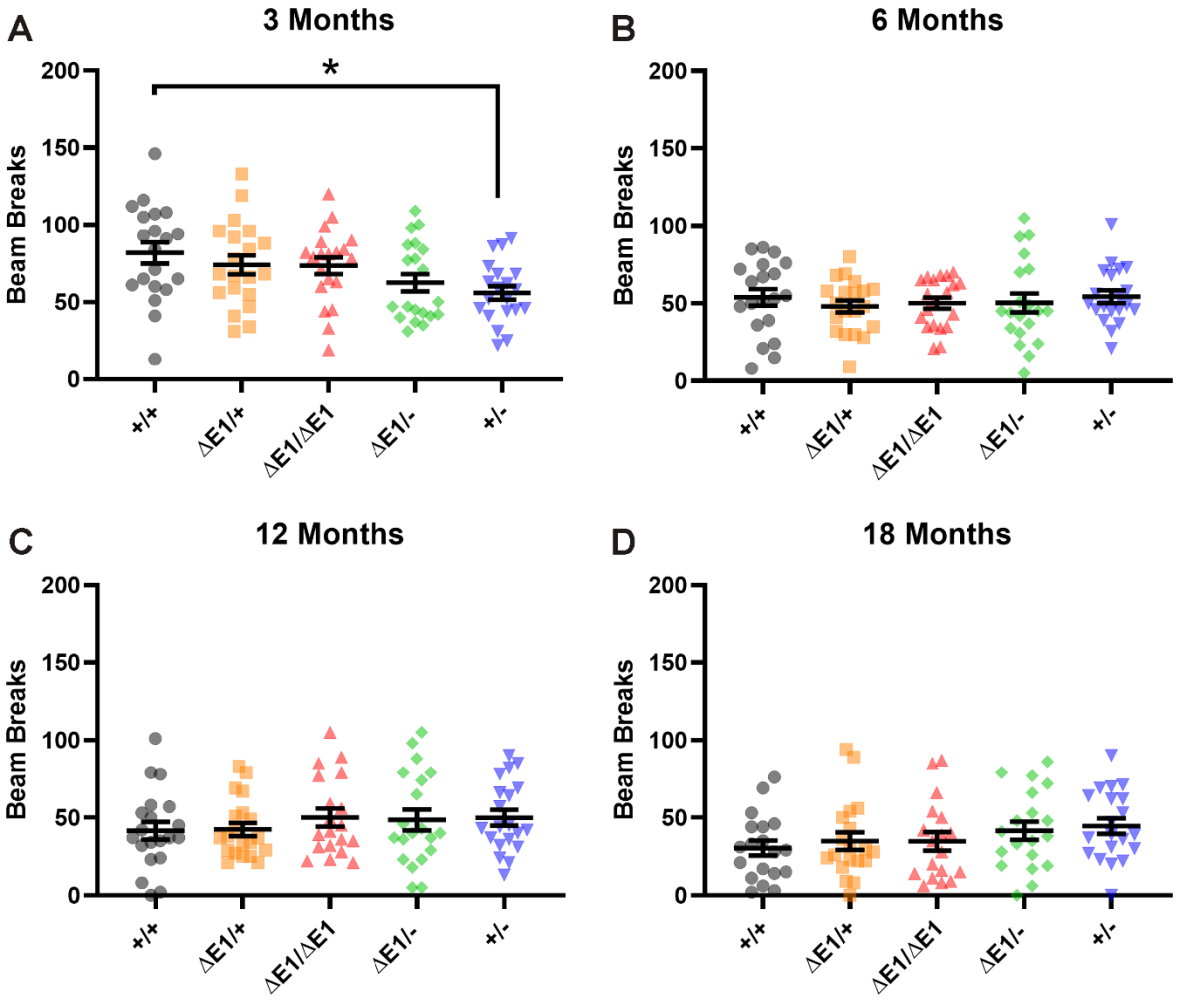

Figure 3-8: Deletion of the Htt N-terminus does not affect vertical activity levels.

$Htt^{+/+}$ (+/+), $Htt^{\Delta E1/+}$ (ΔE1/+), $Htt^{\Delta E1/\Delta E1}$ (ΔE1/ΔE1), $Htt^{\Delta E1/-}$ (ΔE1/-), and $Htt^{+/-}$ (+/-) mice were placed in an activity monitoring apparatus for one 5 min trial at (A) 3, (B) 6, (C) 12, and (D) 18 months of age. Total vertical activity measurements were recorded. 1-way ANOVA with Tukey's multiple comparison test. *p<0.05, mean ± SEM.

3 months: $Htt^{+/+}$: 81.85±6.91, $Htt^{\Delta E1/+}$: 74.05±6.14, $Htt^{\Delta E1/\Delta E1}$: 73.50±5.48, $Htt^{+/-}$: 55.95±4.36, $Htt^{\Delta E1/-}$: 62.50±5.66, p=0.0172, F=3.168, D_F=4; 6 months: $Htt^{+/+}$: 53.85±5.33,

Htt$^{\Delta E1/+}$*:* 48.10±3.86*, Htt*$^{\Delta E1/\Delta E1}$*:* 50.20±3.58*, Htt*$^{+/-}$*:* 54.40±4.08*, Htt*$^{\Delta E1/-}$*:* 50.35±6.13*,* p=0.8624, F=0.3224, D_F=4; 12 months: *Htt*$^{+/+}$*:* 41.60±5.69*, Htt*$^{\Delta E1/+}$*:* 42.40±4.26*, Htt*$^{\Delta E1/\Delta E1}$*:* 50.11±5.83*, Htt*$^{+/-}$*:* 49.95±5.05*, Htt*$^{\Delta E1/-}$*:* 48.50±6.68*,* p=0.6891, F=0.5644, D_F=4; 18 months: *Htt*$^{+/+}$*:* 30.37±4.85*, Htt*$^{\Delta E1/+}$*:* 34.89±5.72*, Htt*$^{\Delta E1/\Delta E1}$*:* 34.72±6.03*, Htt*$^{+/-}$*:* 44.60±5.01*,* *Htt*$^{\Delta E1/-}$*:* 41.63±5.81*,* p=0.3511, F=1.122, D_F=4.

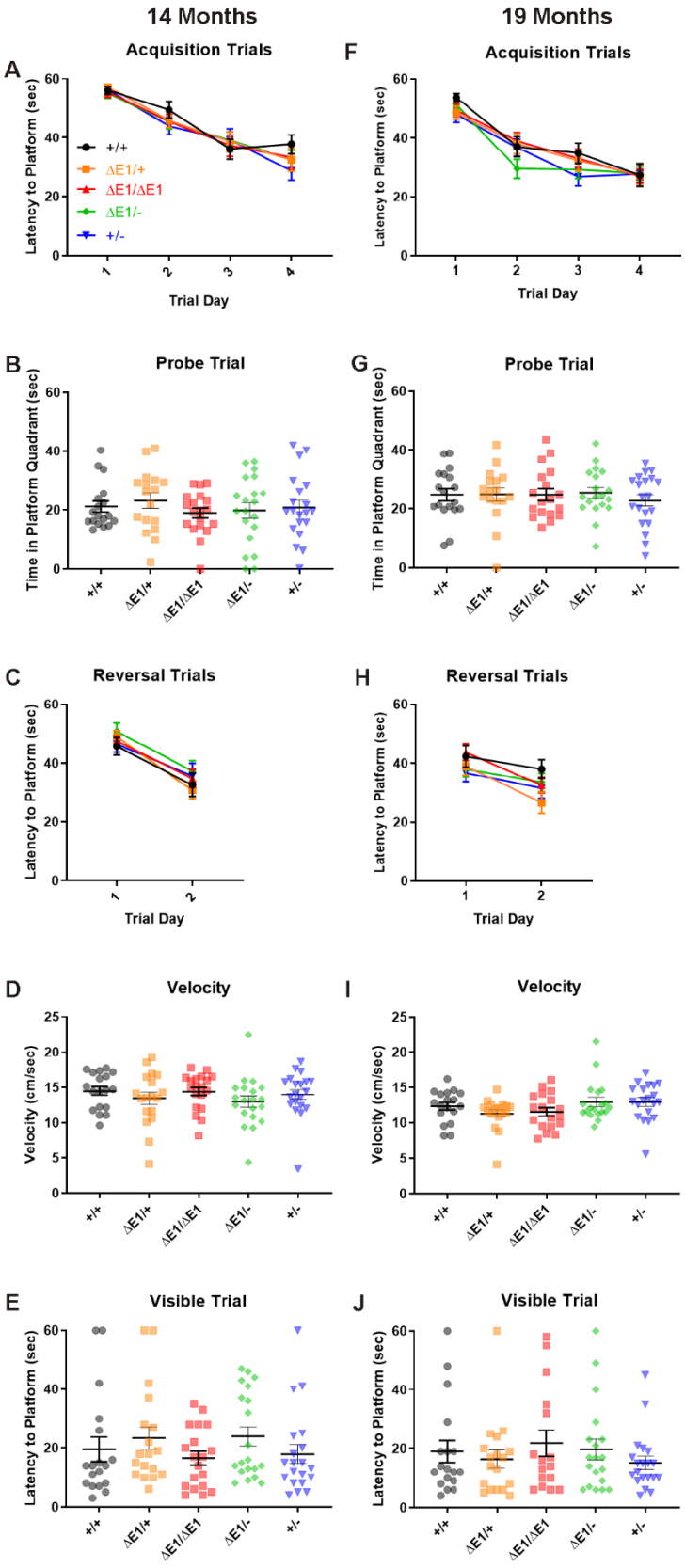
14 Months
19 Months
A
Acquisition Trials
F
Acquisition Trials
Latency to Platform (sec)
Trial Day
+/+
ΔE1/+
ΔE1/ΔE1
ΔE1/-
+/-
B
Probe Trial
G
Probe Trial
Time in Platform Quadrant (sec)
C
Reversal Trials
H
Reversal Trials
D
Velocity
I
Velocity
Velocity (cm/sec)
E
Visible Trial
J
Visible Trial

Figure 3-9: No differences in spatial learning and memory were observed in $Htt^{\Delta E1/+}$, $Htt^{\Delta E1/\Delta E1}$, $Htt^{+/-}$, or $Htt^{\Delta E1/-}$ mice. $Htt^{+/+}$ (+/+), $Htt^{\Delta E1/+}$ (ΔE1/+), $Htt^{\Delta E1/\Delta E1}$ (ΔE1/ΔE1), $Htt^{\Delta E1/-}$ (ΔE1/-), and $Htt^{+/-}$ (+/-) mice were subjected to spatial learning and memory testing over eight consecutive days using the Morris water maze test at 14 (A-E) and 19 (F-J) months of age. The test consisted of a 4-day acquisition phase (A, F) followed by a 1-day probe trial (B, G), and a 2-day reversal trial (C, H). The swim velocity of the mice was measured on the day of the probe trial (D, I). A visible control trial (E, J) was performed on the last day of testing. See Table 3-4 for detailed statistical values of the acquisition and reversal trials. 2-way ANOVA (acquisition and reversal phases) and 1-way ANOVA with Tukey's multiple comparison test (probe trial, visible control trial, and velocity), mean±SEM.

14 months: acquisition trials: $Htt^{+/+}$: 44.86±4.78, $Htt^{\Delta E1/+}$: 43.60±5.31, $Htt^{\Delta E1/\Delta E1}$: 42.96±4.89, $Htt^{+/-}$: 42.04±5.66, $Htt^{\Delta E1/-}$: 43.02±4.77; probe trial: $Htt^{+/+}$: 21.18±1.85, $Htt^{\Delta E1/+}$: 23.15±2.56, $Htt^{\Delta E1/\Delta E1}$: 19.02±1.68, $Htt^{+/-}$: 20.82±2.48, $Htt^{\Delta E1/-}$: 19.88±2.58, p=0.7764, F=0.4442, D_F=3; reversal trials: $Htt^{+/+}$: 39.22±6.56, $Htt^{\Delta E1/+}$: 39.92±9.15, $Htt^{\Delta E1/\Delta E1}$: 41.23±6.36, $Htt^{+/-}$: 41.09±5.39, $Htt^{\Delta E1/-}$: 44.13±6.78; velocity: $Htt^{+/+}$: 14.50±0.61, $Htt^{\Delta E1/+}$: 13.43±0.90, $Htt^{\Delta E1/\Delta E1}$: 14.42±0.60, $Htt^{+/-}$: 14.00±0.72, $Htt^{\Delta E1/-}$: 12.96±0.79, p=0.5248, F=0.8056, D_F=3; visible control: $Htt^{+/+}$: 19.56±4.14, $Htt^{\Delta E1/+}$: 23.39±3.86, $Htt^{\Delta E1/\Delta E1}$: 16.58±2.34, $Htt^{+/-}$: 17.95±3.19, $Htt^{\Delta E1/-}$: 23.95±3.29, p=0.4445, F=0.9402, D_F=3.

19 months: acquisition trials: $Htt^{+/+}$: 38.26±5.56, $Htt^{\Delta E1/+}$: 36.60±4.54, $Htt^{\Delta E1/\Delta E1}$: 37.11±4.77, $Htt^{+/-}$: 34.85±4.90, $Htt^{\Delta E1/-}$: 34.55±5.60; probe trial: $Htt^{+/+}$: 24.88±2.06, $Htt^{\Delta E1/+}$: 24.98±2.27, $Htt^{\Delta E1/\Delta E1}$: 24.89±2.02, $Htt^{+/-}$: 22.89±1.99, $Htt^{\Delta E1/-}$: 25.51±1.84, p=0.9020, F=0.2613, D_F=3; reversal trials: $Htt^{+/+}$: 40.21±2.15, $Htt^{\Delta E1/+}$: 32.88±6.20, $Htt^{\Delta E1/\Delta E1}$: 38.17±5.60, $Htt^{+/-}$: 34.17±2.63, $Htt^{\Delta E1/-}$: 35.83±2.32; velocity: $Htt^{+/+}$: 12.39±0.53,

Htt$^{\Delta E1/+}$*:* 11.35±0.56*, Htt*$^{\Delta E1/\Delta E1}$*:* 11.60±0.59*, Htt*$^{+/-}$*:* 12.98±0.59*, Htt*$^{\Delta E1/-}$*:* 12.98±0.65*,* *p*=0.1669, F=1.659, D_F=3; visible control: *Htt*$^{+/+}$*:* 19.00±3.72*, Htt*$^{\Delta E1/+}$*:* 16.44±3.09*,* *Htt*$^{\Delta E1/\Delta E1}$*:* 21.81±4.44*, Htt*$^{+/-}$*:* 15.20±2.20*, Htt*$^{\Delta E1/-}$*:* 19.74±3.50*, p*=0.6637, F=0.6000, D_F=3.

Genotype (Compared to *Htt*$^{+/+}$)	Trial	14 Months	19 Months
***Htt*$^{\Delta E1/+}$**	**Acquisition**	p=0.6607 F=0.1959 D_F=1	p=0.6377 F=0.2256 D_F=1
***Htt*$^{\Delta E1/\Delta E1}$**	**Acquisition**	p=0.5190 F=0.4241 D_F=1	p=0.7052 F=0.1455 D_F=1
***Htt*$^{+/-}$**	**Acquisition**	p=0.3593 F=0.8618 D_F=1	p=0.2578 F=1.321 D_F=1
***Htt*$^{\Delta E1/-}$**	**Acquisition**	p=0.5128 F=0.4366 D_F=1	p=0.2273 F=1.509 D_F=1
***Htt*$^{\Delta E1/+}$**	**Reversal**	p=0.8504 F=0.03613 D_F=1	p=0.0651 F=3.634 D_F=1
***Htt*$^{\Delta E1/\Delta E1}$**	**Reversal**	p=0.5882 F=0.2987 D_F=1	p=0.5807 F=0.3110 D_F=1
***Htt*$^{+/-}$**	**Reversal**	p=0.6715 F=0.1829 D_F=1	p=0.1400 F=2.277 D_F=1
***Htt*$^{\Delta E1/-}$**	**Reversal**	p=0.2419 F=1.416 D_F=1	p=0.2496 F=1.371 D_F=1

Table 3-6: Statistical values for the results from the acquisition and reversal trials of the Morris water maze test (Fig. 3-7) calculated using 2-way ANOVA. Statistically significant values (p<0.05) are bolded.

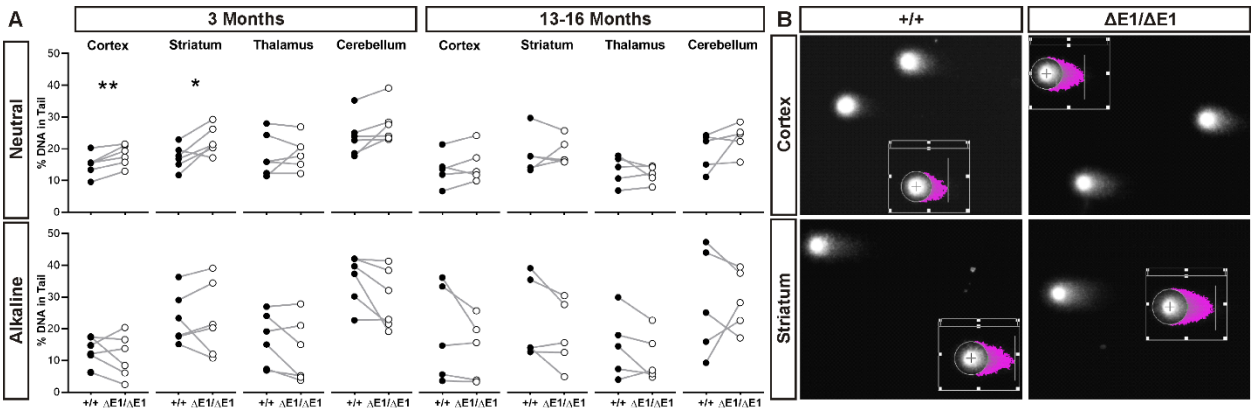

Fig. 3-10: Double strand DNA breaks are increased in 3-month-old *Htt*$^{\Delta E1/\Delta E1}$ mice.

(A) Quantification of neutral and alkaline comet assays from the cortex, striatum, thalamus, and cerebellum of 3- and 13-16-month-old mice. The percentage of DNA in the comet tail under neutral conditions was significantly increased in the cortex and striatum of *Htt*$^{\Delta E1/\Delta E1}$ (ΔE1/ΔE1) mice compared to *Htt*$^{+/+}$ (+/+) mice at 3 months of age. *p<0.05, **p<0.01, mean±SEM, paired t-test, 104-202 nuclei/mouse, 5-6 mice/genotype. (B) Neutral comet assay images from the cortex and striatum of 3-month-old *Htt*$^{+/+}$ and *Htt*$^{\Delta E1/\Delta E1}$ mice. Examples of CaspLab comet quantification analyses are shown in white boxes: comet head circumference (white circle), comet head center (black cross), comet tail area (purple), and end of comet tail (vertical white line) are indicated.
Neutral assay: 3 months: cortex: *Htt*$^{+/+}$: 15.00±1.43%, *Htt*$^{\Delta E1/\Delta E1}$: 18.00±1.35%, p=0.0053; striatum: *Htt*$^{+/+}$: 17.33±1.57%, *Htt*$^{\Delta E1/\Delta E1}$: 22.62±1.78%, p=0.0289; thalamus: *Htt*$^{+/+}$: 18.00±2.73%, *Htt*$^{\Delta E1/\Delta E1}$: 18.85±2.08%, p=0.6579; cerebellum: *Htt*$^{+/+}$: 23.90±2.57%, *Htt*$^{\Delta E1/\Delta E1}$: 27.62±2.48%, p=0.0533; 13-16 months: cortex: *Htt*$^{+/+}$: 13.58±2.37%, *Htt*$^{\Delta E1/\Delta E1}$: 15.17±2.55%, p=0.2315; striatum: *Htt*$^{+/+}$: 18.50±2.95%, *Htt*$^{\Delta E1/\Delta E1}$: 19.20±1.92%, p=0.7558; thalamus: *Htt*$^{+/+}$: 13.31±2.03.%, *Htt*$^{\Delta E1/\Delta E1}$: 11.97±1.21%, p=0.4423; cerebellum: *Htt*$^{+/+}$: 19.34±2.64%, *Htt*$^{\Delta E1/\Delta E1}$: 2332±2.12%, p=0.2148.

Alkaline assay: 3 months: cortex: $Htt^{+/+}$: 13.28±1.73%, $Htt^{\Delta E1/\Delta E1}$: 11.29±2.78%, p=0.3987; striatum: $Htt^{+/+}$: 23.22±3.33%, $Htt^{\Delta E1/\Delta E1}$: 23.01±4.72%, p=0.9382; thalamus: $Htt^{+/+}$: 16.58±3.43%, $Htt^{\Delta E1/\Delta E1}$: 12.95±4.10%, p=0.1408; cerebellum: $Htt^{+/+}$: 35.68±3.15%, $Htt^{\Delta E1/\Delta E1}$: 29.25±3.82%, p=0.0679; 13-16 months: cortex: $Htt^{+/+}$: 18.68±6.83%, $Htt^{\Delta E1/\Delta E1}$: 13.65±4.41%, p=0.1914; striatum: $Htt^{+/+}$: 23.07±5.84%, $Htt^{\Delta E1/\Delta E1}$: 18.25±4.77%, p=0.1288; thalamus: $Htt^{+/+}$: 14.77±4.54%, $Htt^{\Delta E1/\Delta E1}$: 11.11±3.45%, p=0.1771; cerebellum: $Htt^{+/+}$: 28.33±7.53%, $Htt^{\Delta E1/\Delta E1}$: 29.01±4.28%, p=0.9060.

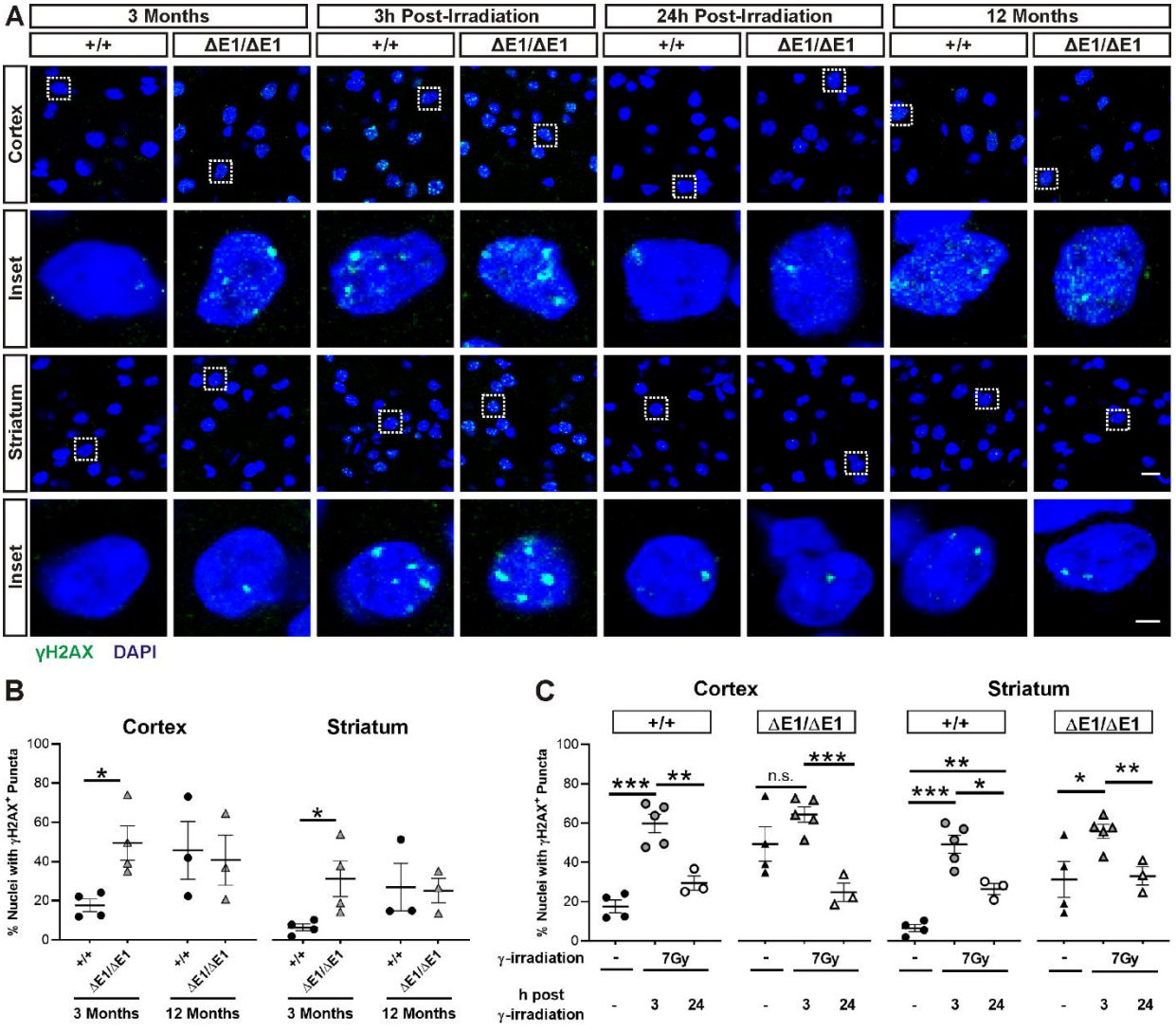

Fig. 3-11: The percentage of nuclei with γH2AX puncta is increased in 3-month-old *Htt*$^{\Delta E1/\Delta E1}$ mice. (A) Cortex and striatum from 3- and 12-month-old *Htt*$^{+/+}$ (+/+) and *Htt*$^{\Delta E1/\Delta E1}$ (ΔE1/ΔE1) mice without γ-irradiation and 3-month-old *Htt*$^{+/+}$ and *Htt*$^{\Delta E1/\Delta E1}$ mice 3 or 24 hours after exposure to 7Gy of γ-irradiation immunostained with a γH2AX antibody (green). Nuclei were labeled with DAPI (blue), scale bar=10μm. White dashed boxes indicate the locations of inset images, scale bar=2μm.

(B) Quantification of the percentage of nuclei containing γH2AX^{+} puncta in 3- and 12-month-old untreated mice. *p<0.05, mean±SEM, unpaired t-test, 8-9 images/mouse, 3-4 mice/genotype.

Cortex: 3 months: *Htt*$^{+/+}$: 17.66±3.18%, *Htt*$^{\Delta E1/\Delta E1}$: 49.50±8.76%, p=0.0142; 12 months: *Htt*$^{+/+}$: 45.77±14.80%, *Htt*$^{\Delta E1/\Delta E1}$: 40.76±12.81%, p=0.8108; striatum: 3 months: *Htt*$^{+/+}$: 6.47±1.79%, *Htt*$^{\Delta E1/\Delta E1}$: 31.35±9.12%, p=0.0368; 12 months: *Htt*$^{+/+}$: 27.14±12.18%, *Htt*$^{\Delta E1/\Delta E1}$: 25.24±6.26%, p=0.8964.

(C) Quantification of the percentage of nuclei containing γH2AX^{+} puncta before and after γ-irradiation. *p<0.05, **p<0.01, ***p<0.001, mean±SEM, unpaired t-test, 8-9 images/mouse, 3-5 mice/genotype.

Cortex: *Htt*$^{+/+}$: 3h post-irradiation: 59.81±4.67%, p=0.0002 compared to control; 24h post-irradiation: 29.54±3.67%, p=0.0583 compared to control, p=0.0043 compared to 3h post-irradiation; *Htt*$^{\Delta E1/\Delta E1}$: 3h post-irradiation: 64.52±3.86%, p=0.1334 compared to control, p=0.4590 compared to *Htt*$^{+/+}$ 3h post-irradiation; 24h post-irradiation: 24.91±4.66%, p=0.0771 compared to control, p=0.0007 compared to 3h post-irradiation, p=0.4788 compared to *Htt*$^{+/+}$ 24h post-irradiation.

Striatum: *Htt*$^{+/+}$: 3h post-irradiation: 48.96±4.57%, p=0.0001 compared to control; 24h post-irradiation: 26.35±2.84%, p=0.0015 compared to control, p=0.0126 compared to 3h post-irradiation; *Htt*$^{\Delta E1/\Delta E1}$: 3h post-irradiation: 55.83±3.52%, p=0.0292 compared to control, p=0.2678 compared to *Htt*$^{+/+}$ 3h post-irradiation; 24h post-irradiation: 33.08±4.74%, p=0.8862 compared to control, p=0.0080 compared to 3h post-irradiation, p=0.2902 compared to *Htt*$^{+/+}$ 24h post-irradiation.

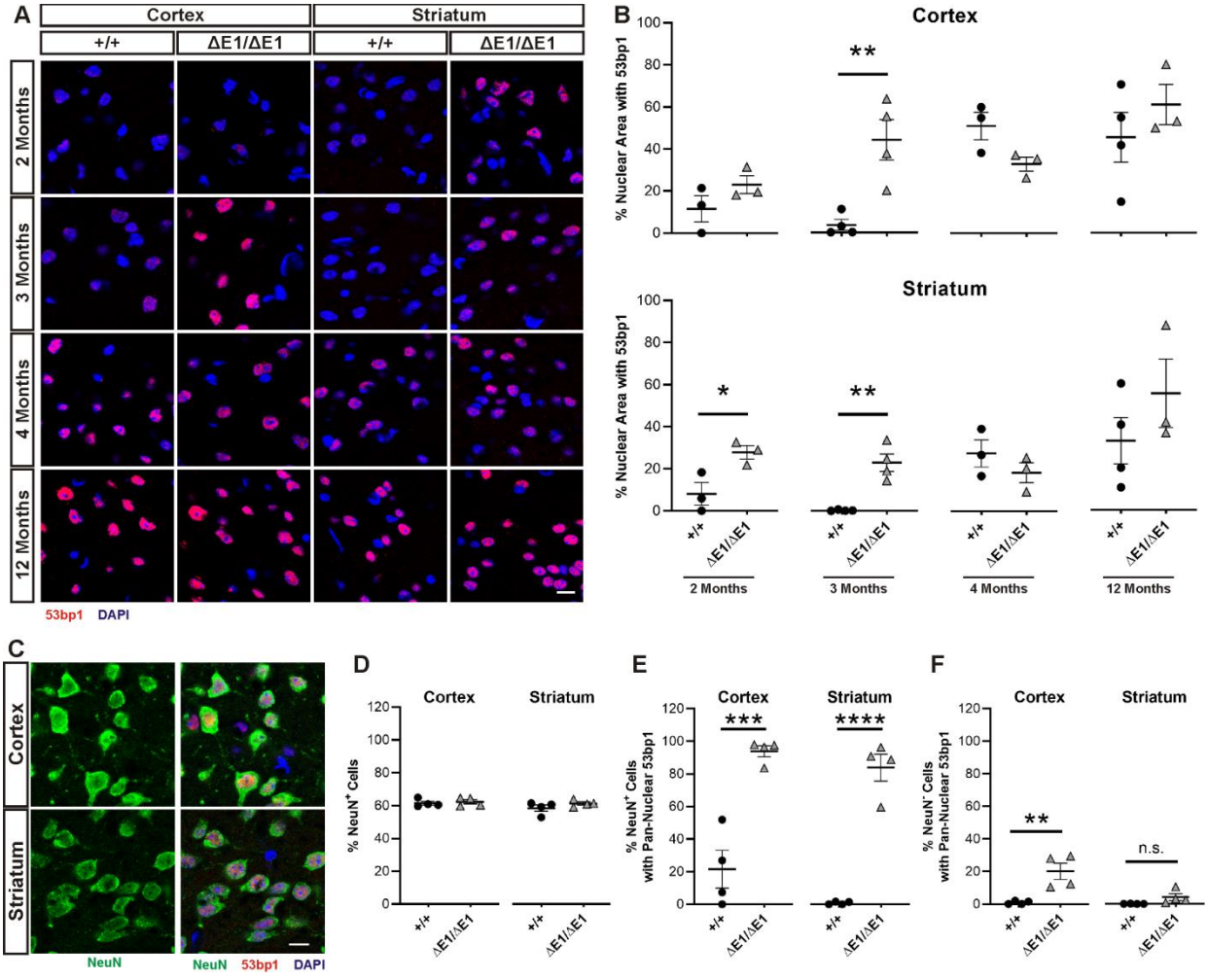

Figure 3-12: Pan-nuclear 53bp1 is elevated in the cortex and striatum of 3-month-old *Htt*$^{\Delta E1/\Delta E1}$ mice. (A) Cortex and striatum from 2-, 3-, 4-, and 12-month-old *Htt*$^{+/+}$ (+/+) and *Htt*$^{\Delta E1/\Delta E1}$ (ΔE1/ΔE1) mice immunostained with a 53bp1 antibody (red). Nuclei were labeled with DAPI (blue), scale bar=10μm.

(B) Quantification of the percentage of the nuclear area with 53bp1. *p<0.05, **p<0.01, mean±SEM, unpaired t-test, 9 images/mouse, 3-4 mice/genotype.

Cortex: 2 months: $Htt^{+/+}$: 11.56±6.22%, $Htt^{\Delta E1/\Delta E1}$: 23.04±4.25%, p=0.2018; 3 months: $Htt^{+/+}$: 3.73±2.61%, $Htt^{\Delta E1/\Delta E1}$: 44.29±9.69%, p=0.0068; 4 months: $Htt^{+/+}$: 51.22±6.6%, $Htt^{\Delta E1/\Delta E1}$: 33.05±3.36%, p=0.0702; 12 months: $Htt^{+/+}$: 45.70±11.875, $Htt^{\Delta E1/\Delta E1}$: 61.30±9.59%, p=0.3790.

Striatum: 2 months: $Htt^{+/+}$: 8.08±5.37%, $Htt^{\Delta E1/\Delta E1}$: 27.77±3.175, p=0.0344; 3 months: $Htt^{+/+}$: 0.26±0.16%, $Htt^{\Delta E1/\Delta E1}$: 23.02±4.14%, p=0.0015; 4 months: $Htt^{+/+}$: 27.72±6.51%, $Htt^{\Delta E1/\Delta E1}$: 18.49±4.80%, p=0.3174; 12 months: $Htt^{+/+}$: 33.13±11.08%, $Htt^{\Delta E1/\Delta E1}$: 55.81±16.35%, p=0.2849.

(C) Images of the cortex and striatum of 3-month-old $Htt^{\Delta E1/\Delta E1}$ mice immunostained with NeuN (green) and 53bp1 antibodies (red). Nuclei were labeled with DAPI (blue), scale bar=10μm.

(D) Quantification of the percentage of total cells that are $NeuN^+$ per image. Mean±SEM, unpaired t-test, 9 images/mouse, 4 mice/genotype. Cortex: $Htt^{+/+}$: 61.53±1.16%, $Htt^{\Delta E1/\Delta E1}$: 62.35±1.31%, p=0.6559; striatum: $Htt^{+/+}$: 58.57±1.94%, $Htt^{\Delta E1/\Delta E1}$: 61.33±0.99%, p=0.2521.

(E) Quantification of the percentage of $NeuN^+$ cells with pan-nuclear 53bp1. ***p<0.001, ****p<0.0001, mean±SEM, unpaired t-test, 9 images/mouse, 4 mice/genotype. Cortex: $Htt^{+/+}$: 21.58±11.62%, $Htt^{\Delta E1/\Delta E1}$: 93.90±3.44%, p=0.0010; striatum: $Htt^{+/+}$: 0.77±0.45%, $Htt^{\Delta E1/\Delta E1}$: 83.90±8.25%, p<0.0001.

(F) Quantification of the percentage of $NeuN^-$ cells with pan-nuclear 53bp1, **p<0.01, mean±SEM, unpaired t-test, 9 images/mouse, 4 mice/genotype. Cortex: $Htt^{+/+}$: 0.89±0.52%, $Htt^{\Delta E1/\Delta E1}$: 20.04±5.01%, p=0.0090; striatum: $Htt^{+/+}$: 0.07±0.07%, $Htt^{\Delta E1/\Delta E1}$: 4.23±2.14%, p=0.0996.

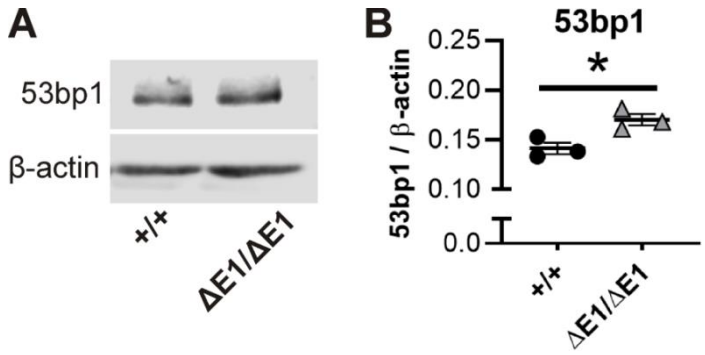

Fig. 3-13: Cortical 53bp1 levels are elevated in 3-month-old *Htt*$^{\Delta E1/\Delta E1}$ mice. (A) Western blots of cortical whole-cell lysates from 3-month-old *Htt*$^{+/+}$ (+/+) and *Htt*$^{\Delta E1/\Delta E1}$ (ΔE1/ΔE1) mice probed with a 53bp1 antibody.

(B) Fluorescence levels were quantified and normalized to β-actin. *p<0.05, mean±SEM, unpaired t-test, 3 mice/genotype. *Htt*$^{+/+}$: 0.14±0.01, *Htt*$^{\Delta E1/\Delta E1}$: 0.17±0.01; p=0.0257.

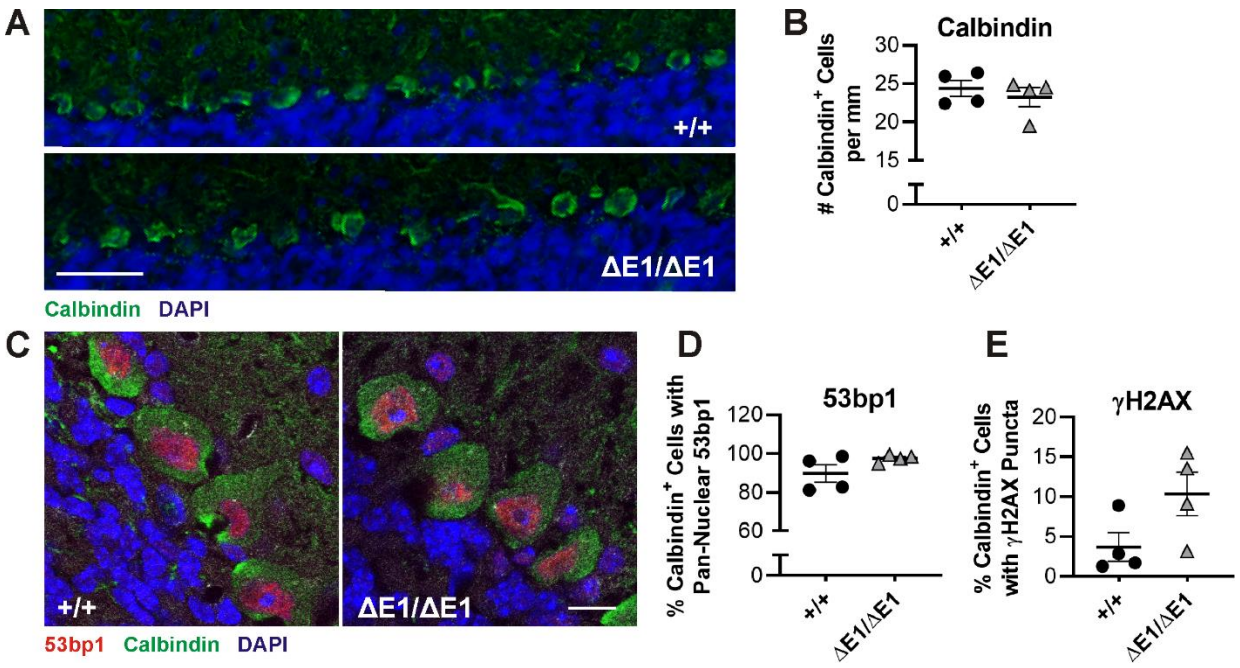

Fig. 3-14: Purkinje cell density and DNA damage marker levels are not altered in 3-month-old *Htt*$^{\Delta E1/\Delta E1}$ mice. (A) Cerebellum from 3-month-old *Htt*$^{+/+}$ (+/+) and *Htt*$^{\Delta E1/\Delta E1}$ (ΔE1/ΔE1) mice immunostained with a calbindin antibody (green). Nuclei were labeled with DAPI (blue), scale bar=50μm.

(B) Quantification of the number of calbindin^{+} cells per mm. Mean±SEM, unpaired t-test, 4 images/mouse, 4 mice/genotype. *Htt*$^{+/+}$: 24.40±1.05 cells, *Htt*$^{\Delta E1/\Delta E1}$: 23.27±1.26 cells, p=0.5156.

(C) Cerebellum from 3-month-old *Htt*$^{+/+}$ (+/+) and *Htt*$^{\Delta E1/\Delta E1}$ (ΔE1/ΔE1) mice immunostained with 53bp1 (red) and calbindin (green) antibodies. Nuclei were labeled with DAPI (blue), scale bar=10μm.

(D) Quantification of the percentage of calbindin^{+} cells with pan-nuclear 53bp1. Mean±SEM, unpaired t-test, 157-224 cells/mouse, 4 mice/genotype. *Htt*$^{+/+}$: 89.73±4.48%, *Htt*$^{\Delta E1/\Delta E1}$: 97.56±1.01%, p=0.1390.

(E) Quantification of the percentage of calbindin^{+} cells with γH2AX puncta. Mean±SEM, unpaired t-test, 157-224 cells/mouse, 4 mice/genotype. *Htt*$^{+/+}$: 3.69±1.78%, *Htt*$^{\Delta E1/\Delta E1}$: 10.37±2.74%, p=0.0870.

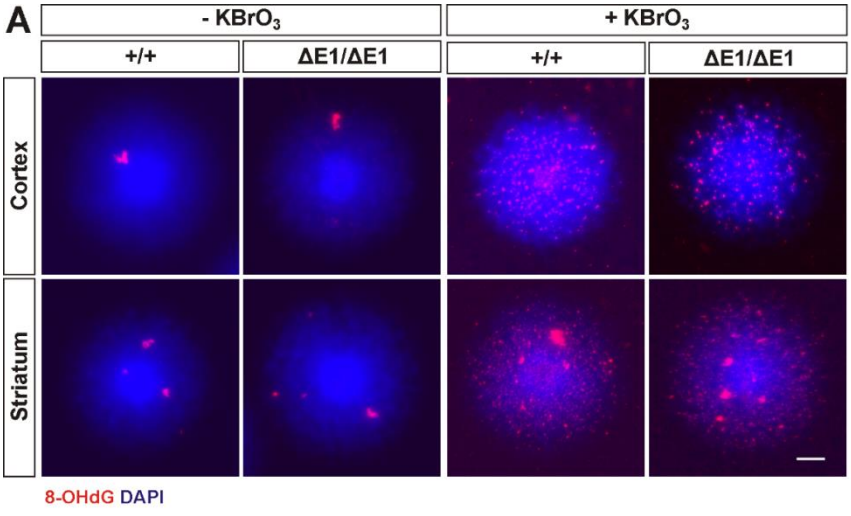
A
- KBrO3
+ KBrO3
+/+
ΔE1/ΔE1
+/+
ΔE1/ΔE1
Cortex
Striatum
8-OHdG DAPI

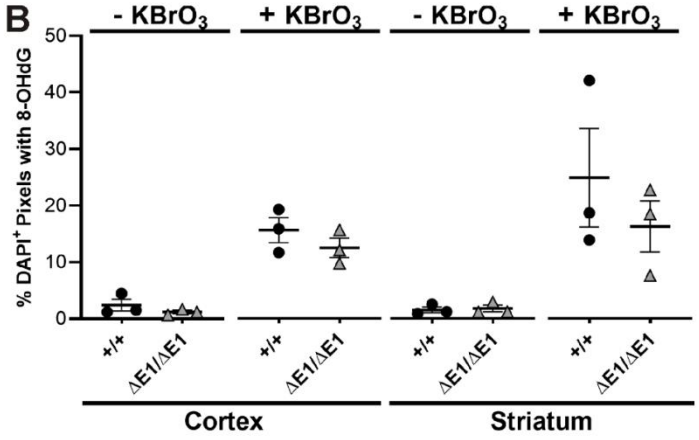
B
- KBrO3
+ KBrO3
- KBrO3
+ KBrO3
% DAPI+ Pixels with 8-OHdG
50
40
30
20
10
0
+/+
ΔE1/ΔE1
+/+
ΔE1/ΔE1
+/+
ΔE1/ΔE1
+/+
ΔE1/ΔE1
Cortex
Striatum

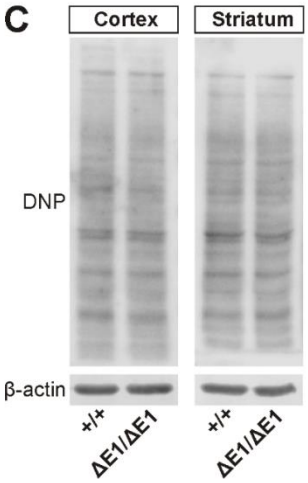
C
Cortex
Striatum
DNP
β-actin
+/+
ΔE1/ΔE1
+/+
ΔE1/ΔE1

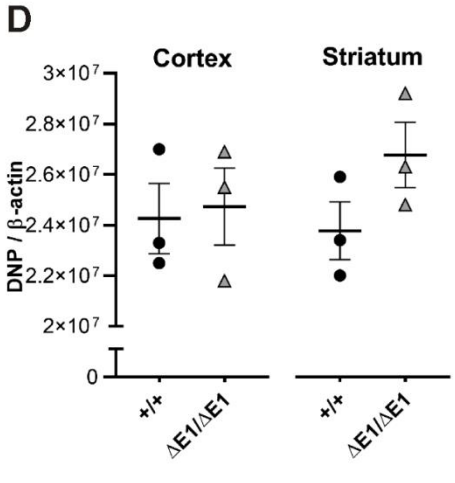
D
Cortex
Striatum
3×10^7
2.8×10^7
2.6×10^7
2.4×10^7
2.2×10^7
2×10^7
0
DNP / β-actin
+/+
ΔE1/ΔE1
+/+
ΔE1/ΔE1

Fig. 3-15: DNA and protein oxidation markers are not significantly altered in *Htt*$^{\Delta E1/\Delta E1}$ mice at 3 months of age. (A) Nuclei isolated from the cortex and striatum of 3-month-old *Htt*$^{\Delta E1/\Delta E1}$ (ΔE1/ΔE1) and *Htt*$^{+/+}$ (+/+) mice with or without $KBrO_3$ treatment and immunostained with an 8-OHdG antibody (red). Nuclei were labeled with DAPI (blue), scale bar = 10μm.

(B) Quantification of the percentage of DAPI$^+$ pixels that are 8-OHdG$^+$. Mean±SEM, unpaired t-test, 19-20 images/mouse, 3 mice/genotype. Cortex: without $KBrO_3$: *Htt*$^{+/+}$: 2.40±1.04%, *Htt*$^{\Delta E1/\Delta E1}$: 1.17±0.29%, p=0.3229; with $KBrO_3$: *Htt*$^{+/+}$: 15.64±2.20%, *Htt*$^{\Delta E1/\Delta E1}$: 12.51±1.72%, p=0.3247; striatum: without $KBrO_3$: *Htt*$^{+/+}$: 1.57±0.51%, *Htt*$^{\Delta E1/\Delta E1}$: 1.81±0.59%, p=0.7717; with $KBrO_3$: *Htt*$^{+/+}$: 24.90±8.72%, *Htt*$^{\Delta E1/\Delta E1}$: 16.27±4.51%, p=0.4285.

(C) Western blots of cortical and striatal lysates probed with a DNP antibody to evaluate protein carbonyl levels.

(D) Protein carbonyl levels were quantified and normalized to β-actin. Mean±SEM, unpaired t-test, 3 mice/genotype. Cortex: *Htt*$^{+/+}$: $2.43x10^7$±$1.39x10^6$, *Htt*$^{\Delta E1/\Delta E1}$: $2.47x10^7$±$1.52x10^6$, p=0.8317; striatum: *Htt*$^{+/+}$: $2.38x10^7$±$1.14x10^6$, *Htt*$^{\Delta E1/\Delta E1}$: $2.68x10^7$±$1.29x10^6$, p=0.1566.

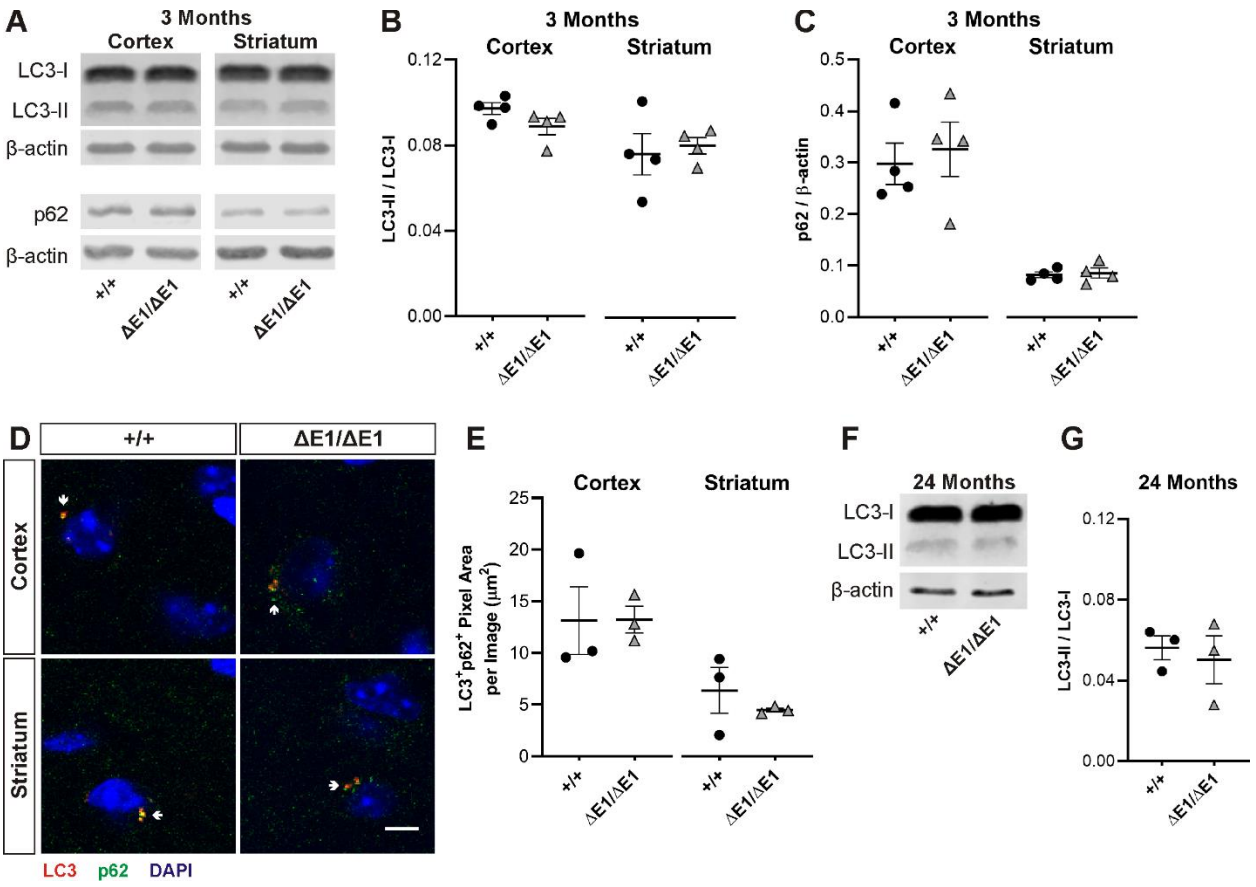

Fig. 3-16: Autophagy markers are not altered in *Htt*$^{\Delta E1/\Delta E1}$ mice. (A) Western blots of cortical and striatal total microsomal fractions from 3-month-old *Htt*$^{+/+}$ (+/+) and *Htt*$^{\Delta E1/\Delta E1}$ (ΔE1/ΔE1) mice probed with LC3 and p62/SQSTM1 (p62) antibodies.

(B) LC3-II fluorescence levels in (A) were quantified and normalized to LC3-I. Mean±SEM, unpaired t-test, 4 mice/genotype. Cortex: *Htt*$^{+/+}$: 0.097±0.003, *Htt*$^{\Delta E1/\Delta E1}$: 0.089±0.004, p=0.1245; striatum: *Htt*$^{+/+}$: 0.076±0.010, *Htt*$^{\Delta E1/\Delta E1}$: 0.080±0.004; p=0.7160.

(C) p62 fluorescence levels in (A) were quantified and normalized to β-actin. Mean±SEM, unpaired t-test, 4 mice/genotype. Cortex: *Htt*$^{+/+}$: 0.298±0.040, *Htt*$^{\Delta E1/\Delta E1}$: 0.326±0.053, p=0.6860; striatum: *Htt*$^{+/+}$: 0.082±0.006, *Htt*$^{\Delta E1/\Delta E1}$: 0.086±0.010, p=0.7449.

(D) Cortex and striatum from 3-month-old *Htt*$^{+/+}$ and *Htt*$^{\Delta E1/\Delta E1}$ mice immunostained with LC3 (red) and p62 (green) antibodies. Nuclei were labeled with DAPI (blue), scale bar=5 μm. White arrows indicate LC3^{+}p62^{+} puncta.

(E) Quantification of the LC3^{+}p62^{+} pixel area per image. Mean±SEM, unpaired t-test, 3 mice/genotype. Cortex: *Htt*$^{+/+}$: 13.13±3.26 μm, *Htt*$^{\Delta E1/\Delta E1}$: 13.22±1.29 μm, p=0.9808; striatum: *Htt*$^{+/+}$: 6.37±2.22 μm, *Htt*$^{\Delta E1/\Delta E1}$: 4.47±0.19 μm, p=0.4419.

(F) Western blots of whole-brain microsomal lysates from 24-month-old *Htt*$^{+/+}$ and *Htt*$^{\Delta E1/\Delta E1}$ mice probed with an LC3 antibody.

(G) LC3-II fluorescence levels in (F) were quantified and normalized to LC3-I. Mean±SEM, unpaired t-test, 3 mice/genotype. *Htt*$^{+/+}$: 0.056±0.006, *Htt*$^{\Delta E1/\Delta E1}$: 0.050±0.012, p=0.6772.

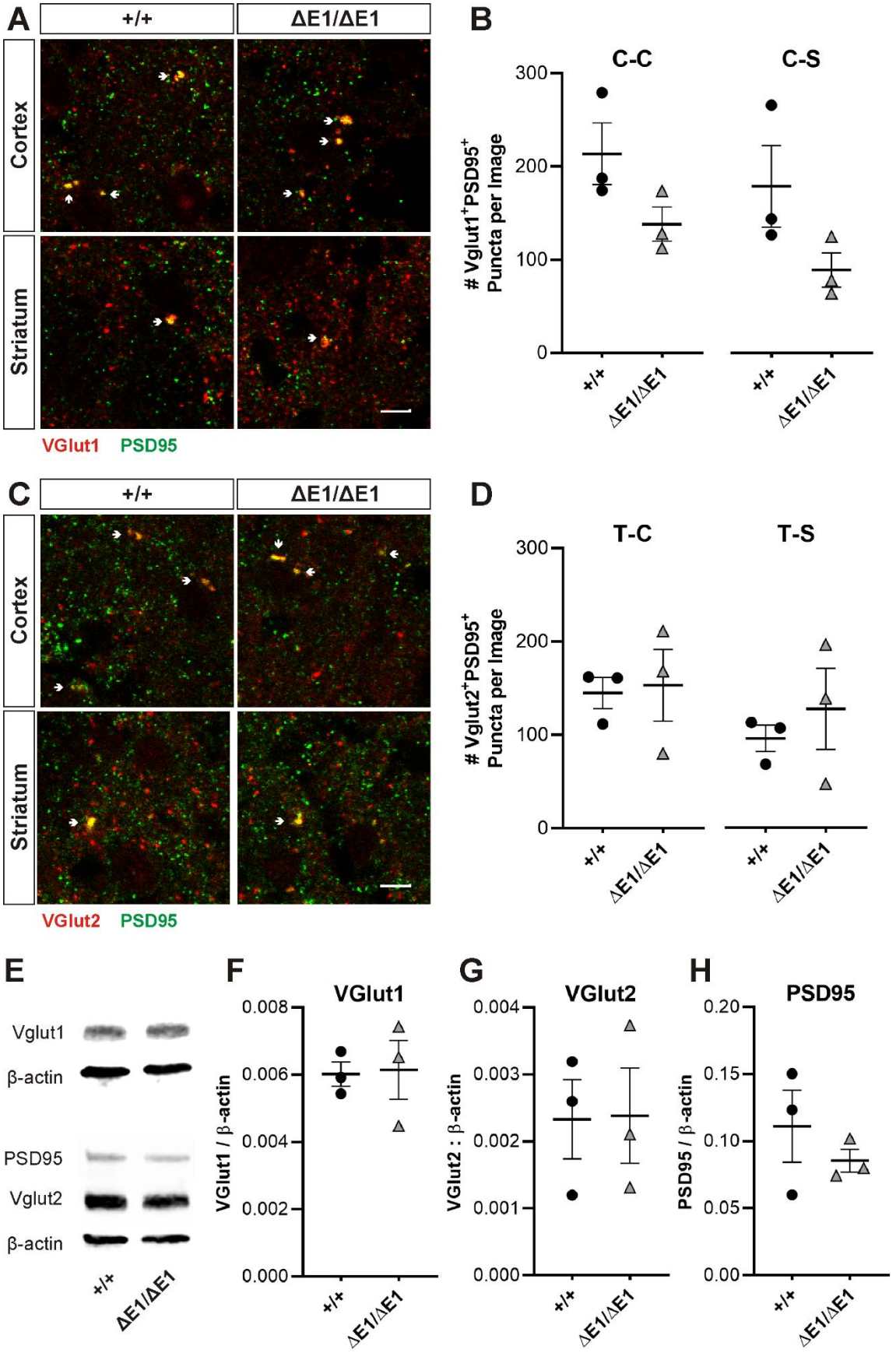
A
+/+
ΔE1/ΔE1
Cortex
Striatum
VGlut1 PSD95
B
C-C
C-S
Vglut1+PSD95+ Puncta per Image
300
200
100
0
+/+
ΔE1/ΔE1
C
+/+
ΔE1/ΔE1
Cortex
Striatum
VGlut2 PSD95
D
T-C
T-S
Vglut2+PSD95+ Puncta per Image
300
200
100
0
+/+
ΔE1/ΔE1
E
Vglut1
β-actin
PSD95
Vglut2
β-actin
+/+
ΔE1/ΔE1
F
VGlut1
VGlut1 / β-actin
0.008
0.006
0.004
0.002
0.000
+/+
ΔE1/ΔE1
G
VGlut2
VGlut2 : β-actin
0.004
0.003
0.002
0.001
0.000
+/+
ΔE1/ΔE1
H
PSD95
PSD95 / β-actin
0.20
0.15
0.10
0.05
0.00
+/+
ΔE1/ΔE1

Fig. 3-17: Synapse numbers are not altered in *Htt*$^{\Delta E1/\Delta E1}$ mice at 18 months of age.

(A) Cortex and striatum from 18-month-old *Htt*$^{+/+}$ (+/+) and *Htt*$^{\Delta E1/\Delta E1}$ (ΔE1/ΔE1) mice immunostained with VGlut1 (red) and PSD95 (green) antibodies, scale bar=5 μm. White arrows indicate Vglut1^{+}PSD95^{+} puncta.

(B) Quantification of the number of VGlut1^{+}PSD95^{+} puncta per image. Mean±SEM, unpaired t-test, 3 mice/genotype. Corticocortical (C-C): *Htt*$^{+/+}$: 213.7±33.1, *Htt*$^{\Delta E1/\Delta E1}$: 138.2±18.4, p=0.1167; corticostriatal (C-S): *Htt*$^{+/+}$: 178.8±43.8, *Htt*$^{\Delta E1/\Delta E1}$: 89.0±18.4, p=0.1316.

(C) Cortex and striatum from 18-month-old *Htt*$^{+/+}$ and *Htt*$^{\Delta E1/\Delta E1}$ mice immunostained with VGlut2 (red) and PSD95 (green) antibodies, scale bar=5 μm. White arrows indicate Vglut2^{+}PSD95^{+} puncta.

(D) Quantification of the number of VGlut2^{+}PSD95^{+} puncta per image. Mean±SEM, unpaired t-test, 3 mice/genotype. Thalamocortical (T-C): *Htt*$^{+/+}$: 144.8±16.6, *Htt*$^{\Delta E1/\Delta E1}$: 153.1±38.6, p=0.8524; thalamostriatal (T-S): *Htt*$^{+/+}$: 96.2±14.0, *Htt*$^{\Delta E1/\Delta E1}$: 127.6±43.5, p=0.5292.

(E) Western blots of whole-brain total microsomal lysates from 24-month-old *Htt*$^{+/+}$ and *Htt*$^{\Delta E1/\Delta E1}$ mice probed with Vglut1, VGlut2, and PSD95 antibodies.

Fluorescence levels of (F) Vglut1, (G) Vglut2, and (H) PSD95 were quantified and normalized to β-actin. Mean±SEM, unpaired t-test, 3 mice/genotype. Vglut1: *Htt*$^{+/+}$: 0.0060±0.0004, *Htt*$^{\Delta E1/\Delta E1}$: 0.0061±0.0009, p=0.8974; Vglut2: *Htt*$^{+/+}$: 0.0023±0.0006, *Htt*$^{\Delta E1/\Delta E1}$: 0.0024±0.0007, p=0.9565; PSD95: *Htt*$^{+/+}$: 0.111±0.027, *Htt*$^{\Delta E1/\Delta E1}$: 0.085±0.008, p=0.4111.

Chapter IV: Characterization of normal *Htt* N-terminal deletion alleles expressed in trans with a mutant *Htt* allele

Introduction

Deletion of Htt's three N-terminal domains in homozygosity results in only modest phenotypes. However, because loss of normal Htt function is likely to contribute to HD pathogenesis and the Htt N-terminus may be able to respond to cellular stress, these domains may modulate Htt's ability to perform its normal functions in an HD model and affect disease progression. To examine this possibility, the $Htt^{\Delta E1}$ allele was crossed into a knock-in HD mouse model expressing a mutant *Htt* allele with 140 CAG repeats ($Htt^{140Q/\Delta E1}$), and the progression of HD model phenotypes was compared to wild type controls ($Htt^{+/+}$), a heterozygous HD mouse model ($Htt^{140Q/+}$), and a hemizygous HD mouse model ($Htt^{140Q/-}$). The $Htt^{140Q/+}$ model has been well characterized and exhibits progressive motor dysfunction including an early phase of hyperactivity at 1 month of age followed by hypoactivity at 4 months of age, and gait abnormalities at 12 months of age [120]. HD model mice with in trans deletions of either the N17 domain ($Htt^{140Q/\Delta N17}$), the polyQ domain, ($Htt^{140Q/\Delta Q}$) or both the polyQ and PRR domains of Htt ($Htt^{140Q/\Delta QP}$) exhibit altered behavioral phenotypes compared to $Htt^{140Q/+}$ mice [8, 121]. On the accelerating rotarod test, $Htt^{140Q/\Delta QP}$ and $Htt^{140Q/\Delta N17}$ mice were impaired compared to $Htt^{140Q/+}$ mice, and were also more hypoactive compared than the $Htt^{140Q/+}$ mice in the open field test [121]. However, both $Htt^{140Q/\Delta QP}$ and $Htt^{140Q/\Delta N17}$ mice exhibited improved spatial learning and memory in the Morris water maze compared to $Htt^{140Q/+}$ mice, who have reduced spatial learning and memory performance compared to $Htt^{+/+}$ mice [121]. Similarly, $Htt^{140Q/\Delta Q}$ mice exhibit improved rotarod and Barnes maze performance

compared to *Htt*$^{140Q/+}$ mice, and do not display a hypoactivity phenotype [8]. The effect of removing all three domains in the context of an HD model, however, is unknown.

Mutant Htt inclusions are first detectable in *Htt*$^{140Q/+}$ mice starting at 4 months of age in the striatum, nucleus accumbens, and olfactory tubercle [120]. As the mouse ages, mutant Htt aggregates can also be found in the cortex and globus pallidus [120]. Deletion of the normal Htt polyQ domain in trans to an *Htt*^{140Q} allele results in a reduced aggregate burden, suggesting that the *Htt* allele in trans to the *Htt*^{140Q} allele can affect aggregation kinetics, possibly by increasing mHtt clearance [8]. Deletion of the PRR in cis to an *Htt*^{140Q} allele also reduces aggregate burden, suggesting that the polyQ flanking domains are able to influence aggregation within the *Htt*^{140Q} model [122]. In addition to aggregation kinetics, cellular functions that are both influenced by the Htt N-terminal domains and affected in HD, such as synapse numbers and autophagy, may be altered in *Htt* N-terminal deletion HD model mice. Glutamatergic synapse number and function are altered in HD models [71, 73, 76], and deletion of Htt's N17 domain in homozygosity causes a reduction in thalamostriatal glutamatergic synapses in aged mice [4]. Autophagy is impaired in HD [82], but deletion of the polyQ domain in trans to an *Htt*^{140Q} allele increases the levels of autophagy markers observed in mouse brains [8]. However, autophagy is also impaired in primary neuronal cultures from both *Htt*$^{140Q/\Delta QP}$ and *Htt*$^{140Q/\Delta N17}$ mice [121]. Because deletions of individual domains within Htt's N-terminus do not consistently affect HD phenotype progression, characterizing the deletion of the entire region is a necessary step in determining how these domains function together in vivo.

Through longitudinal behavioral analysis of *Htt*$^{140Q/\Delta E1}$ mice and analysis of Htt subcellular localization, autophagy markers, and synapse markers in *Htt*$^{140Q/\Delta E1}$, *Htt*$^{140Q/\Delta QP}$, and *Htt*$^{140Q/\Delta N17}$ mice, I have further characterized the role of the Htt N-terminus in modulating HD mouse model phenotypes. I have found that expression of the Htt exon 1 N-terminal deletion allele delays the onset of some motor deficits, but not the spatial learning and memory deficits observed in HD model mice, suggesting that deletion of the Htt N-terminus may result in a delay in some aspects of HD mouse model pathogenesis. Autophagy markers, however, remain unaltered in *Htt*$^{140Q/\Delta E1}$, *Htt*$^{140Q/\Delta QP}$, and *Htt*$^{140Q/\Delta N17}$ mice, synaptic markers are only modestly altered in *Htt*$^{140Q/\Delta E1}$ mice, and Htt's subcellular localization is not altered in *Htt*$^{140Q/\Delta E1}$, *Htt*$^{140Q/\Delta Q}$, *Htt*$^{140Q/\Delta QP}$, or *Htt*$^{140Q/\Delta N17}$ mice.

Results

Htt$^{140Q/\Delta E1}$ *mice exhibit normal lifespans and body weight through 19 months of age*

Htt$^{140Q/+}$, *Htt*$^{140Q/\Delta E1}$, and *Htt*$^{140Q/-}$ male mice survive through 19 months of age (Table 4-1). At 3 and 6 months of age, the body weight (Fig. 4-1) of *Htt*$^{140Q/-}$ mice is reduced compared to *Htt*$^{140Q/+}$ (3 months: p =0.0017, 6 months: p =0.0195, Tukey's multiple comparison test), *Htt*$^{140Q/\Delta E1}$ (3 months: p =0.0003, 6 months: p =0.0016, Tukey's multiple comparison test), and *Htt*$^{+/+}$ (3 months: p =0.0071, 6 months: p =0.0006, Tukey's multiple comparison test) mice (Fig. 4-1). The body weight of *Htt*$^{140Q/-}$ mice is also reduced at 12 and 18 months of age compared to *Htt*$^{+/+}$ (12 months: p =0.0004, 18 months: p =0.0008, Tukey's multiple comparison test) and *Htt*$^{140Q/\Delta E1}$ (12 months: p =0.0368, 18 months: p =0.0097, Tukey's multiple comparison test) mice.

Additionally, the body weight of *Htt*$^{140Q/+}$ mice is significantly reduced compared to *Htt*$^{+/+}$ mice at 18 months of age (p =0.0464, Tukey's multiple comparison test).

Deletion of the Htt N-terminus does not affect Htt subcellular localization in HD model mice.

To determine whether deletion of the Htt N-terminus affects Htt's subcellular distribution in the context of an HD model, whole brain lysates from 6-month-old *Htt*$^{+/+}$, *Htt*$^{140Q/\Delta E1}$, *Htt*$^{140Q/+}$, and *Htt*$^{140Q/-}$ mice were separated into microsomal, cytosolic, and nuclear fractions and analyzed by western blotting (Fig. 4-2). There were no differences in the levels of cytosolic (C), nuclear (N), or total microsomal (M) WT-Htt and ΔE1-Htt from the *Htt*$^{140Q/+}$ and *Htt*$^{140Q/\Delta E1}$ mice (WT-Htt C: ~35%, N: ~52%, M: ~56%, ΔE1-Htt: C: ~31%, N: ~70%, M: ~40% compared to *Htt*$^{+/+}$ levels). Additionally, no differences in the levels of cytosolic, nuclear, or total microsomal 140Q-Htt from *Htt*$^{140Q/\Delta E1}$, *Htt*$^{140Q/+}$, and *Htt*$^{140Q/-}$ mice was observed. Lysates from 6-month-old *Htt*$^{140Q/+}$, *Htt*$^{140Q/\Delta Q}$, *Htt*$^{140Q/\Delta QP}$, and *Htt*$^{140Q/\Delta N17}$ mice were separated into microsomal, cytosolic, and nuclear fractions, and analyzed by western blotting (Fig. 4-3), and no differences were observed in the levels of WT-Htt, ΔQ-Htt, ΔQP-Htt, or ΔN17-Htt in any of the fractions, or in the levels of 140Q-Htt between genotypes in any of the fractions.

Characterization of motor phenotypes in Htt$^{140Q/\Delta E1}$ *mice.*

To investigate whether *Htt*$^{\Delta E1}$ expressed in trans to an HD model allele influences the progression of HD mouse model motor and cognitive phenotypes, male *Htt*$^{+/+}$, *Htt*$^{140Q/\Delta E1}$, *Htt*$^{140Q/+}$, and *Htt*$^{140Q/-}$ mice (see Table 4-1 for the number of animals used at each experimental time point) were subjected to longitudinal activity cage (Fig. 4-4, 4-5,

4-6), forelimb grip strength (Fig. 4-7), accelerating rotarod (Fig. 4-8), and Morris water maze testing (Fig. 4-9). At 3 months of age, $Htt^{140Q/\Delta E1}$ mice traveled a further total distance in the activity cage (Fig. 4-4) in comparison to $Htt^{140Q/-}$ mice (p=0.0438, Tukey's multiple comparison test). At 6, 12, and 18 months of age, $Htt^{140Q/+}$ (6 months: p=0.0001; 12 months: p<0.0001, 18 months: p=0.0093, Tukey's multiple comparison test), $Htt^{140Q/\Delta E1}$ (6 months: p=0.0057; 12 months: p<0.0001, 18 months: p<0.0001, Tukey's multiple comparison test), and $Htt^{140Q/-}$ mice (6 months: p=0.0003; 12 months: p<0.0001, 18 months: p=0.0027, Tukey's multiple comparison test) all traveled less than $Htt^{+/+}$ mice. $Htt^{140Q/+}$ and $Htt^{140Q/-}$ mice have reduced horizontal activity (Fig. 4-5) compared to $Htt^{+/+}$ ($Htt^{140Q/+}$: p =0.0467, $Htt^{140Q/-}$: p =0.0124, Tukey's multiple comparison test) and $Htt^{140Q/\Delta E1}$ ($Htt^{140Q/+}$: p =0.0316, $Htt^{140Q/-}$: p =0.0079, Tukey's multiple comparison test) mice at 3 months of age. By 6 months of age, the horizontal activity of $Htt^{140Q/\Delta E1}$ mice is not significantly different from either the $Htt^{140Q/+}$, $Htt^{140Q/-}$, or $Htt^{+/+}$ mice, however $Htt^{140Q/+}$ and $Htt^{140Q/-}$ mice still exhibit reduced horizontal activity compared to $Htt^{+/+}$ ($Htt^{140Q/+}$: p =0.0.0067, $Htt^{140Q/-}$: p =0.0002, Tukey's multiple comparison test). At 12 and 18 months of age, $Htt^{140Q/\Delta E1}$ mice also exhibit reduced horizontal activity levels compared to $Htt^{+/+}$ mice (p <0.0001, Tukey's multiple comparison test) and are indistinguishable from $Htt^{140Q/+}$ (p <0.0001, Tukey's multiple comparison test) and $Htt^{140Q/-}$ (p <0.0001, Tukey's multiple comparison test) mice. There were no differences in vertical activity levels (Fig, 4-6) at 3 or 6 months of age. At 12 months of age, $Htt^{140Q/+}$ (p<0.0001, Tukey's multiple comparison test), $Htt^{140Q/\Delta E1}$ (p=0.0002, Tukey's multiple comparison test), and $Htt^{140Q/-}$ mice (p=0.0013, Tukey's multiple comparison test) all exhibited reduced vertical activity levels compared to $Htt^{+/+}$ mice. At 18 months of age, $Htt^{140Q/\Delta E1}$ mice exhibited reduced levels of vertical activity compared to $Htt^{+/+}$ mice (p=0.0023, Tukey's multiple comparison test).

There are no differences in forelimb grip strength (Fig. 4-7) at 3 months of age. $Htt^{140Q/-}$ mice exhibit reduced forelimb grip strength at 6 months of age compared to $Htt^{+/+}$ mice (p =0.0129, Tukey's multiple comparison test). At 12 months of age, $Htt^{140Q/-}$ (p =0.0002, Tukey's multiple comparison test) and $Htt^{140Q/+}$ mice (p =0.0035, Tukey's multiple comparison test) exhibit reduced grip strength compared to $Htt^{140Q/\Delta E1}$ and $Htt^{+/+}$ mice. By 18 months of age, the forelimb grip strength of $Htt^{140Q/-}$ (p <0.0001, Tukey's multiple comparison test), $Htt^{140Q/+}$ (p =0.0230, Tukey's multiple comparison test), and $Htt^{140Q/\Delta E1}$ mice (p =0.0388, Tukey's multiple comparison test) is reduced compared to $Htt^{+/+}$ mice.

The $Htt^{\Delta E1}$ allele does not significantly alter rotarod performance in HD model mice (Fig. 4-8), although $Htt^{140Q/-}$ mice outperform $Htt^{140Q/+}$ and $Htt^{140Q/\Delta E1}$ mice at 6 ($Htt^{140Q/+}$: p = 0.0167, F=6.263, D_F =1, $Htt^{140Q/\Delta E1}$: p =0.0274, F=5.265, D_F =1 , 2-way ANOVA) and 12 months of age ($Htt^{140Q/+}$: p = 0.0.260, F=5.364, D_F =1, $Htt^{140Q/\Delta E1}$: p =0.0140, F=6.634, D_F =1 , 2-way ANOVA), and continue to outperform $Htt^{140Q/+}$ mice at 18 months of age (p =0.0323, F=4.946, D_F =1, 2-way ANOVA). At 18 months of age $Htt^{140Q/+}$ mice also exhibit a rotarod deficit compared to $Htt^{+/+}$ mice (p =0.0318, F=5.015, D_F =1, 2-way ANOVA).

Deletion of the Htt N-terminus does not affect spatial learning and memory performance in HD model mice.

While HD model mice display spatial learning and memory deficits compared to wild type mice in the Morris water maze test, deletion of the N-terminal domains of normal Htt does not affect performance at 10, 14, or 19 months of age (Fig. 4-9). At 10 months of age, $Htt^{140Q/+}$ (p <0.0001, F=26.70, D_F =1, 2-way ANOVA) $Htt^{140Q/\Delta E1}$

(p<0.0001, F=42.8, D_F =1, 2-way ANOVA), and $Htt^{140Q/-}$ (p <0.0001, F=25.96, D_F =1, 2-way ANOVA) mice all exhibited a deficit compared to $Htt^{+/+}$ mice in the reversal phase of the Morris water maze test. $Htt^{140Q/+}$ (p =0.0048, Tukey's multiple comparison test) and $Htt^{140Q/\Delta E1}$ (p =0.0018, Tukey's multiple comparison test) mice also spent less time in the platform quadrant during the probe trial than $Htt^{+/+}$ mice. However, $Htt^{140Q/+}$ (visible platform trial: p =0.0251, velocity: p =0.0007, Tukey's multiple comparison test) and $Htt^{140Q/\Delta E1}$ (visible platform trial: p =0.0217, velocity: p =0.0020, Tukey's multiple comparison test) mice exhibit deficits in the visible control trial and reduced velocity during the probe trial compared to $Htt^{+/+}$ mice. $Htt^{140Q/+}$ mice also swam significantly more slowly than $Htt^{140Q/-}$ mice (p =0.0348, Tukey's multiple comparison test), which may be a confounding factor when interpreting their Morris water maze performance. No significant differences between genotypes in any of the measurements recorded were observed at 14 months of age. $Htt^{140Q/+}$ (p =0.0015, F=11.84, D_F =1, 2-way ANOVA) $Htt^{140Q/\Delta E1}$ (p =0.0001, F=19.18, D_F =1, 2-way ANOVA), and $Htt^{140Q/-}$ (p =0.0001, F=18.53, D_F =1, 2-way ANOVA) mice all exhibited a deficit compared to $Htt^{+/+}$ mice during the acquisition phase at 19 months of age. $Htt^{140Q/\Delta E1}$ mice additionally exhibit reduced velocity compared to $Htt^{+/+}$ mice during the probe trial at 19 months of age (p =0.0008, Tukey's multiple comparison test). No other differences were observed.

Analyses of glutamatergic synaptic markers in $Htt^{140Q/+}$, $Htt^{140Q/\Delta QP}$, $Htt^{140Q/\Delta N17}$ and $Htt^{140Q/\Delta E1}$ mice

To determine whether there is a generalized reduction in glutamatergic synapses in Htt N-terminal deletion HD model mice, whole brain total microsomal fractions were analyzed by western blotting for the glutamatergic synapse markers PSD95, Vglut1, and

Vglut2 at 6 months of age in *Htt*$^{140Q/+}$, *Htt*$^{140Q/\Delta Q}$, *Htt*$^{140Q/\Delta QP}$, and *Htt*$^{140Q/\Delta N17}$ mice, and at 6 and 24 months of age in *Htt*$^{+/+}$, *Htt*$^{140Q/+}$, *Htt*$^{140Q/\Delta E1}$, and *Htt*$^{140Q/-}$ mice. At 6 months of age, PSD95 levels (Fig. 4-10A) were significantly reduced in the brains of *Htt*$^{140Q/+}$ and *Htt*$^{140Q/-}$ mice compared to *Htt*$^{+/+}$ mice (*Htt*$^{140Q/+}$: p=0.0419, *Htt*$^{140Q/-}$: p=0.0111, Tukey's multiple comparisons test), and reduced in *Htt*$^{140Q/-}$ mice compared to *Htt*$^{140Q/\Delta E1}$ (p=0.0139, Tukey's multiple comparisons test). Additionally, there was a trend toward a reduction in PSD95 levels in the brains of *Htt*$^{140Q/+}$ mice compared to *Htt*$^{140Q/\Delta E1}$ (p=0.0533, Tukey's multiple comparisons test). PSD95 contains an SH3 domain that can bind to the PRR within the Htt N-terminus [74]. Therefore, it is possible that the Htt N-terminus may regulate the localization of PSD95. To determine whether microsomal PSD95 levels were reduced in the *Htt*$^{140Q/+}$ and *Htt*$^{140Q/-}$ mice or whether PSD95 was mislocalized, cytosolic fractions from 6-month-old *Htt*$^{+/+}$, *Htt*$^{140Q/+}$, *Htt*$^{140Q/\Delta E1}$, and *Htt*$^{140Q/-}$ mice were also analyzed by western blotting for PSD95 levels (Fig. 4-10B). Very little PSD95 was detected in the cytosol, and there were no differences between genotypes. Therefore, the difference in microsomal PSD95 levels is likely due to a difference in PSD95 levels and not a difference in PSD95 subcellular localization. At 12 months of age (Fig. 4-10 C) there was a significant decrease in the levels of PSD95 in *Htt*$^{140Q/\Delta E1}$ mice compared to *Htt*$^{+/+}$ mice (p=0.0254, Tukey's multiple comparisons test). No differences in PSD95 levels were detected at 24 months of age (Fig. 4-10D), and no differences in Vglut1 or Vglut2 levels were detected at 6 or 24 months of age (Fig. 4-11). No differences in Vglut1, Vglut2, or PSD95 levels at 6 months of age were detected in *Htt*$^{140Q/+}$, *Htt*$^{140Q/\Delta Q}$, *Htt*$^{140Q/\Delta QP}$, and *Htt*$^{140Q/\Delta N17}$ mice (Fig. 4-12).

Autophagy markers are not altered in the brains of $Htt^{140Q/+}$, $Htt^{140Q/\Delta QP}$, $Htt^{140Q/\Delta N17}$ or $Htt^{140Q/\Delta E1}$ mice

Levels of LC3-II and p62 were evaluated in whole brain total microsomal fractions from 6-month-old $Htt^{+/+}$, $Htt^{140Q/+}$, $Htt^{140Q/\Delta E1}$, and $Htt^{140Q/-}$ mice (Fig. 4-13A, 4-13B) and 6- and 12-month-old $Htt^{+/+}$, $Htt^{140Q/+}$, $Htt^{140Q/\Delta QP}$, and $Htt^{140Q/\Delta N17}$ mice (Fig. 4-14) by western blotting. LC3-II levels were also evaluated in whole brain total microsomal fractions from 24-month-old $Htt^{+/+}$, $Htt^{140Q/+}$, $Htt^{140Q/\Delta E1}$, and $Htt^{140Q/-}$ mice (Fig. 4-13C). There were no differences between genotypes in the ratio of total microsomal LC3-II to LC3-I or in the levels of total microsomal p62 at either 6, 12, or 24 months of age.

Discussion

Although $Htt^{140Q/+}$, $Htt^{140Q/\Delta E1}$, and $Htt^{140Q/-}$ mice exhibit normal lifespans through 19 months of age, the body weight of $Htt^{140Q/-}$ mice is reduced throughout their adult lifespan, and $Htt^{140Q/+}$ mice exhibit a reduced body weight at 18 months of age compared to $Htt^{+/+}$ mice. This data is consistent with prior work showing that Htt levels correlate with body weight in mice [60], and that HD patients exhibit reduced body weight with disease progression [19]. The body weight of the $Htt^{140Q/\Delta E1}$ mice was not changed compared to $Htt^{+/+}$ mice even at 18 months of age, suggesting that HD-related body weight reduction is delayed or rescued in $Htt^{140Q/\Delta E1}$ mice. Similarly, the horizontal activity levels of $Htt^{140Q/\Delta E1}$ mice was reduced compared to $Htt^{+/+}$ mice starting at 12 months of age, while it was reduced in $Htt^{140Q/+}$ and $Htt^{140Q/-}$ mice at 3 months of age. Forelimb grip strength was reduced in $Htt^{140Q/\Delta E1}$ mice at 18 months of age, in $Htt^{140Q/+}$ mice at 12 months of age, and in $Htt^{140Q/-}$ mice at 6 months of age. Taken together, this data suggests that expression of the $Htt^{\Delta E1}$ allele in an HD model may delay some HD motor

phenotypes. However, expression of the *Htt*$^{\Delta E1}$ allele does not affect all motor functions impacted by HD. While HD models exhibited reductions in the total distance traveled and vertical activity during activity monitoring and altered rotarod performance, expression of the *Htt*$^{/\Delta E1}$ allele did not cause a delay in the onset of deficits in these tests.

Spatial learning and memory performance in HD model mice was not affected by expression of the *Htt*$^{\Delta E1}$ allele. This result was surprising considering the improvement in spatial learning and memory performance demonstrated by the *Htt*$^{140Q/\Delta Q}$, *Htt*$^{140Q/\Delta QP}$, and *Htt*$^{140Q/\Delta N17}$ mice [8, 121]. However, similar to the *Htt*$^{\Delta Q/\Delta Q}$, *Htt*$^{\Delta QP/\Delta QP}$, and *Htt*$^{\Delta N17/\Delta N17}$ mice, the *Htt*$^{140Q/\Delta Q}$, *Htt*$^{140Q/\Delta QP}$, and *Htt*$^{140Q/\Delta N17}$ mice were tested on a mixed 129Sv x C57BL/6J genetic background [4, 5, 8, 121], while the *Htt*$^{140Q/\Delta E1}$ mice were tested on a C57BL/6J congenic genetic background, and therefore direct comparisons between genotypes may be difficult.

Htt$^{140Q/+}$ and *Htt*$^{140Q/-}$ mice exhibit a reduction in PSD95 levels that is not observed in *Htt*$^{140Q/\Delta E1}$ mice at 6 months of age. However, no differences in the levels of Vglut1 or Vglut2 were observed between genotypes, suggesting that the alteration in PSD95 levels may represent a change in the composition of the post-synaptic density rather than an alteration in synapse number. At 12 months of age, however, only *Htt*$^{140Q/\Delta E1}$ mice exhibit reduced levels of PSD95 compared to *Htt*$^{+/+}$ controls, and by 24 months of age there are no differences in the levels of PSD95 between genotypes. This phenotype may represent either an increase in PSD95 levels in the HD model mice with age or a decrease in PSD95 levels in the control mice with age. However, the variability in PSD95 levels between mice of the same genotype also increased with age, especially

in the *Htt*$^{+/+}$ control mice. A larger sample size may therefore be needed to detect any significant differences in PSD95 levels in aged mice.

Although autophagosome formation is decreased in primary neuronal cultures from *Htt*$^{140Q/\Delta QP}$ and *Htt*$^{140Q/\Delta N17}$ mice [121], no differences in LC3-II levels were observed by western blotting between *Htt*$^{140Q/+}$, *Htt*$^{140Q/\Delta QP}$, and *Htt*$^{140Q/\Delta N17}$ mice or between *Htt*$^{140Q/+}$, *Htt*$^{140Q/\Delta E1}$, and *Htt*$^{140Q/-}$ mice. Additionally, the significant increase in p62 levels in primary neuronal cultures from *Htt*$^{140Q/\Delta N17}$ mice [121] was not replicated in the brains of *Htt*$^{140Q/\Delta N17}$ mice. Because p62 is able to respond to a wide variety of cellular stressors (for review, see [123]), the increase in p62 observed in *Htt*$^{140Q/\Delta N17}$ neuronal cultures may represent an altered response to cellular stress in vitro that is not present in vivo. Whether primary neuronal cultures from *Htt*$^{140Q/\Delta E1}$ mice would exhibit similar autophagosome formation deficits and elevated p62 levels is not known.

While *Htt*$^{140Q/\Delta E1}$ mice exhibit a delay in the onset of some HD motor phenotypes, the cause is unclear. Based on the levels of PSD95 in the brains of *Htt*$^{140Q/+}$, *Htt*$^{140Q/\Delta E1}$, and *Htt*$^{140Q/-}$ mice compared to *Htt*$^{+/+}$ mice at 6 months of age, one possibility is a delay in synaptic dysfunction in *Htt*$^{140Q/\Delta E1}$ mice compared to *Htt*$^{140Q/\Delta E1}$ and *Htt*$^{140Q/-}$ mice. A more thorough characterization of *Htt*$^{140Q/\Delta E1}$ mice, including analyses of DNA damage accumulation and repair, synaptic function, HD progression markers such as DARPP32 expression, astrogliosis, lipofuscin accumulation, and Htt aggregate properties including kinetics, brain regional localization, subcellular localization, and size will be required to fully understand the effects of deleting the normal Htt N-terminus in *Htt*$^{140Q/\Delta E1}$ mice. Additionally, an unbiased approach such as RNA sequencing could be used to identify

other cellular processes that may be altered in the brains of *Htt*$^{140Q/\Delta E1}$ mice in comparison to either *Htt*$^{+/+}$ or *Htt*$^{140Q/+}$ mice.

Age	$Htt^{+/+}$	$Htt^{140Q/+}$	$Htt^{140Q/\Delta E1}$	$Htt^{140Q/-}$
3 Months	20	20	20	20
6 Months	20	20	20	20
10 Months	19	20	20	20
12 Months	19	20	20	20
14 Months	18	20	20	19
18 Months	17	20	19	19

Table 4-1: Number of mice used at each experimental time point for behavioral testing.

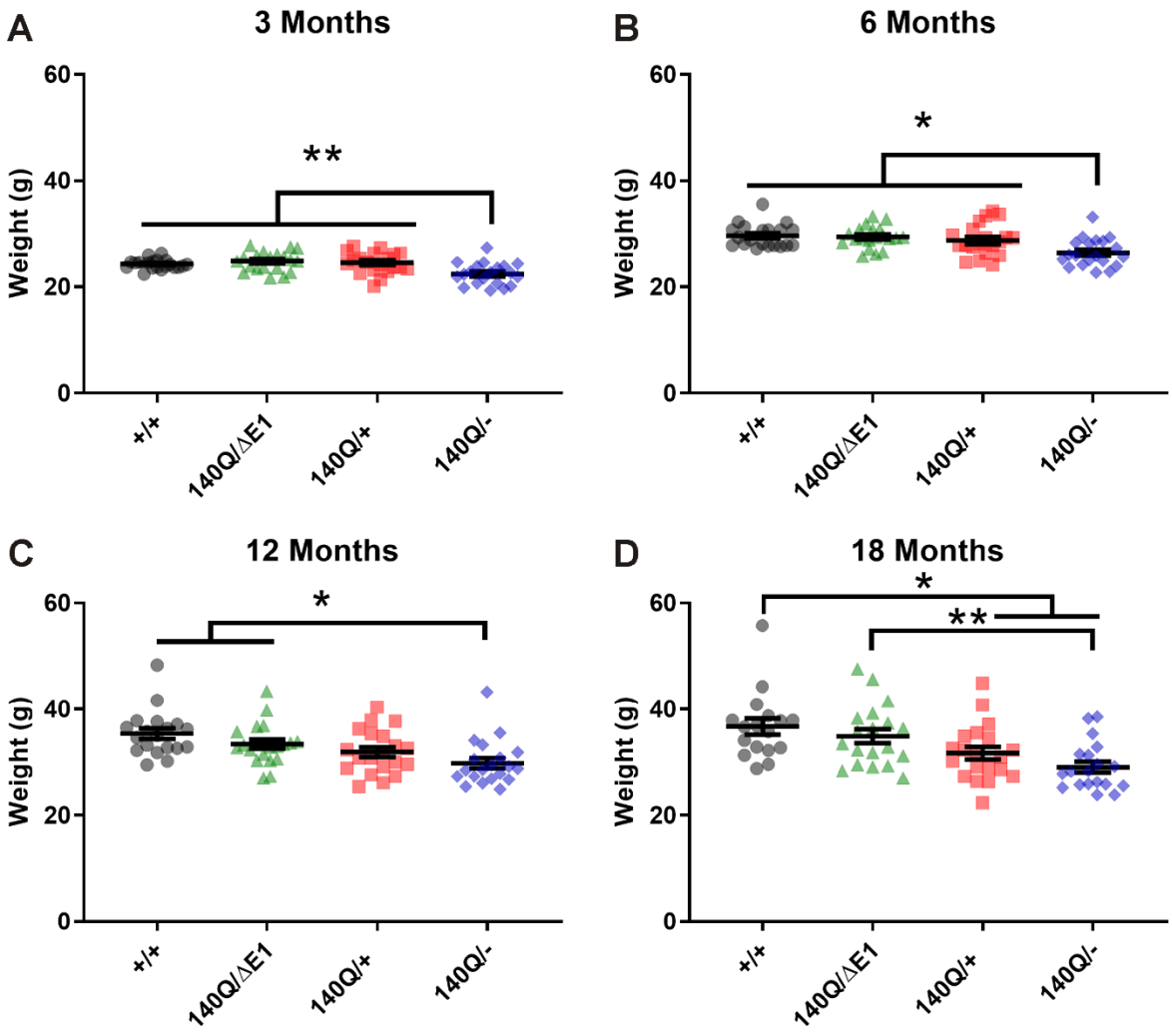

Figure 4-1: Body weight is reduced in *Htt*$^{140Q/-}$ mice. *Htt*$^{+/+}$ (+/+), *Htt*$^{140Q/\Delta E1}$ (140Q/ΔE1), *Htt*$^{140Q/+}$ (140Q/+), and *Htt*$^{140Q/-}$ (140Q/-) mice were weighed at (A) 3, (B) 6, (C) 12, and (D) 18 months of age. 1-way ANOVA with Tukey's multiple comparison test. Mean±SEM with individual data points shown. 3 months: *Htt*$^{+/+}$: 24.26±0.20 g, *Htt*$^{140Q/\Delta E1}$: 24.80±0.41 g *Htt*$^{140Q/+}$: 24.51±0.45 g, *Htt*$^{140Q/-}$: 22.40±0.46 g, p=0.0002, F=7.550, D_F=3; 6 months: *Htt*$^{+/+}$: 29.64±0.48 g, *Htt*$^{140Q/\Delta E1}$: 29.40±0.46 g, *Htt*$^{140Q/+}$: 28.76±0.66 g, *Htt*$^{140Q/-}$: 26.42±0.59 g, p=0.0003, F=7.045, D_F=3; 12 months: *Htt*$^{+/+}$: 35.37±0.99 g, *Htt*$^{140Q/\Delta E1}$:

33.41±0.86 g, *Htt*$^{140Q/+}$*:* 31.92±0.93 g*, Htt*$^{140Q/-}$: 29.81±0.95 g, p=0.0007, F=6.294, D_F=3; 18 months: *Htt*$^{+/+}$: 36.64±1.64 g, *Htt*$^{140Q/\Delta E1}$*:* 34.90±1.32 g, *Htt*$^{140Q/+}$*:* 31.71±1.18 g*, Htt*$^{140Q/-}$: 29.10±1.03 g, p=0.0005, F=6.592, D_F=3.

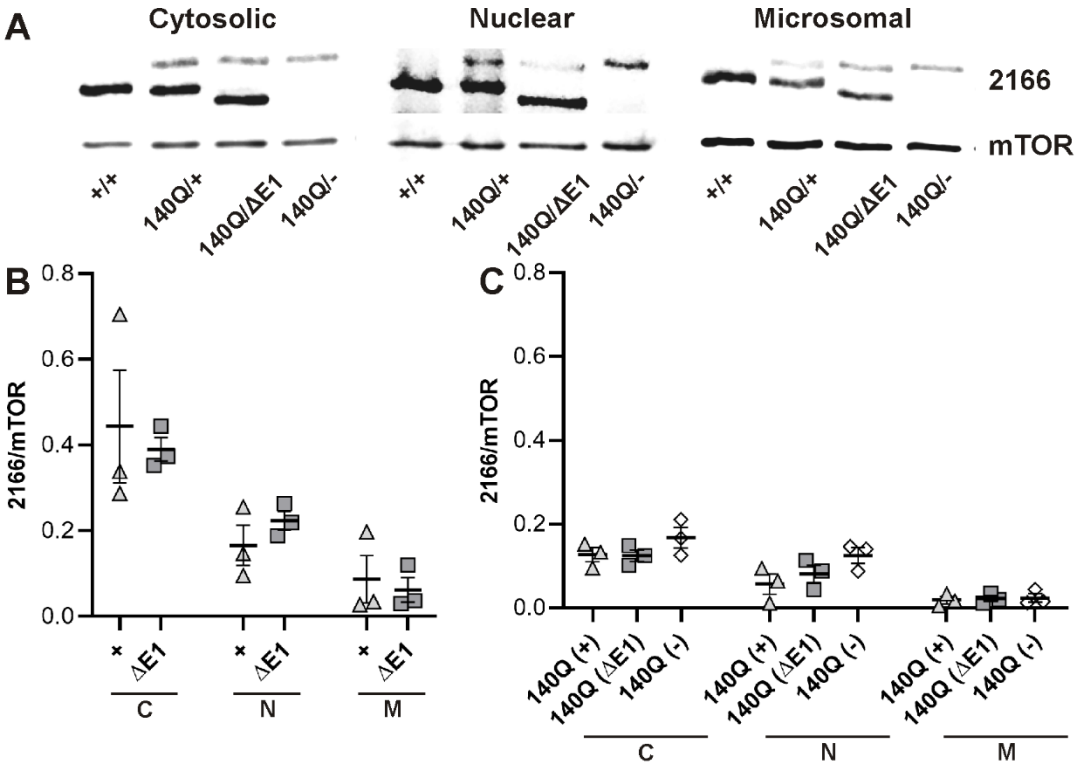

Figure 4-2: Deletion of the Htt N-terminus does not affect Htt subcellular distribution in HD model mice. (A) Total Htt levels were quantified from western blots of protein lysates from whole brain cytosolic, nuclear, and total microsomal fractions from 6-month-old *Htt*$^{+/+}$, *Htt*$^{140Q/\Delta E1}$, *Htt*$^{140Q/+}$, and *Htt*$^{140Q/-}$ mice probed with Htt (2166) and mTOR antibodies.

(B) The fluorescent intensities of WT-Htt (+) and ΔE1-Htt (ΔE1) were quantified and normalized to mTOR. N=3/genotype, unpaired t-test. Mean±SEM.

(C) The fluorescent intensity of 140Q-Htt (140Q) was quantified and normalized to mTOR. N=3/genotype, 1-way ANOVA with Tukey's multiple comparison test. Mean±SEM.

Cytosolic: *Htt*$^{+/+}$: 1.25±0.72, *Htt*$^{140Q/+}$: WT-Htt: 0.44±0.13, Htt140Q: 0.13±0.02, *Htt*$^{140Q/\Delta E1}$: ΔE1-Htt*:* 0.39±0.03*,* 140Q-Htt: 0.12±0.01, *Htt*$^{140Q/-}$: 0.17±0.02, ΔE1-Htt compared to WT-Htt: p=0.7115; 140Q-Htt: p=0.2708, F=1.637, D_F=2.

Nuclear: *Htt*$^{+/+}$: 0.32±0.03, *Htt*$^{140Q/+}$: WT-Htt: 0.17±0.05, Htt140Q: 0.06±0.02, *Htt*$^{140Q/\Delta E1}$: ΔE1-Htt*:* 0.22±0.02*,* 140Q-Htt: 0.08±0.02, *Htt*$^{140Q/-}$: 0.12±0.02, ΔE1-Htt compared to WT-Htt: p=0.3276; 140Q-Htt: p=0.1526, F=2.614, D_F=2.

Total microsomal: *Htt*$^{+/+}$: 0.155±0.085, *Htt*$^{140Q/+}$: WT-Htt: 0.086±0.056, Htt140Q: 0.005±0.034, *Htt*$^{140Q/\Delta E1}$: ΔE1-Htt*:* 0.062±0.029*,* 140Q-Htt: 0.012±0.035, *Htt*$^{140Q/-}$: 0.016±0.044, ΔE1-Htt compared to WT-Htt: p=0.7148; 140Q-Htt: p=0.9092, F=0.09673, D_F=2.

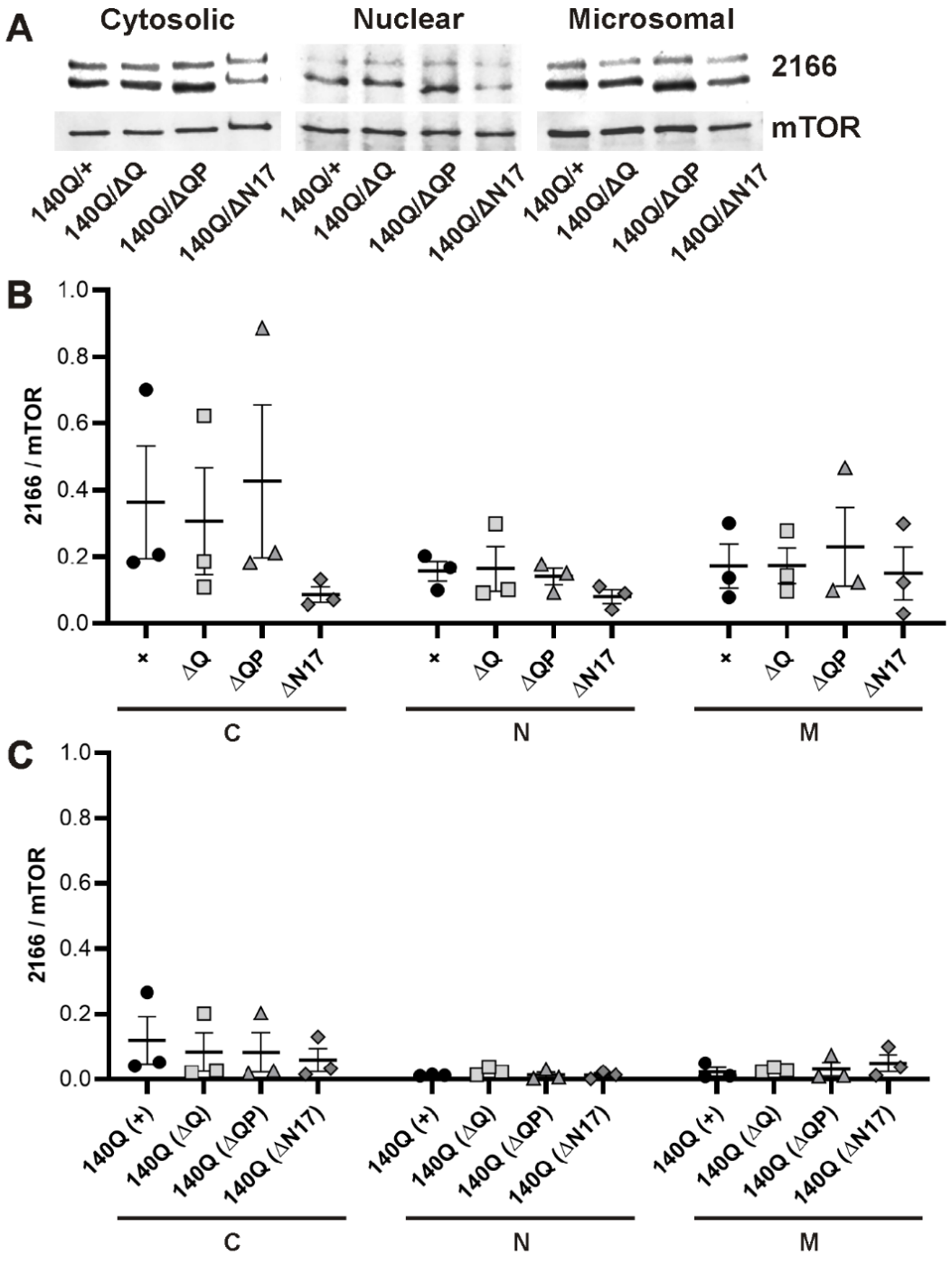
A
Cytosolic
Nuclear
Microsomal
2166
mTOR
140Q/+
140Q/ΔQ
140Q/ΔQP
140Q/ΔN17
B
2166 / mTOR
1.0
0.8
0.6
0.4
0.2
0.0
×
ΔQ
ΔQP
ΔN17
C
N
M
C
2166 / mTOR
140Q (+)
140Q (ΔQ)
140Q (ΔQP)
140Q (ΔN17)
C
N
M

Figure 4-3: Htt's subcellular localization is not altered in the brains of *Htt$^{140Q/\Delta Q}$*, *Htt$^{140Q/\Delta QP}$*, and *Htt$^{140Q/\Delta N17}$* mice. (A) Total Htt levels were quantified from western blots of protein lysates from whole brain cytosolic, nuclear, and total microsomal fractions from 6-month-old *Htt$^{140Q/+}$*, *Htt$^{140Q/\Delta Q}$*, *Htt$^{140Q/\Delta QP}$*, and *Htt$^{140Q/\Delta N17}$* mice probed with Htt (2166) and mTOR antibodies.

(B) The fluorescent intensities of WT-Htt (+), ΔQ-Htt (ΔQ), ΔQP-Htt (ΔQP), and ΔN17-Htt (ΔN17) were quantified and normalized to mTOR. N=3/genotype, unpaired t-test. Mean±SEM.

(C) The fluorescent intensity of 140Q-Htt (140Q) was quantified and normalized to mTOR. N=3/genotype, 1-way ANOVA with Tukey's multiple comparison test. Mean±SEM.

Cytosolic: *Htt$^{140Q/+}$*: WT-Htt: 0.36±0.17, Htt140Q: 0.12±0.07, *Htt$^{140Q/\Delta Q}$*: ΔQ-Htt*:* 0.31±0.16*,* 140Q-Htt: 0.08±0.06, *Htt$^{140Q/\Delta QP}$*: ΔQP-Htt*:* 0.43±0.23*,* 140Q-Htt: 0.08±0.06, *Htt$^{140Q/\Delta N17}$*: ΔN17-Htt*:* 0.09±0.02*,* 140Q-Htt: 0.06±0.04, WT-Htt, ΔQ-Htt, ΔQP-Htt, ΔN17-Htt: p=0.5204, F=0.8157, D_F=3; 140Q-Htt: p=0.9053, F=0.1825, D_F=3.

Nuclear: *Htt$^{140Q/+}$*: WT-Htt: 0.157±0.030, Htt140Q: 0.012±0.002, *Htt$^{140Q/\Delta Q}$*: ΔQ-Htt*:* 0.164±0.067*,* 140Q-Htt: 0.025±0.007, *Htt$^{140Q/\Delta QP}$*: ΔQP-Htt*:* 0.141±0.025*,* 140Q-Htt: 0.014±0.009, *Htt$^{140Q/\Delta N17}$*: ΔN17-Htt*:* 0.081±0.021*,* 140Q-Htt: 0.013±0.007, WT-Htt, ΔQ-Htt, ΔQP-Htt, ΔN17-Htt: p=0.4903, F=0.8818, D_F=3; 140Q-Htt: p=0.5111, F=0.8357, D_F=3.

Microsomal: *Htt*$^{140Q/+}$: WT-Htt: 0.172±0.066, Htt140Q: 0.023±0.013, *Htt*$^{140Q/\Delta Q}$: ΔQ-Htt*:* 0.173±0.054*,* 140Q-Htt: 0.030±0.004, *Htt*$^{140Q/\Delta QP}$: ΔQP-Htt*:* 0.230±0.119*,* 140Q-Htt: 0.031±0.021, *Htt*$^{140Q/\Delta N17}$: ΔN17-Htt*:* 0.151±0.079*,* 140Q-Htt: 0.050±0.026, WT-Htt, ΔQ-Htt, ΔQP-Htt, ΔN17-Htt: p=0.9147, F=0.1684, D_F=3; 140Q-Htt: p=0.3982, F=0.7581, D_F=3.

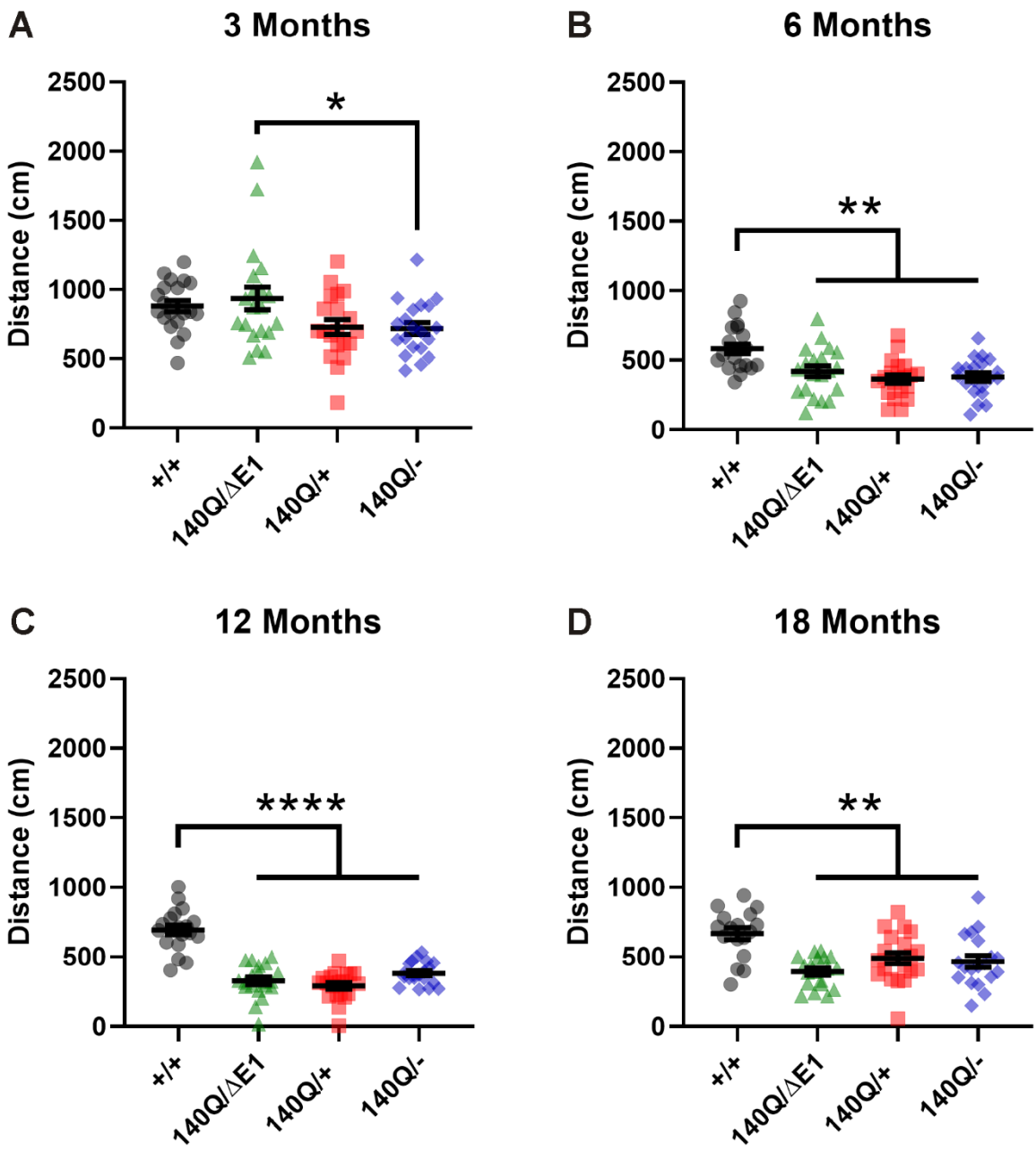

Figure 4-4: Total distance traveled during activity monitoring is reduced in HD model mice. *Htt*$^{+/+}$ (+/+), *Htt*$^{140Q/\Delta E1}$ (140Q/ΔE1), *Htt*$^{140Q/+}$ (140Q/+), and *Htt*$^{140Q/-}$ (140Q/-) mice were placed in an activity monitoring apparatus for one 5-minute trial at each

experimental time point. Total distance traveled at (A) 3, (B) 6, (C) 12, and (D) 18 months of age were recorded. 1-way ANOVA with Tukey's multiple comparison test. *p<0.05, **p<0.01, ****p<0.0001, mean±SEM.

3 months: $Htt^{+/+}$: 881.8±40.6 cm, $Htt^{140Q/\Delta E1}$: 936.8±81.6 cm, $Htt^{140Q/+}$: 730.8±53.1 cm, $Htt^{140Q/-}$: 720.7±43.6 cm, p=0.0170, F=3.612, D_F=3; 6 months: $Htt^{+/+}$: 582.5±35.0 cm, $Htt^{140Q/\Delta E1}$: 420.0±38.6 cm, $Htt^{140Q/+}$: 365.3±30.3 cm, $Htt^{140Q/-}$: 379.4±30.2 cm, p<0.0001, F=8.762, D_F=3; 12 months: $Htt^{+/+}$: 692.9±34.3 cm, $Htt^{140Q/\Delta E1}$: 326.5±26.6 cm, $Htt^{140Q/+}$: 290.5±22.9 cm, $Htt^{140Q/-}$: 380.6±18.0 cm, p<0.0001, F=49.29, D_F=3; 18 months: $Htt^{+/+}$: 666.8±42.6 cm, $Htt^{140Q/\Delta E1}$: 392.0±25.1 cm, $Htt^{140Q/+}$: 490.2±39.4 cm, $Htt^{140Q/-}$: 466.1±42.8 cm, p<0.0001, F=8.838, D_F=3.

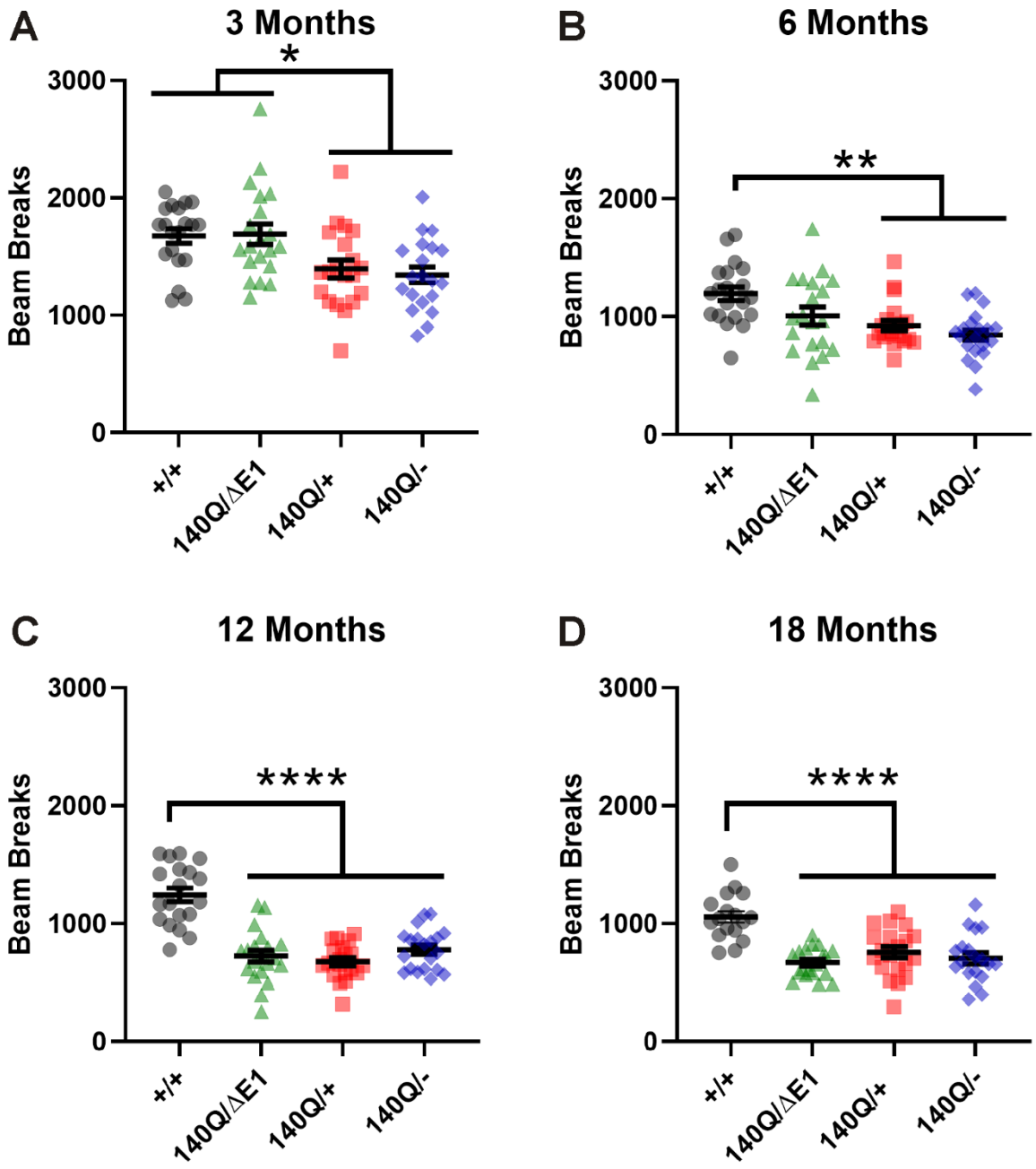

Figure 4-5: Reduced horizontal activity in HD model mice is delayed in *Htt*$^{140Q/\Delta E1}$ mice. *Htt*$^{+/+}$ (+/+), *Htt*$^{140Q/\Delta E1}$ (140Q/ΔE1), *Htt*$^{140Q/+}$ (140Q/+), and *Htt*$^{140Q/-}$ (140Q/-) mice were placed in an activity monitoring apparatus for one 5-minute trial at each

experimental time point. Horizontal activity measurements at (A) 3, (B) 6, (C) 12, and (D) 18 months of age were recorded. 1-way ANOVA with Tukey's multiple comparison test. *p<0.05, **p<0.01, ****p<0.0001, mean±SEM.

3 months: $Htt^{+/+}$: 1674±62 , $Htt^{140Q/\Delta E1}$: 1690±88, $Htt^{140Q/+}$: 1395±76, $Htt^{140Q/-}$: 1344±68, p=0.0010, F=5.993, D_F=3; 6 months: $Htt^{+/+}$: 1193±57, $Htt^{140Q/\Delta E1}$: 1005±75, $Htt^{140Q/+}$: 924±43, $Htt^{140Q/-}$: 842±45, p=0.0003, F=7.019, D_F=3; 12 months: $Htt^{+/+}$: 1242±59, $Htt^{140Q/\Delta E1}$: 723±50, $Htt^{140Q/+}$: 675±33, $Htt^{140Q/-}$: 777±39, p<0.0001, F=31.60, D_F=3; 18 months: $Htt^{+/+}$: 1056±48, $Htt^{140Q/\Delta E1}$: 668±28, $Htt^{140Q/+}$: 754±46, $Htt^{140Q/-}$: 704±48, p<0.0001, F=15.65, D_F=3.

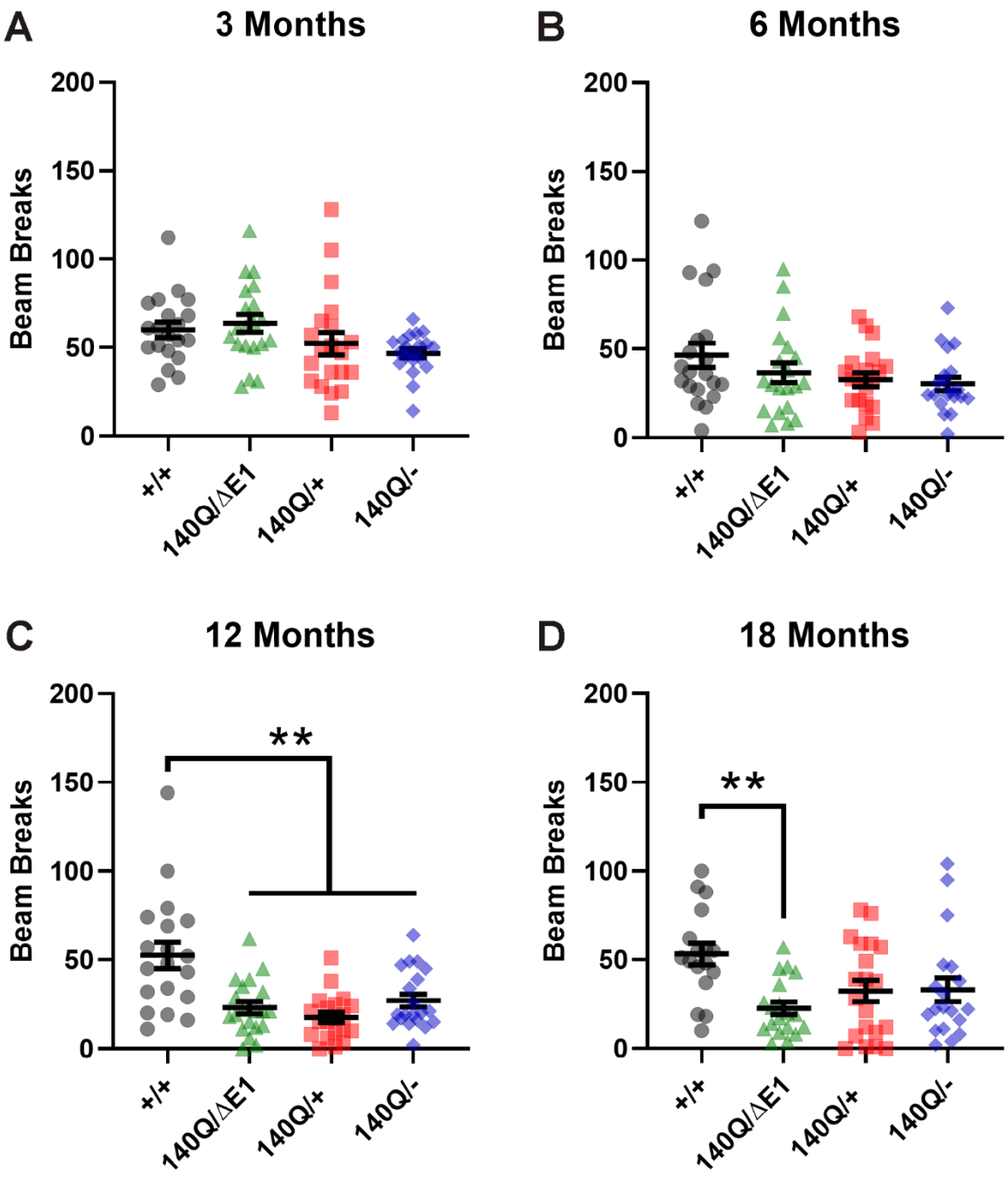

Figure 4-6: Vertical activity is reduced in HD model mice. *Htt*$^{+/+}$ (+/+), *Htt*$^{140Q/\Delta E1}$ (140Q/ΔE1), *Htt*$^{140Q/+}$ (140Q/+), and *Htt*$^{140Q/-}$ (140Q/-) mice were placed in an activity monitoring apparatus for one 5-minute trial at each experimental time point. Vertical

activity measurements at (A) 3, (B) 6, (C) 12, and (D) 18 months of age were recorded. 1-way ANOVA with Tukey's multiple comparison test. **p<0.01, mean±SEM.

3 months: $Htt^{+/+}$: 60.05±4.30, $Htt^{140Q/\Delta E1}$: 63.70±6.37, $Htt^{140Q/+}$: 52.20±6.37, $Htt^{140Q/-}$: 46.65±2.60, p=0.0584, F=2.597, D_F=3; 6 months: $Htt^{+/+}$: 46.35±6.84, $Htt^{140Q/\Delta E1}$: 36.60±5.53, $Htt^{140Q/+}$: 32.70±3.93, $Htt^{140Q/-}$: 30.35±3.73, p=0.1427, F=1.865, D_F=3; 12 months: $Htt^{+/+}$: 52.63±7.49, $Htt^{140Q/\Delta E1}$: 23.10±3.45, $Htt^{140Q/+}$: 17.55±2.85, $Htt^{140Q/-}$: 27.05±3.66, p<0.0001, F=10.94, D_F=3; 18 months: $Htt^{+/+}$: 53.29±6.15, $Htt^{140Q/\Delta E1}$: 22.63±3.61, $Htt^{140Q/+}$: 32.40±5.98, $Htt^{140Q/-}$: 33.11±6.72, p=0.0044, F=4.757, D_F=3.

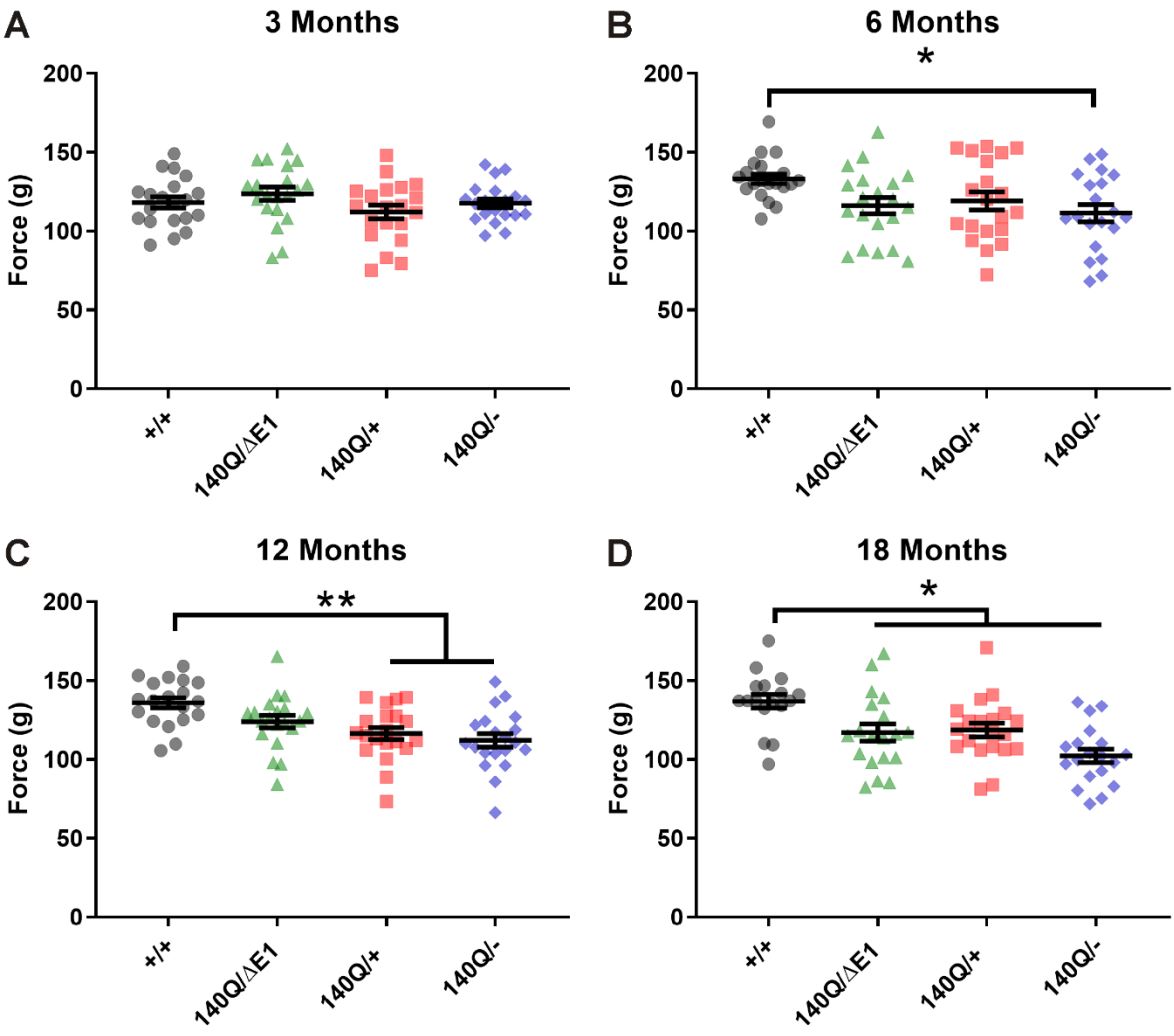

Figure 4-7: Deletion of the Htt N-terminus delays a reduction of forelimb grip strength in *Htt*$^{140Q/\Delta E1}$ mice. The forelimb grip strength of *Htt*$^{+/+}$ (+/+), *Htt*$^{140Q/\Delta E1}$ (140Q/ΔE1), *Htt*$^{140Q/+}$ (140Q/+), and *Htt*$^{140Q/-}$ (140Q/-) mice was tested at (A) 3, (B) 6, (C) 12, and (D) 18 months of age. Three trials per mouse were performed at each experimental time point. 1-way ANOVA with Tukey's multiple comparison test. *p<0.05, **p<0.01, mean±SEM.

3 months: $Htt^{+/+}$: 118.14±3.49 g, $Htt^{140Q/\Delta E1}$: 123.52±4.18 g, $Htt^{140Q/+}$: 112.06±4.30 g, $Htt^{140Q/-}$: 117.51±2.75 g, p=0.2015, F=1.579, D_F=3; 6 months: $Htt^{+/+}$: 133.17±3.03 g, $Htt^{140Q/\Delta E1}$: 116.11±5.11 g, $Htt^{140Q/+}$: 119.04±5.65 g, $Htt^{140Q/-}$: 111.38±5.43 g, p=0.0165, F=3.635, D_F=3; 12 months: $Htt^{+/+}$: 135.92±3.37 g, $Htt^{140Q/\Delta E1}$: 123.82±3.92 g, $Htt^{140Q/+}$: 116.37±3.79 g, $Htt^{140Q/-}$: 112.02±4.23 g, p=0.0002, F=7.257, D_F=3; 18 months: $Htt^{+/+}$: 136.82±4.47 g, $Htt^{140Q/\Delta E1}$: 117.00±5.44 g $Htt^{140Q/+}$: 118.56±4.40 g, $Htt^{140Q/-}$: 102.31±4.26 g, p<0.0001, F=8.712, D_F=3.

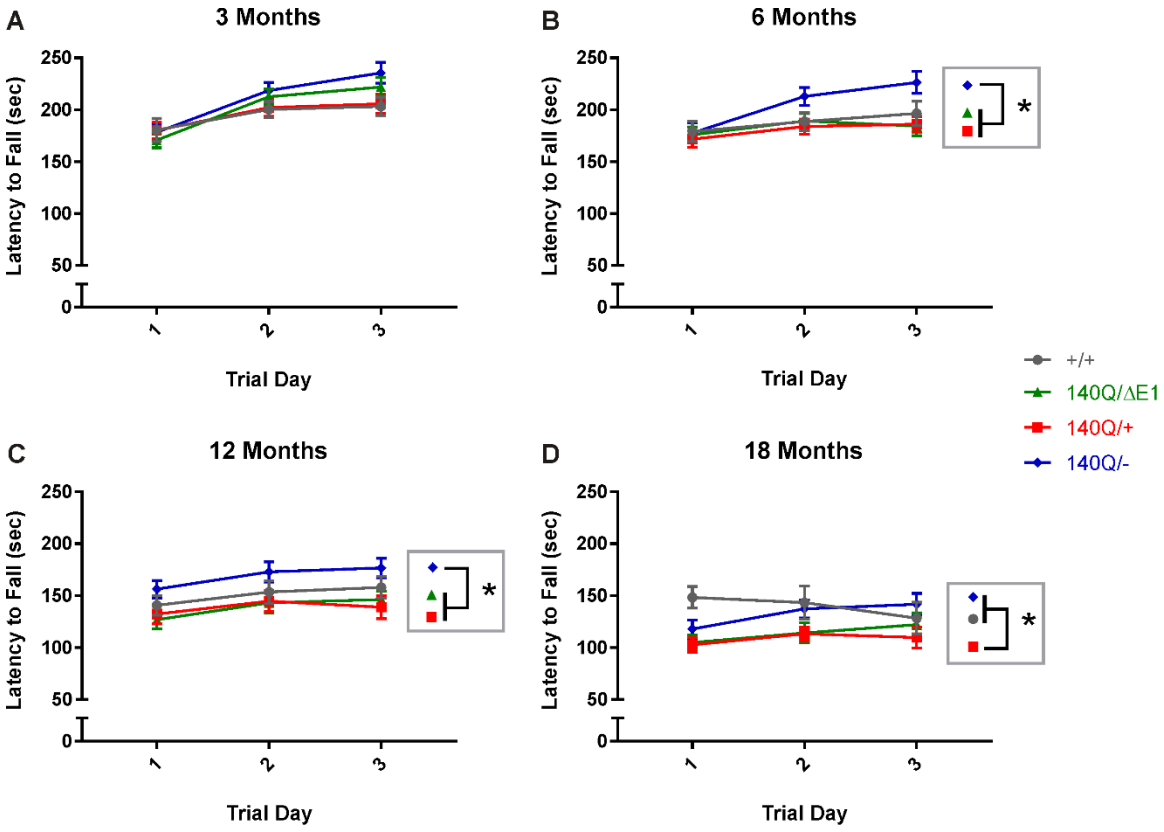

Figure 4-8: *Htt*$^{140Q/-}$ mice exhibit enhanced rotarod performance compared to *Htt*$^{140Q/ΔE1}$ and *Htt*$^{140Q/+}$ mice. *Htt*$^{+/+}$ (+/+), *Htt*$^{140Q/ΔE1}$ (140Q/ΔE1), *Htt*$^{140Q/+}$ (140Q/+), and *Htt*$^{140Q/-}$ (140Q/-) mice were subjected to rotarod testing at (A) 3, (B) 6, (C) 12, and (D) 18 months of age for three trials per day over 3 days. See Table 4-2 for detailed statistical values. 2-way ANOVA. Mean±SEM shown.

3 months: *Htt*$^{+/+}$: 194.6±5.5 sec, *Htt*$^{140Q/ΔE1}$: 201.7±5.4 sec, *Htt*$^{140Q/+}$: 195.9±5.1 sec, *Htt*$^{140Q/-}$: 210.7±6.0 sec, 6 months: *Htt*$^{+/+}$: 188.1±5.8 sec, *Htt*$^{140Q/ΔE1}$: 183.0±4.6 sec, *Htt*$^{140Q/+}$: 180.5±4.4 sec, *Htt*$^{140Q/-}$: 205.6±6.1 sec, 12 months: *Htt*$^{+/+}$: 150.6±5.9 sec, *Htt*$^{140Q/ΔE1}$: 138.6±5.1 sec, *Htt*$^{140Q/+}$: 138.5±5.8 sec, *Htt*$^{140Q/-}$: 168.5±5.3 sec, 18 months: *Htt*$^{+/+}$: 139.8±8.1 sec, *Htt*$^{140Q/ΔE1}$: 113.6±5.5 sec, *Htt*$^{140Q/+}$: 108.4±4.6 sec, *Htt*$^{140Q/-}$: 132.2±5.5 sec.

Genotype 1	Genotype 2	3 Month	6 Month	12 Month	18 Month
***Htt*$^{+/+}$**	***Htt*$^{140Q/\Delta E1}$**	*p*=0.5131 F=0.4359 D_F=1	*p*=0.6406 F=0.2215 D_F=1	*p*=0.3381 F=0.9417 D_F=1	*p*=0.0973 F=2.913 D_F=1
***Htt*$^{+/+}$**	***Htt*$^{140Q/+}$**	*p*=0.9093 F=0.01315 D_F=1	*p*=0.4909 F=0.4839 D_F=1	*p*=0.3830 F=0.7794 D_F=1	***p*=0.0318** **F=5.015** **D_F=1**
***Htt*$^{+/+}$**	***Htt*$^{140Q/-}$**	*p*=0.1633 F=2.021 D_F=1	*p*=0.1588 F=2.066 D_F=1	*p*=0.1706 F=1.953 D_F=1	*p*=0.6173 F=0.2545 D_F=1
***Htt*$^{140Q/\Delta E1}$**	***Htt*$^{140Q/+}$**	*p*=0.5764 F=0.3176 D_F=1	*p*=0.7571 F=0.09708 D_F=1	*p*=0.9933 F=0.00007069 D_F=1	*p*=0.6367 F=0.2268 D_F=1
***Htt*$^{140Q/\Delta E1}$**	***Htt*$^{140Q/-}$**	*p*=0.3933 F=0.7454 D_F=1	***p*=0.0274** **F=5.265** **D_F=1**	***p*=0.0140** **F=6.634** **D_F=1**	*p*=0.1310 F=2.388 D_F=1
***Htt*$^{140Q/+}$**	***Htt*$^{140Q/-}$**	*p*=0.1827 F=1.843 D_F=1	***p*=0.0167** **F=6.263** **D_F=1**	***p*=0.0260** **F=5.364** **D_F=1**	***p*=0.0323** **F=4.946** **D_F=1**

Table 4-2: Statistical values for the accelerating rotarod results (Fig. 4-5) calculated using 2-way ANOVA. Statistically significant values ($p<0.05$) are bolded.

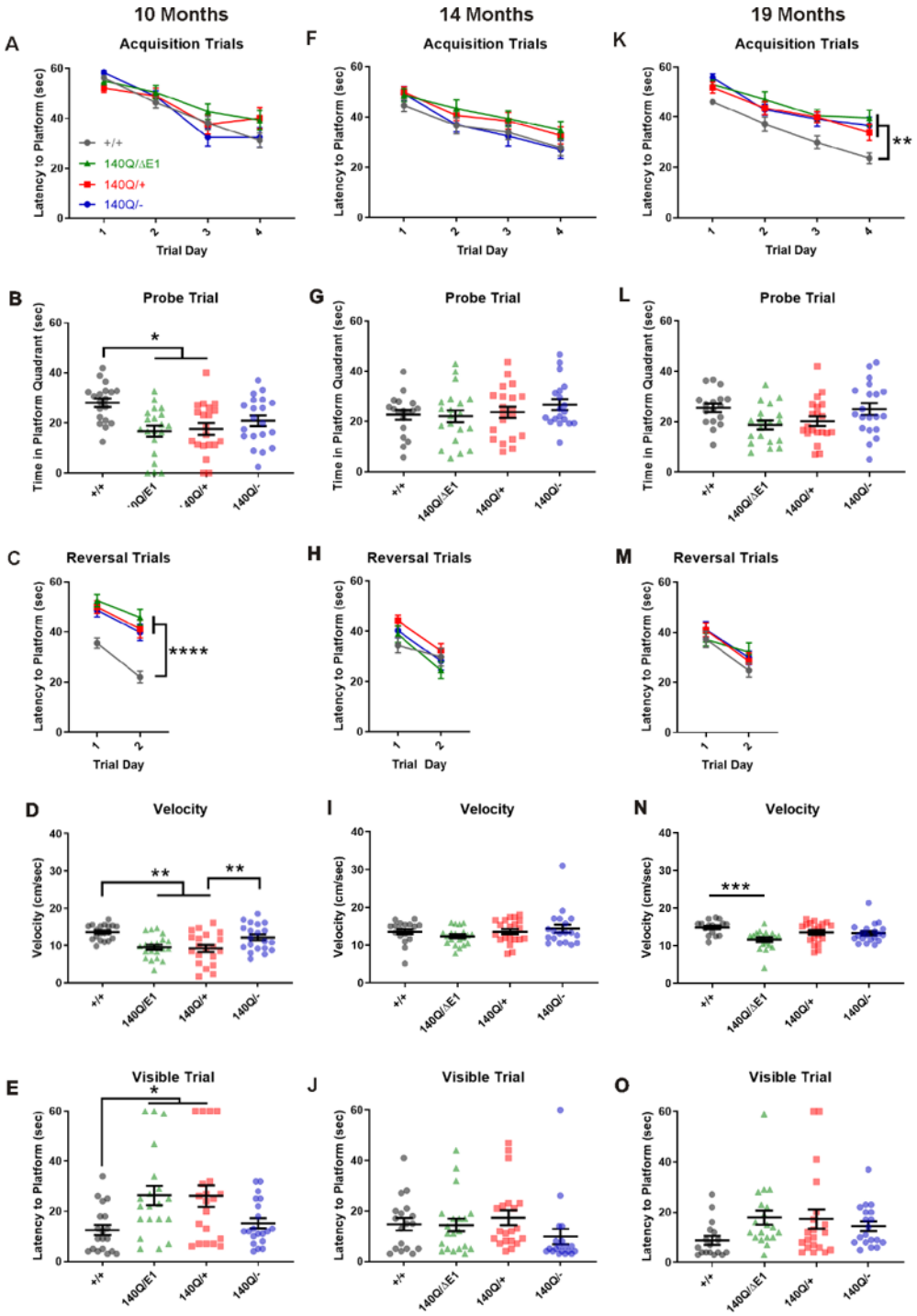
10 Months
14 Months
19 Months
A
Acquisition Trials
F
Acquisition Trials
K
Acquisition Trials
Latency to Platform (sec)
Trial Day
+/+
140Q/ΔE1
140Q/+
140Q/-
**
B
Probe Trial
G
Probe Trial
L
Probe Trial
Time in Platform Quadrant (sec)
*
+/+
140Q/ΔE1
140Q/+
140Q/-
C
Reversal Trials
H
Reversal Trials
M
Reversal Trials
****
Trial Day
D
Velocity
I
Velocity
N
Velocity
Velocity (cm/sec)
**
**
***
E
Visible Trial
J
Visible Trial
O
Visible Trial
*

Figure 4-9: HD model mice exhibit deficits in spatial learning and memory that are not affected by deletion of the normal Htt N-terminus. $Htt^{+/+}$ (+/+), $Htt^{140Q/\Delta E1}$ (140Q/ΔE1), $Htt^{140Q/+}$ (140Q/+), and $Htt^{140Q/-}$ (140Q/-) mice were subjected to spatial learning and memory testing at 10 (A-E), 14 (F-J), and 19 months of age (K-O) as previously described. See Table 4-3 for detailed statistical values for the acquisition and reversal phases. 2-way ANOVA, mean±SEM shown (acquisition and reversal phases) and 1-way ANOVA with Tukey's multiple comparison test, mean±SEM (probe trial, visible control trial, and velocity).

10 months: acquisition trials: $Htt^{+/+}$: 43.05±1.56 sec, $Htt^{140Q/\Delta E1}$: 46.93±1.60 sec, $Htt^{140Q/+}$: 44.78±1.78 sec, $Htt^{140Q/-}$: 43.06±1.91 sec, probe trial: $Htt^{+/+}$: 28.07±1.75 sec, $Htt^{140Q/\Delta E1}$: 16.75±2.19 sec, $Htt^{140Q/+}$: 17.65±2.30 sec, $Htt^{140Q/-}$: 20.87±2.12 sec, p=0.0013, F=5.794, D_F=3; reversal trials: $Htt^{+/+}$: 28.78±1.87 sec, $Htt^{140Q/\Delta E1}$: 49.16±2.20 sec, $Htt^{140Q/+}$: 45.48±2.27 sec, $Htt^{140Q/-}$: 44.26±2.20 sec; velocity: $Htt^{+/+}$: 13.54±0.46 cm/sec , $Htt^{140Q/\Delta E1}$: 9.58±0.69 cm/sec, $Htt^{140Q/+}$: 9.22±0.94 cm/sec, $Htt^{140Q/-}$: 12.13±0.78 cm/sec, p=0.0002, F=7.634, D_F=3; visible control: $Htt^{+/+}$: 12.53±2.12 sec, $Htt^{140Q/\Delta E1}$: 26.35±3.91 sec, $Htt^{140Q/+}$: 26.10±4.35 sec, $Htt^{140Q/-}$: 15.25±2.01 sec, p=0.0043, F=4.762, D_F=3.

14 months: acquisition trials: $Htt^{+/+}$: 35.68±3.48 sec, $Htt^{140Q/\Delta E1}$: 41.48±2.95 sec, $Htt^{140Q/+}$: 40.33±2.55 sec , $Htt^{140Q/-}$: 36.35±4.72 sec, probe trial: $Htt^{+/+}$: 22.68±1.96 sec, $Htt^{140Q/\Delta E1}$: 22.07±2.40 sec, $Htt^{140Q/+}$: 23.68±2.30 sec, $Htt^{140Q/-}$: 26.74±2.14 sec, p=0.4620, F=0.8675, D_F=3; reversal trials: $Htt^{+/+}$: 32.08±2.38 sec, $Htt^{140Q/\Delta E1}$: 31.68±7.21 sec, $Htt^{140Q/+}$: 38.23±5.93 sec, $Htt^{140Q/-}$: 34.24±6.10 sec; velocity: $Htt^{+/+}$: 13.54±0.69 cm/sec, $Htt^{140Q/\Delta E1}$: 12.32±0.51 cm/sec, $Htt^{140Q/+}$: 13.55±0.70 cm/sec, $Htt^{140Q/-}$: 14.36±1.10 cm/sec, p=0.3182, F=1.194, D_F=3; visible control: $Htt^{+/+}$: 14.78±2.46 sec, $Htt^{140Q/\Delta E1}$: 14.45±2.58 sec, $Htt^{140Q/+}$: 17.35±2.92 sec, $Htt^{140Q/-}$: 9.84±3.07 sec, p=0.2905, F=1.272, D_F=3.

19 months: acquisition trials: $Htt^{+/+}$: 34.21±4.85 sec, $Htt^{140Q/\Delta E1}$: 45.00±3.12 sec, $Htt^{140Q/+}$: 42.27±3.72 sec, $Htt^{140Q/-}$: 43.58±4.24 sec, probe trial: $Htt^{+/+}$: 25.45±1.70 sec, $Htt^{140Q/\Delta E1}$: 18.74±1.76 sec , $Htt^{140Q/+}$: 20.25±1.93 sec, $Htt^{140Q/-}$: 24.98±2.31 sec, p=0.0414, F=2.888, D_F=3; reversal trials: $Htt^{+/+}$: 31.01±6.16 sec, $Htt^{140Q/\Delta E1}$: 34.55±2.49 sec, $Htt^{140Q/+}$: 34.68±6.26 sec, $Htt^{140Q/-}$: 35.49±5.65 sec, velocity: $Htt^{+/+}$: 14.84±0.49 cm/sec, $Htt^{140Q/\Delta E1}$: 11.55±0.58 cm/sec, $Htt^{140Q/+}$: 13.49±0.60 cm/sec, $Htt^{140Q/-}$: 13.27±0.57 cm/sec, p=0.0018, F=5.509, D_F=3; visible control: $Htt^{+/+}$: 8.82±1.73 sec, $Htt^{140Q/\Delta E1}$: 17.84±2.87 sec, $Htt^{140Q/+}$: 17.25±3.90 sec, $Htt^{140Q/-}$: 14.37±1.90 sec, p=0.1191, F=2.018, D_F=3.

Genotype 1	Genotype 2	Trial	10 Month	14 Month	19 Month
***Htt*$^{+/+}$**	***Htt*$^{140Q/\Delta E1}$**	**Acquisition**	*p*=0.1789 F=1.877 D_F=1	*p*=0.0816 F=3.211 D_F=1	***p*=0.0001** **F=19.18** **D_F=1**
***Htt*$^{+/+}$**	***Htt*$^{140Q/+}$**	**Acquisition**	*p*=0.5382 F=0.3861 D_F=1	*p*=0.1027 F=2.804 D_F=1	***p*=0.0015** **F=11.84** **D_F=1**
***Htt*$^{+/+}$**	***Htt*$^{140Q/-}$**	**Acquisition**	*p*=0.9969 F=0.00001515 D_F=1	*p*=0.8133 F=0.05644 D_F=1	***p*=0.0001** **F=18.53** **D_F=1**
***Htt*$^{140Q/\Delta E1}$**	***Htt*$^{140Q/+}$**	**Acquisition**	*p*=0.5233 F=0.4151 D_F=1	*p*=0.7267 F=0.1240 D_F=1	*p*=0.3222 F=1.007 D_F=1
***Htt*$^{140Q/\Delta E1}$**	***Htt*$^{140Q/-}$**	**Acquisition**	*p*=0.2358 F=1.451 D_F=1	*p*=0.1302 F=2.396 D_F=1	*p*=0.5917 F=0.2929 D_F=1
***Htt*$^{140Q/+}$**	***Htt*$^{140Q/-}$**	**Acquisition**	*p*=0.5911 F=0.2936 D_F=1	*p*=0.1769 F=1.895 D_F=1	*p*=0.6036 F=0.2742 D_F=1
***Htt*$^{+/+}$**	***Htt*$^{140Q/\Delta E1}$**	**Reversal**	***p*<0.0001** **F=42.89** **D_F=1**	*p*=0.9188 F=0.01054 D_F=1	*p*=0.3511 F=0.8938 D_F=1
***Htt*$^{+/+}$**	***Htt*$^{140Q/+}$**	**Reversal**	***p*<0.0001** **F=26.70** **D_F=1**	*p*=0.0985 F=2.877 D_F=1	*p*=0.3085 F=1.068 D_F=1
***Htt*$^{+/+}$**	***Htt*$^{140Q/-}$**	**Reversal**	***p*<0.0001** **F=25.96** **D_F=1**	*p*=0.6004 F=0.2794 D_F=1	*p*=0.2173 F=1.580 D_F=1
***Htt*$^{140Q/\Delta E1}$**	***Htt*$^{140Q/+}$**	**Reversal**	*p*=0.3394 F=0.9361 D_F=1	*p*=0.0716 F=3.436 D_F=1	*p*=0.9693 F=0.001501 D_F=1
***Htt*$^{140Q/\Delta E1}$**	***Htt*$^{140Q/-}$**	**Reversal**	*p*=0.1724 F=1.934 D_F=1	*p*=0.5214 F=0.4190 D_F=1	*p*=0.7888 F=0.07285 D_F=1
***Htt*$^{140Q/+}$**	***Htt*$^{140Q/-}$**	**Reversal**	*p*=0.7188 F=0.1315 D_F=1	*p*=0.2796 F=1.204 D_F=1	*p*=0.8089 F=0.05935 D_F=1

Table 4-3: Statistical values for the results of the acquisition and reversal phases of the Morris water maze test (Fig. 4-6) calculated using 2-way ANOVA. Statistically significant values ($p<0.05$) are bolded.

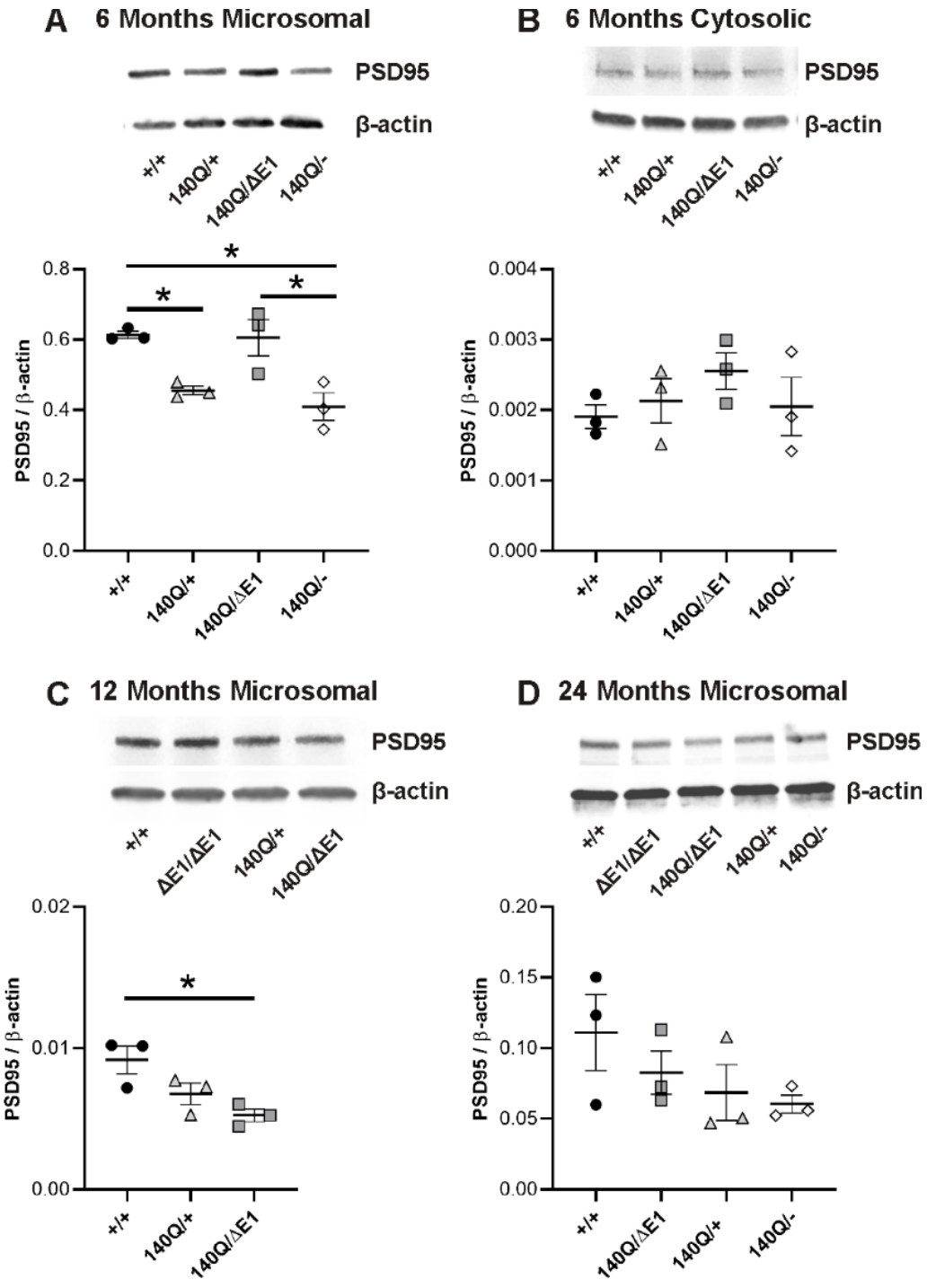

Figure 4-10: PSD95 levels are reduced in *Htt*$^{140Q/+}$ and *Htt*$^{140Q/-}$ mice at 6 months of age, and in *Htt*$^{140Q/\Delta E1}$ mice at 12 months of age. Western blots of (A) 6-month-old

microsomal, (B) 6-month-old cytosolic (C) 12-month-old microsomal and (D) 24-month-old microsomal fractions of whole-brain protein lysates from *Htt*$^{+/+}$, *Htt*$^{140Q/+}$, *Htt*$^{140Q/\Delta E1}$, and *Htt*$^{140Q/-}$ mice were probed with a PSD95 antibody. The fluorescent intensity of each band was calculated and normalized to β-actin as a loading control. See Fig 3-17 for analysis of 24-month-old *Htt*$^{+/+}$ and *Htt*$^{\Delta E1/\Delta E1}$ PSD95 levels. There were no differences in 12-month-old *Htt*$^{+/+}$ and *Htt*$^{\Delta E1/\Delta E1}$ PSD95 levels (*Htt*$^{\Delta E1/\Delta E1}$:0.0088±0.0002, p=0.7247, unpaired t-test). 3 mice/genotype, 1-way ANOVA with Tukey's multiple comparison test. Mean±SEM.

6 months: microsomal: *Htt*$^{+/+}$: 0.61±0.01, *Htt*$^{140Q/+}$: 0.46±0.01, *Htt*$^{140Q/\Delta E1}$: 0.60±0.05, *Htt*$^{140Q/-}$: 0.41±0.04, p=0.0050, F=9.607, D_F=3; cytosolic: *Htt*$^{+/+}$: 0.0019±0.0002, *Htt*$^{140Q/+}$: 0.0021±0.0003, *Htt*$^{140Q/\Delta E1}$: 0.0026±0.0003, *Htt*$^{140Q/-}$: 0.0020±0.0004, p=0.5037, F=0.8519, D_F=3.

12 months: *Htt*$^{+/+}$: 0.0092±0.0010, *Htt*$^{140Q/\Delta E1}$: 0.0068±0.0008, *Htt*$^{140Q/+}$: 0.0052±0.0004, p=0.0294, F=6.723, D_F=2.

24 months: *Htt*$^{+/+}$: 0.111±0.027, *Htt*$^{140Q/\Delta E1}$: 0.083±0.015, *Htt*$^{140Q/+}$: 0.068±0.020, *Htt*$^{140Q/-}$: 0.060±0.006, p=0.3015, F=1.440, D_F=3.

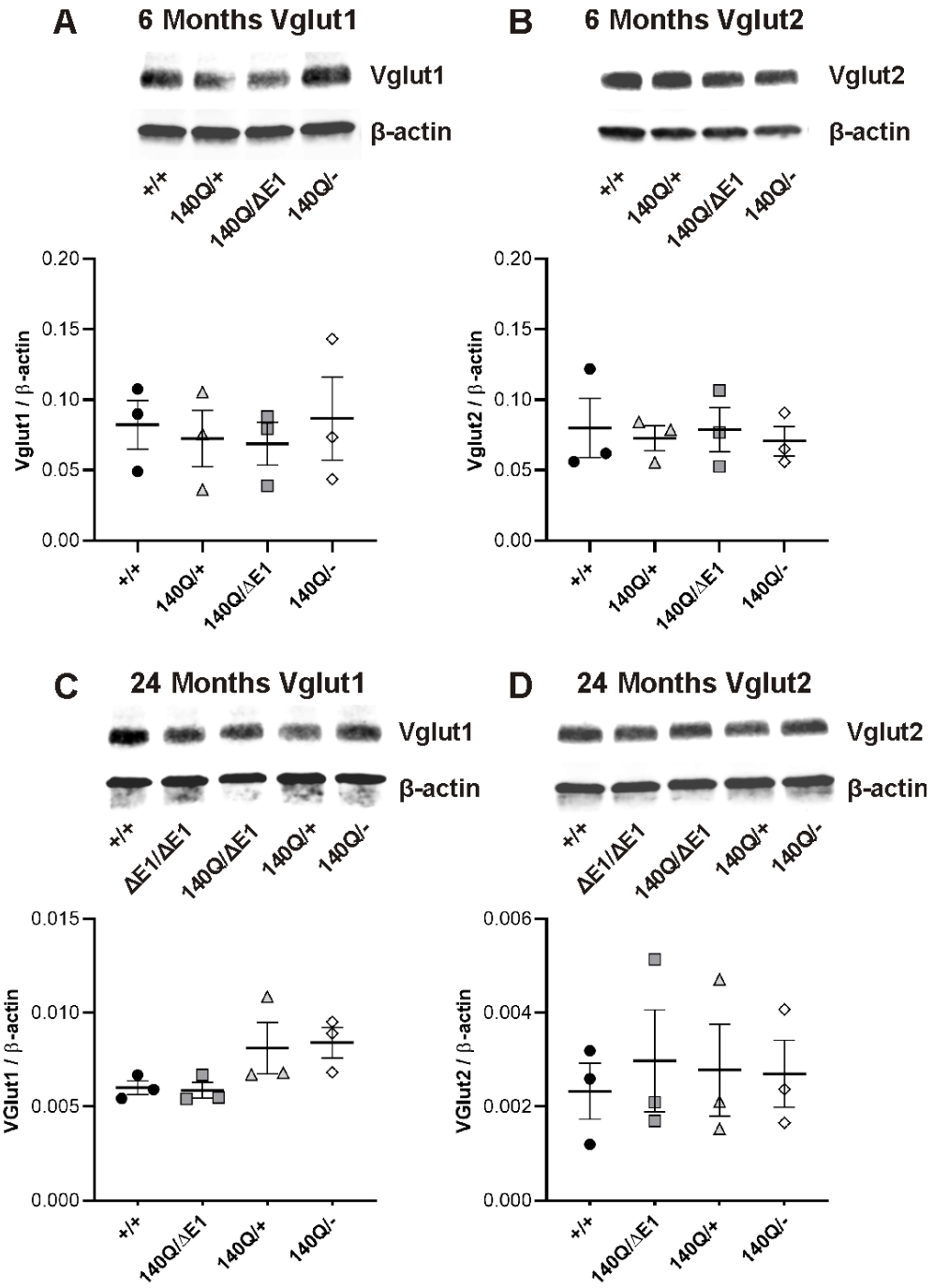

Figure 4-11: Vglut1 and Vglut2 levels are not altered in *Htt*$^{140Q/+}$, *Htt*$^{140Q/\Delta E1}$, and *Htt*$^{140Q/-}$ mice. Western blots of protein lysates from whole brain microsomal fractions of (A, B) 6-, and (C, D) 24-month-old *Htt*$^{+/+}$, *Htt*$^{140Q/+}$, *Htt*$^{140Q/\Delta E1}$, and *Htt*$^{140Q/-}$ mice were

probed with (A, C) Vglut1 and (B, D) Vglut2 antibodies. The fluorescent intensity of each band was calculated and normalized to β-actin as a loading control. See Fig 3-17 for analysis of 24-month-old $Htt^{+/+}$ and $Htt^{\Delta E1/\Delta E1}$ Vglut1 and Vglut2 levels. 3 mice/genotype, 1-way ANOVA with Tukey's multiple comparison test. Mean±SEM.

6 months: Vglut1: $Htt^{+/+}$: 0.082±0.017, $Htt^{140Q/+}$: 0.072±0.020, $Htt^{140Q/\Delta E1}$: 0.069±0.015, $Htt^{140Q/-}$: 0.087±0.030, p=0.9236, F=0.1549, D_F=3; Vglut2: $Htt^{+/+}$: 0.080±0.021, $Htt^{140Q/+}$: 0.073±0.009, $Htt^{140Q/\Delta E1}$: 0.079±0.016, $Htt^{140Q/-}$: 0.071±0.010, p=0.9607, F=0.09488, D_F=3.

24 months: Vglut1: $Htt^{+/+}$: 0.0060±0.0004, $Htt^{140Q/\Delta E1}$: 0.0059±0.0004, $Htt^{140Q/+}$: 0.0081±0.0014, $Htt^{140Q/-}$: 0.0084±0.0008, p=0.1265, F=2.577, D_F=3; Vglut2: $Htt^{+/+}$: 0.0023±0.0006, $Htt^{140Q/\Delta E1}$: 0.0030±0.0011, $Htt^{140Q/+}$: 0.0028±0.0010, $Htt^{140Q/-}$: 0.0027±0.0007, p=0.9586, F=0.09848, D_F=3.

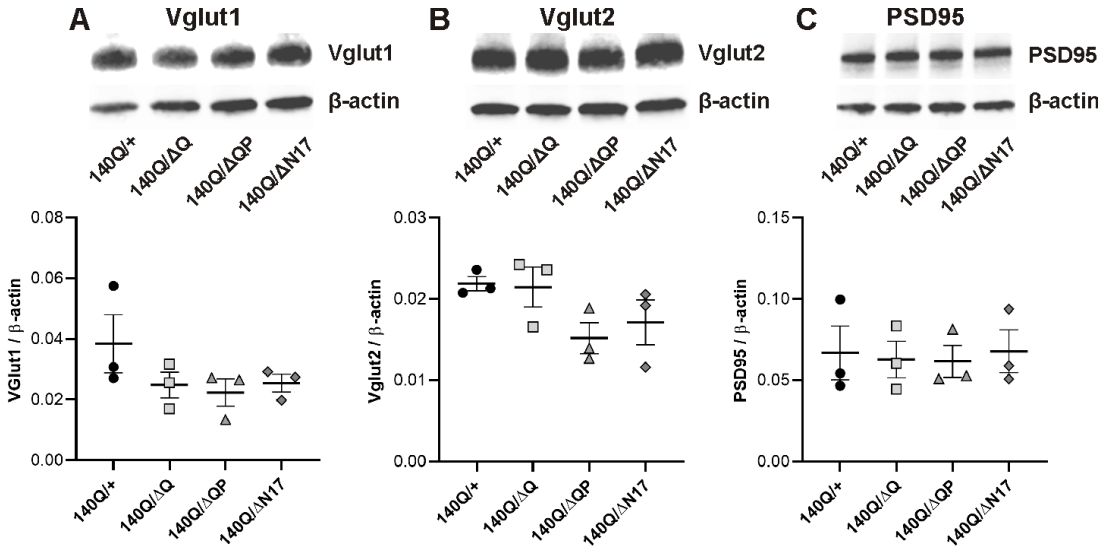

Figure 4-12: No differences were observed in synaptic marker levels from whole brain samples collected from Htt$^{140Q/+}$, Htt$^{140Q/\Delta Q}$, Htt$^{140Q/\Delta QP}$, and Htt$^{140Q/\Delta N17}$ mice.

Western blots of protein lysates from whole brain total microsomal fractions of 6-month-old *Htt$^{140Q/+}$, Htt$^{140Q/\Delta Q}$, Htt$^{140Q/\Delta QP}$,* and *Htt$^{140Q/\Delta N17}$* mice were probed with (A) Vglut1, (B) Vglut2, and (C) PSD95 antibodies. The fluorescent intensity of each band was calculated and normalized to β-actin as a loading control. 3 mice/genotype, 1-way ANOVA with Tukey's multiple comparison test. Mean±SEM.

Vglut1: *Htt$^{140Q/+}$*: 0.0384±0.010, *Htt$^{140Q/\Delta Q}$*: 0.0248±0.004, *Htt$^{140Q/\Delta QP}$*: 0.0224±0.004, *Htt$^{140Q/\Delta N17}$*: 0.0255±0.003, p=0.2842, F=1.511, D_F=3; Vglut2: *Htt$^{140Q/+}$*: 0.022±0.001, *Htt$^{140Q/\Delta Q}$*: 0.021±0.002, *Htt$^{140Q/\Delta QP}$*: 0.015±0.002, *Htt$^{140Q/\Delta N17}$*: 0.017±0.003, p=0.1439, F=2.394, D_F=3; PSD95: *Htt$^{140Q/+}$*: 0.067±0.017, *Htt$^{140Q/\Delta Q}$*: 0.063±0.011, *Htt$^{140Q/\Delta QP}$*: 0.062±0.010, *Htt$^{140Q/\Delta N17}$*: 0.068±0.013, p=0.0.9639, F=0.08926, D_F=3.

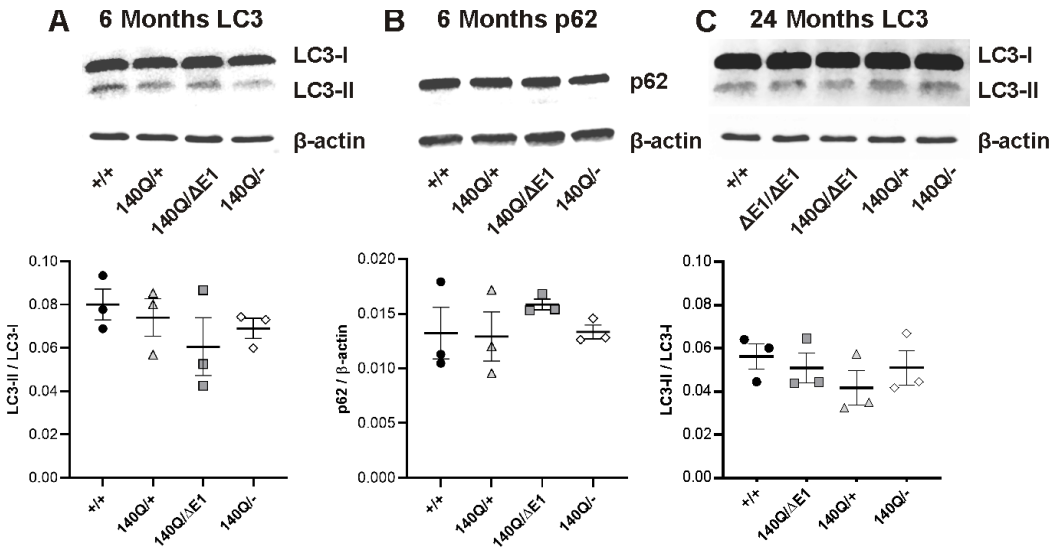

Figure 4-13: No differences were found in the levels of autophagy markers from whole brain total microsomal fractions collected from 6- and 24-month-old *Htt*$^{+/+}$, *Htt*$^{140Q/+}$, *Htt*$^{140Q/\Delta E1}$, and *Htt*$^{140Q/-}$ mice. Western blots of protein lysates from whole brain microsomal fractions of (A, B) 6- and (C) 24-month-old *Htt*$^{+/+}$, *Htt*$^{140Q/+}$, *Htt*$^{140Q/\Delta E1}$, and *Htt*$^{140Q/-}$ mice were probed with (A, C) LC3 and (B) p62 antibodies. For LC3 quantification, the ratio of the fluorescent intensity of LC3-II to LC3-I was calculated. The fluorescent intensity of each p62 band was calculated and normalized to β-actin as a loading control. See Fig 3-16 for analysis of 24-month-old *Htt*$^{+/+}$ and *Htt*$^{\Delta E1/\Delta E1}$ LC3 levels. 3 mice/genotype, 1-way ANOVA with Tukey's multiple comparison test. Mean±SEM.

6 months: LC3: *Htt*$^{+/+}$: 0.080±0.007, *Htt*$^{140Q/+}$: 0.074±0.009, *Htt*$^{140Q/\Delta E1}$: 0.061±0.013, *Htt*$^{140Q/-}$: 0.069±0.005, p=0.5142, F=0.8291, D_F=3; p62: *Htt*$^{+/+}$: 0.0132±0.0024, *Htt*$^{140Q/+}$: 0.0129±0.0022, *Htt*$^{140Q/\Delta E1}$: 0.0158±0.0005, *Htt*$^{140Q/-}$: 0.0133±0.0006, p=0.6058, F=0.6482, D_F=3.

24 months: LC3: $Htt^{+/+}$: 0.056±0.006, $Htt^{140Q/\Delta E1}$: 0.051±0.007, $Htt^{140Q/+}$: 0.042±0.008, $Htt^{140Q/-}$: 0.051±0.008, p=0.5730, F=0.7095, D_F=3.

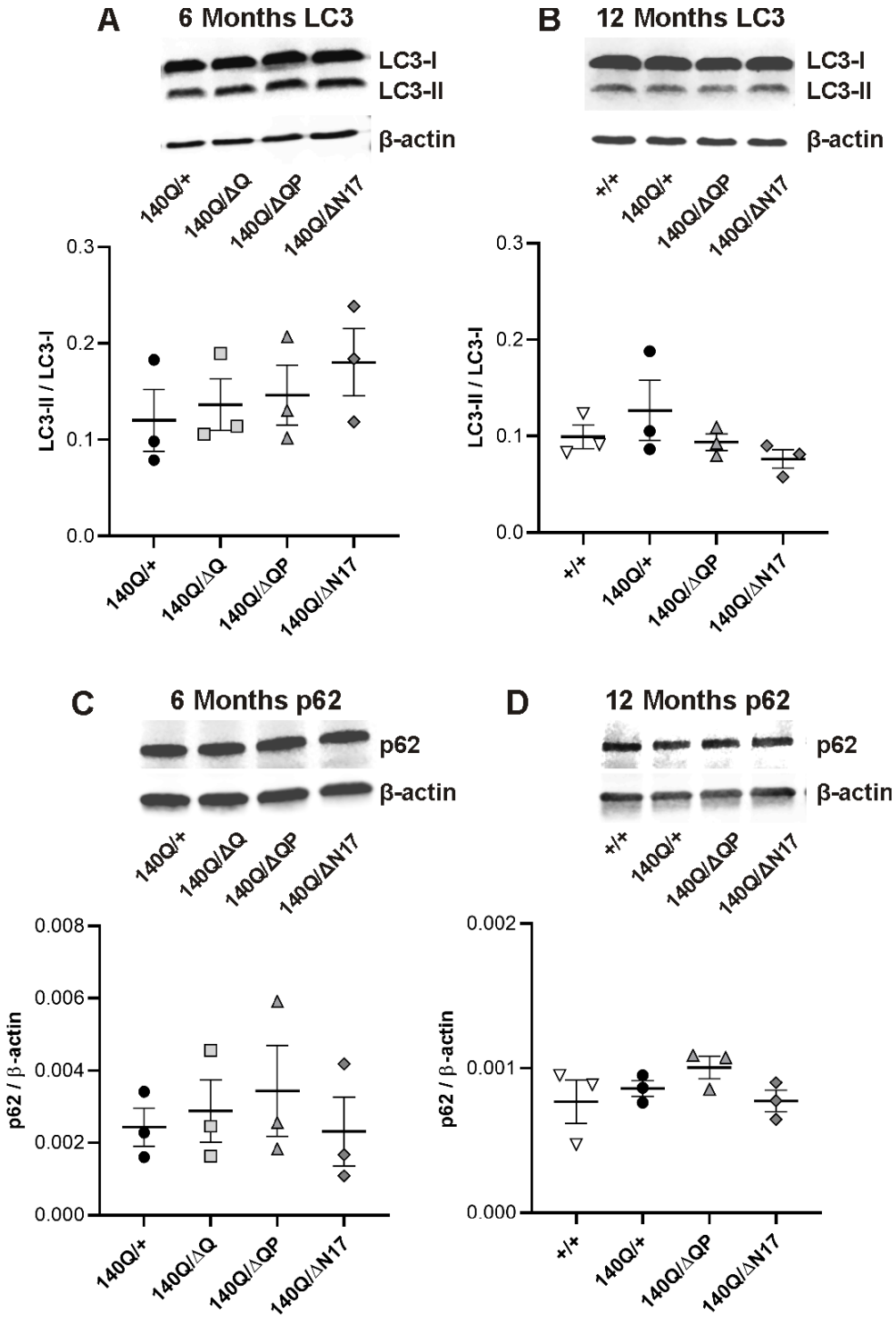
A
6 Months LC3
LC3-I
LC3-II
β-actin
140Q/+
140Q/ΔQ
140Q/ΔQP
140Q/ΔN17
LC3-II / LC3-I
0.3
0.2
0.1
0.0
B
12 Months LC3
+/+
C
6 Months p62
p62
p62 / β-actin
0.008
0.006
0.004
0.002
0.000
D
12 Months p62
0.002
0.001

Figure 4-14: No differences were found in the levels of autophagy markers from fractionated whole brain samples collected from 6- and 12-month-old *Htt*$^{+/+}$, *Htt*$^{140Q/+}$, *Htt*$^{140Q/\Delta QP}$, and *Htt*$^{140Q/\Delta N17}$ mice. Western blots of protein lysates from whole brain total microsomal fractions of (A, C) 6-month-old *Htt*$^{140Q/+}$, *Htt*$^{140Q/\Delta Q}$, *Htt*$^{140Q/\Delta QP}$, and *Htt*$^{140Q/\Delta N17}$ and (B, D) 12-month-old *Htt*$^{+/+}$, *Htt*$^{140Q/+}$, *Htt*$^{140Q/\Delta QP}$, and *Htt*$^{140Q/\Delta N17}$ mice were probed with (A, B) LC3 and (C, D) p62 antibodies. For LC3 quantification, the ratio of the fluorescent intensity of LC3-II to LC3-I was calculated. The fluorescent intensity of each p62 band was calculated and normalized to β-actin. 3 mice/genotype, 1-way ANOVA with Tukey's multiple comparison test. Mean±SEM.

6 months: LC3: *Htt*$^{140Q/+}$: 0.12±0.03, *Htt*$^{140Q/\Delta Q}$: 0.14±0.03, *Htt*$^{140Q/\Delta QP}$: 0.15±0.03, *Htt*$^{140Q/\Delta N17}$: 0.18±0.03, p=0.5986, F=0.6614, D_F=3; p62: *Htt*$^{140Q/+}$: 0.0024±0.0005, *Htt*$^{140Q/\Delta Q}$: 0.0029±0.0009, *Htt*$^{140Q/\Delta QP}$: 0.0034±0.0013, *Htt*$^{140Q/\Delta N17}$: 0.0023±0.0010, p=0.8286, F=0.2943, D_F=3.

12 months: LC3: *Htt*$^{+/+}$: 0.099±0.012 *Htt*$^{140Q/+}$: 0.127±0.031, *Htt*$^{140Q/\Delta QP}$: 0.094±0.009, *Htt*$^{140Q/\Delta N17}$: 0.076±0.010, p=0.3249, F=1.351, D_F=3; p62: *Htt*$^{+/+}$: 0.00077±0.00015, *Htt*$^{140Q/+}$: 0.00086±0.00005, *Htt*$^{140Q/\Delta QP}$: 0.00100±0.00008, *Htt*$^{140Q/\Delta N17}$: 0.00077±0.00007, p=0.3304, F=1.332, D_F=3.

Chapter V: Conclusions and future directions

The three N-terminal domains of HTT have been previously characterized in vitro, in single- and double-domain deletion mouse models, and in young mice. Here I report a longitudinal characterization of a knock-in mouse model with the three N-terminal domains of Htt deleted in homozygosity (*Htt*$^{\Delta E1/\Delta E1}$), heterozygosity (*Htt*$^{\Delta E1/+}$), and hemizygosity (*Htt*$^{\Delta E1/-}$), as well as in trans to an HD mouse model allele (*Htt*$^{140Q/\Delta E1}$). I found that progeny from *Htt*$^{\Delta E1/+}$ intercrosses and *Htt*$^{\Delta E1/+}$ x *Htt*$^{+/-}$ intercrosses were born at the expected Mendelian frequency, however, progeny from *Htt*$^{\Delta E1/+}$ intercrosses were born with an allele-specific sex distortion. Therefore, while the Htt N-terminus is not required for Htt's critical functions during embryonic development, it likely regulates some aspect of Htt's functions in the testis.

In a longitudinal behavioral study of *Htt*$^{\Delta E1/\Delta E1}$, *Htt*$^{\Delta E1/+}$, and *Htt*$^{\Delta E1/-}$ mice, I found that motor and spatial learning and memory function were, for the most part, comparable to wild type (*Htt*$^{+/+}$) or hemizygous (*Htt*$^{+/-}$) control mice. *Htt*$^{\Delta E1/\Delta E1}$ mice, however, exhibited a modest, non-progressive rotarod deficit in comparison to *Htt*$^{1+/+}$ mice. Interestingly, this phenotype was not observed in the *Htt*$^{140Q/\Delta E1}$ mice, suggesting that the *Htt*^{140Q} allele may retain some of the normal functions of the Htt N-terminus. Additionally, the late-onset rotarod deficit observed in the *Htt*$^{140Q/+}$ mice was absent in the *Htt*$^{140Q/\Delta E1}$ mice, and while *Htt*$^{140Q/\Delta E1}$ mice exhibited deficits in forelimb grip strength and horizontal activity levels compared to *Htt*$^{+/+}$ mice, the onset of these deficits was delayed in comparison to *Htt*$^{140Q/+}$ mice. Deletion of the Htt N-terminus is therefore likely to affect motor function through distinct mechanisms, where it causes a specific and non-progressive motor deficit in homozygosity, and where it delays the onset of the more generalized and

progressive HD motor phenotype in heterozygosity with the expression of an HD mouse model allele. Further studies are required to identify and characterize each of these mechanisms.

Based on prior studies of Htt's N-terminal domains, I have identified several cellular pathways including autophagy [8], glutamatergic synapse number [4], and DNA damage repair [23] that may be affected by deletion of the Htt N-terminus. Although I did not observe an alteration in glutamatergic synapse numbers or autophagosome markers in $Htt^{\Delta E1/\Delta E1}$ mice, I did observe an increase in DNA double strand breaks and elevated pan-nuclear 53bp1 levels in 3-month-old $Htt^{\Delta E1/\Delta E1}$ mice compared to $Htt^{+/+}$ mice that did not persist with age. While repair of acute DNA damage by γ-irradiation was not significantly altered in the $Htt^{\Delta E1/\Delta E1}$ mice, further studies are needed to determine whether the elevation in DNA DSBs in $Htt^{\Delta E1/\Delta E1}$ mice is caused by a subtle deficit in DNA damage repair, an increase in the induction of DNA damage, or a combination of both. Additionally, further studies are needed to determine the cause and consequences of the increased levels of pan-nuclear 53bp1 and its potential association with the increased levels of DNA damage I observed in the $Htt^{\Delta E1/\Delta E1}$ mice.

Autophagy markers were not altered, and synapse markers were only modestly changed in $Htt^{140Q/\Delta E1}$ mice in comparison to $Htt^{140Q/+}$ and $Htt^{+/+}$ mice. However, molecular markers of HD progression such as mutant Htt aggregation, levels of the striatal marker DARPP32, lipofuscin accumulation, and astrogliosis were not examined in the $Htt^{140Q/\Delta E1}$ mice. Investigating these and other possible consequences of HD progression such as

altered synaptic function, elevated DNA damage levels, reduced DNA damage repair efficiency, and elevated oxidative damage levels may provide insight into the cause of the delay in behavioral HD model phenotypes observed in the *Htt*$^{140Q/\Delta E1}$ mice.

Taken together, the mild effects of removing the Htt N-terminus in *Htt*$^{\Delta E1/\Delta E1}$ mice and the delay in HD motor phenotype onset in *Htt*$^{140Q/\Delta E1}$ mice suggest that removing the Htt N-terminus may be a promising strategy for treating HD motor symptoms. However, many additional studies on the safety of deleting the Htt N-terminus remain to be completed before the efficacy of Htt N-terminal deletion as a treatment can be evaluated. This project focuses on the effects of removing the Htt N-terminus on specific aspects of Htt's function that were identified based on prior studies. Therefore, this work should be supplemented with unbiased transcriptomic and proteomic studies of both brain and peripheral tissues from *Htt*$^{\Delta E1/\Delta E1}$ and *Htt*$^{140Q/\Delta E1}$ mice to more systematically investigate the role of the Htt N-terminus. Additionally, the Htt N-terminus may regulate Htt's response to environmental changes. Investigating how *Htt*$^{\Delta E1/\Delta E1}$ and *Htt*$^{140Q/\Delta E1}$ mice respond to variations in the standard laboratory environment including increased environmental enrichment, access to a varied diet, and exposure to infectious agents, among other alterations, will be required to fully characterize these mice. Once the function of the mouse Htt N-terminus is well understood, similar experiments should then be repeated in model organisms with longer lifespans and more complex nervous systems to gain a more accurate understanding of how the HTT N-terminus may function in systems that are more similar to healthy humans and to HD patients.

References

1. DiGiovanni, L.F., et al., *Huntingtin N17 domain is a reactive oxygen species sensor regulating huntingtin phosphorylation and localization.* Hum Mol Genet, 2016.

2. Sittler, A., et al., *SH3GL3 associates with the Huntingtin exon 1 protein and promotes the formation of polygln-containing protein aggregates.* Mol Cell, 1998. **2**(4): p. 427-36.

3. Faber, P.W., et al., *Huntingtin interacts with a family of WW domain proteins.* Hum Mol Genet, 1998. **7**(9): p. 1463-74.

4. Andre, E.A., et al., *Generation and Characterization of Knock-in Mouse Models Expressing Versions of Huntingtin with Either an N17 or a Combined PolyQ and Proline-Rich Region Deletion.* J Huntingtons Dis, 2017. **6**(1): p. 47-62.

5. Clabough, E.B. and S.O. Zeitlin, *Deletion of the triplet repeat encoding polyglutamine within the mouse Huntington's disease gene results in subtle behavioral/motor phenotypes in vivo and elevated levels of ATP with cellular senescence in vitro.* Hum Mol Genet, 2006. **15**(4): p. 607-23.

6. Neveklovska, M., et al., *Deletion of the huntingtin proline-rich region does not significantly affect normal huntingtin function in mice.* J Huntingtons Dis, 2012. **1**(1): p. 71-87.

7. Liu, X., et al., *N-terminal Huntingtin Knock-In Mice: Implications of Removing the N-terminal Region of Huntingtin for Therapy.* PLoS Genet, 2016. **12**(5): p. e1006083.

8. Zheng, S., et al., *Deletion of the huntingtin polyglutamine stretch enhances neuronal autophagy and longevity in mice.* PLoS Genet, 2010. **6**(2): p. e1000838.

9. The Huntington's Disease Collaborative Research Group, *A novel gene containing a trinucleotide repeat that is expanded and unstable on Huntington's disease chromosomes.* Cell, 1993. **72**(6): p. 971-83.

10. Wexler, N.S., et al., *Homozygotes for Huntington's disease.* Nature, 1987. **326**(6109): p. 194-7.

11. Rubinsztein, D.C., et al., *Phenotypic characterization of individuals with 30-40 CAG repeats in the Huntington disease (HD) gene reveals HD cases with 36 repeats and apparently normal elderly individuals with 36-39 repeats.* Am J Hum Genet, 1996. **59**(1): p. 16-22.

12. Saft, C., et al., *Mitochondrial impairment in patients and asymptomatic mutation carriers of Huntington's disease.* Mov Disord, 2005. **20**(6): p. 674-9.

13. DiFiglia, M., et al., *Aggregation of huntingtin in neuronal intranuclear inclusions and dystrophic neurites in brain.* Science, 1997. **277**(5334): p. 1990-3.

14. Dragatsis, I., M.S. Levine, and S. Zeitlin, *Inactivation of Hdh in the brain and testis results in progressive neurodegeneration and sterility in mice.* Nat Genet, 2000. **26**(3): p. 300-6.

15. Van Raamsdonk, J.M., et al., *Loss of wild-type huntingtin influences motor dysfunction and survival in the YAC128 mouse model of Huntington disease.* Hum Mol Genet, 2005. **14**(10): p. 1379-92.

16. Pringsheim, T., et al., *The incidence and prevalence of Huntington's disease: a systematic review and meta-analysis.* Mov Disord, 2012. **27**(9): p. 1083-91.

17. Duyao, M., et al., *Trinucleotide repeat length instability and age of onset in Huntington's disease.* Nat Genet, 1993. **4**(4): p. 387-92.

18. Paulsen, J.S., et al., *Neuropsychiatric aspects of Huntington's disease.* J Neurol Neurosurg Psychiatry, 2001. **71**(3): p. 310-4.

19. van der Burg, J.M.M., M. Björkqvist, and P. Brundin, *Beyond the brain: widespread pathology in Huntington's disease.* The Lancet Neurology, 2009. **8**(8): p. 765-774.

20. Heemskerk, A.W. and R.A. Roos, *Aspiration pneumonia and death in Huntington's disease.* PLoS Curr, 2012. **4**: p. RRN1293.

21. Rui, Y.N., et al., *Huntingtin functions as a scaffold for selective macroautophagy.* Nat Cell Biol, 2015. **17**(3): p. 262-75.

22. Ochaba, J., et al., *Potential function for the Huntingtin protein as a scaffold for selective autophagy.* Proc Natl Acad Sci U S A, 2014. **111**(47): p. 16889-94.

23. Maiuri, T., et al., *Huntingtin is a scaffolding protein in the ATM oxidative DNA damage response complex.* Hum Mol Genet, 2017. **26**(2): p. 395-406.

24. Caviston, J.P., et al., *Huntingtin facilitates dynein/dynactin-mediated vesicle transport.* Proc Natl Acad Sci U S A, 2007. **104**(24): p. 10045-50.

25. Andrade, M.A., et al., *Comparison of ARM and HEAT protein repeats.* J Mol Biol, 2001. **309**(1): p. 1-18.

26. Tartari, M., et al., *Phylogenetic comparison of huntingtin homologues reveals the appearance of a primitive polyQ in sea urchin.* Mol Biol Evol, 2008. **25**(2): p. 330-8.

27. Benn, C.L., et al., *Huntingtin modulates transcription, occupies gene promoters in vivo, and binds directly to DNA in a polyglutamine-dependent manner.* J Neurosci, 2008. **28**(42): p. 10720-33.

28. Caron, N.S., et al., *Polyglutamine domain flexibility mediates the proximity between flanking sequences in huntingtin.* Proc Natl Acad Sci U S A, 2013. **110**(36): p. 14610-5.

29. Maiuri, T., et al., *The huntingtin N17 domain is a multifunctional CRM1 and Ran-dependent nuclear and cilial export signal.* Hum Mol Genet, 2013. **22**(7): p. 1383-94.

30. Atwal, R.S., et al., *Huntingtin has a membrane association signal that can modulate huntingtin aggregation, nuclear entry and toxicity.* Hum Mol Genet, 2007. **16**(21): p. 2600-15.

31. Thompson, L.M., et al., *IKK phosphorylates Huntingtin and targets it for degradation by the proteasome and lysosome.* Journal of Cell Biology, 2009. **187**(7): p. 1083-99.

32. Gu, X., et al., *Serines 13 and 16 are critical determinants of full-length human mutant huntingtin induced disease pathogenesis in HD mice.* Neuron, 2009. **64**(6): p. 828-40.

33. Chiki, A., et al., *Mutant Exon1 Huntingtin Aggregation is Regulated by T3 Phosphorylation-Induced Structural Changes and Crosstalk between T3 Phosphorylation and Acetylation at K6.* Angew Chem Int Ed Engl, 2017. **56**(19): p. 5202-5207.

34. Wellington, C.L., et al., *Caspase cleavage of mutant huntingtin precedes neurodegeneration in Huntington's disease.* J Neurosci, 2002. **22**(18): p. 7862-72.

35. Gafni, J., et al., *Inhibition of calpain cleavage of huntingtin reduces toxicity: accumulation of calpain/caspase fragments in the nucleus.* J Biol Chem, 2004. **279**(19): p. 20211-20.

36. Cooper, J.K., et al., *Truncated N-terminal fragments of huntingtin with expanded glutamine repeats form nuclear and cytoplasmic aggregates in cell culture [In Process Citation].* Hum Mol Genet, 1998. **7**(5): p. 783-90.

37. Zheng, S., et al., *A series of N-terminal epitope tagged Hdh knock-in alleles expressing normal and mutant huntingtin: their application to understanding the effect of increasing the length of normal Huntingtin's polyglutamine stretch on CAG140 mouse model pathogenesis.* Mol Brain, 2012. **5**: p. 28.

38. Dyer, R.B. and C.T. McMurray, *Mutant protein in Huntington disease is resistant to proteolysis in affected brain.* Nat Genet, 2001. **29**(3): p. 270-8.

39. Shirasaki, D.I., et al., *Network organization of the huntingtin proteomic interactome in mammalian brain.* Neuron, 2012. **75**(1): p. 41-57.

40. Nasir, J., et al., *Targeted disruption of the Huntington's disease gene results in embryonic lethality and behavioral and morphological changes in heterozygotes.* Cell, 1995. **81**(5): p. 811-23.

41. Duyao, M.P., et al., *Inactivation of the mouse Huntington's disease gene homolog Hdh.* Science, 1995. **269**(5222): p. 407-10.

42. Zeitlin, S., et al., *Increased apoptosis and early embryonic lethality in mice nullizygous for the Huntington's disease gene homologue.* Nat Genet, 1995. **11**(2): p. 155-63.

43. Wang, G., et al., *Ablation of huntingtin in adult neurons is nondeleterious but its depletion in young mice causes acute pancreatitis.* Proc Natl Acad Sci U S A, 2016. **113**(12): p. 3359-64.

44. Yu, M.S. and N. Tanese, *Huntingtin Is Required for Neural But Not Cardiac/Pancreatic Progenitor Differentiation of Mouse Embryonic Stem Cells In vitro.* Front Cell Neurosci, 2017. **11**: p. 33.

45. Arteaga-Bracho, E.E., et al., *Postnatal and adult consequences of loss of huntingtin during development: Implications for Huntington's disease.* Neurobiol Dis, 2016. **96**: p. 144-155.

46. Godin, J.D., et al., *Huntingtin is required for mitotic spindle orientation and mammalian neurogenesis.* Neuron, 2010. **67**(3): p. 392-406.

47. Molina-Calavita, M., et al., *Mutant huntingtin affects cortical progenitor cell division and development of the mouse neocortex.* J Neurosci, 2014. **34**(30): p. 10034-40.

48. Lopes, C., et al., *Dominant-Negative Effects of Adult-Onset Huntingtin Mutations Alter the Division of Human Embryonic Stem Cells-Derived Neural Cells.* PLoS One, 2016. **11**(2): p. e0148680.

49. Gemayel, R., et al., *Variable Glutamine-Rich Repeats Modulate Transcription Factor Activity.* Mol Cell, 2015. **59**(4): p. 615-27.

50. Schaffar, G., et al., *Cellular toxicity of polyglutamine expansion proteins: mechanism of transcription factor deactivation.* Mol Cell, 2004. **15**(1): p. 95-105.

51. Zhai, W., et al., *In vitro analysis of huntingtin-mediated transcriptional repression reveals multiple transcription factor targets.* Cell, 2005. **123**(7): p. 1241-53.

52. Gauthier, L.R., et al., *Huntingtin controls neurotrophic support and survival of neurons by enhancing BDNF vesicular transport along microtubules.* Cell, 2004. **118**(1): p. 127-38.

53. Hofer, M., et al., *Regional distribution of brain-derived neurotrophic factor mRNA in the adult mouse brain.* EMBO J, 1990. **9**(8): p. 2459-64.

54. Altar, C.A., et al., *Anterograde transport of brain-derived neurotrophic factor and its role in the brain.* Nature, 1997. **389**(6653): p. 856-60.

55. Bulgari, D., D.L. Deitcher, and E.S. Levitan, *Loss of Huntingtin stimulates capture of retrograde dense-core vesicles to increase synaptic neuropeptide stores.* Eur J Cell Biol, 2017. **96**(5): p. 402-406.

56. Grima, J.C., et al., *Mutant Huntingtin Disrupts the Nuclear Pore Complex.* Neuron, 2017. **94**(1): p. 93-107 e6.

57. Gasset-Rosa, F., et al., *Polyglutamine-Expanded Huntingtin Exacerbates Age-Related Disruption of Nuclear Integrity and Nucleocytoplasmic Transport.* Neuron, 2017. **94**(1): p. 48-57 e4.

58. Pouladi, M.A., et al., *Full-length huntingtin levels modulate body weight by influencing insulin-like growth factor 1 expression.* Hum Mol Genet, 2010. **19**(8): p. 1528-38.

59. Kudwa, A.E., et al., *Increased Body Weight of the BAC HD Transgenic Mouse Model of Huntington's Disease Accounts for Some but Not All of the Observed HD-like Motor Deficits.* PLoS Curr, 2013. **5**.

60. Van Raamsdonk, J.M., et al., *Body weight is modulated by levels of full-length huntingtin.* Hum Mol Genet, 2006. **15**(9): p. 1513-23.

61. Borlongan, C.V., et al., *Behavioral pathology induced by repeated systemic injections of 3-nitropropionic acid mimics the motoric symptoms of Huntington's disease.* Brain Research, 1995. **697**(1-2): p. 254-257.

62. Ismailoglu, I., et al., *Huntingtin protein is essential for mitochondrial metabolism, bioenergetics and structure in murine embryonic stem cells.* Dev Biol, 2014. **391**(2): p. 230-40.

63. Hamilton, J., et al., *Energy Metabolism and Mitochondrial Superoxide Anion Production in Pre-symptomatic Striatal Neurons Derived from Human-Induced Pluripotent Stem Cells Expressing Mutant Huntingtin.* Mol Neurobiol, 2020. **57**(2): p. 668-684.

64. Hamilton, J., et al., *Oxidative metabolism in YAC128 mouse model of Huntington's disease.* Hum Mol Genet, 2015. **24**(17): p. 4862-78.

65. The HD iPSC Consortium, *Bioenergetic deficits in Huntington's disease iPSC-derived neural cells and rescue with glycolytic metabolites.* Hum Mol Genet, 2019.

66. Seong, I.S., et al., *HD CAG repeat implicates a dominant property of huntingtin in mitochondrial energy metabolism.* Hum Mol Genet, 2005. **14**(19): p. 2871-80.

67. Orr, A.L., et al., *N-terminal mutant huntingtin associates with mitochondria and impairs mitochondrial trafficking.* J Neurosci, 2008. **28**(11): p. 2783-92.

68. Yano, H., et al., *Inhibition of mitochondrial protein import by mutant huntingtin.* Nat Neurosci, 2014. **17**(6): p. 822-31.

69. Song, W., et al., *Mutant huntingtin binds the mitochondrial fission GTPase dynamin-related protein-1 and increases its enzymatic activity.* Nat Med, 2011. **17**(3): p. 377-82.

70. Buren, C., et al., *Impaired development of cortico-striatal synaptic connectivity in a cell culture model of Huntington's disease.* Neurobiol Dis, 2016. **87**: p. 80-90.

71. Deng, Y.P., et al., *Differential loss of thalamostriatal and corticostriatal input to striatal projection neuron types prior to overt motor symptoms in the Q140 knock-in mouse model of Huntington's disease.* Front Syst Neurosci, 2014. **8**: p. 198.

72. Melief, E.J., et al., *Loss of glutamate signaling from the thalamus to dorsal striatum impairs motor function and slows the execution of learned behaviors.* NPJ Parkinsons Dis, 2018. **4**: p. 23.

73. Kolodziejczyk, K. and L.A. Raymond, *Differential changes in thalamic and cortical excitatory synapses onto striatal spiny projection neurons in a Huntington disease mouse model.* Neurobiol Dis, 2016. **86**: p. 62-74.

74. Sun, Y., et al., *Polyglutamine-expanded huntingtin promotes sensitization of N-methyl-D-aspartate receptors via post-synaptic density 95.* J Biol Chem, 2001. **276**(27): p. 24713-8.

75. Fan, J., et al., *Interaction of postsynaptic density protein-95 with NMDA receptors influences excitotoxicity in the yeast artificial chromosome mouse model of Huntington's disease.* J Neurosci, 2009. **29**(35): p. 10928-38.

76. McKinstry, S.U., et al., *Huntingtin is required for normal excitatory synapse development in cortical and striatal circuits.* J Neurosci, 2014. **34**(28): p. 9455-72.

77. Burrus, C.J., et al., *Striatal Projection Neurons Require Huntingtin for Synaptic Connectivity and Survival.* Cell Rep, 2020. **30**(3): p. 642-657 e6.

78. Parsons, M.P., et al., *Bidirectional control of postsynaptic density-95 (PSD-95) clustering by Huntingtin.* J Biol Chem, 2014. **289**(6): p. 3518-28.

79. Ethell, I.M. and Y. Yamaguchi, *Cell surface heparan sulfate proteoglycan syndecan-2 induces the maturation of dendritic spines in rat hippocampal neurons.* J Cell Biol, 1999. **144**(3): p. 575-86.

80. Kabeya, Y., et al., *LC3, GABARAP and GATE16 localize to autophagosomal membrane depending on form-II formation.* J Cell Sci, 2004. **117**(Pt 13): p. 2805-12.

81. Pankiv, S., et al., *p62/SQSTM1 binds directly to Atg8/LC3 to facilitate degradation of ubiquitinated protein aggregates by autophagy.* J Biol Chem, 2007. **282**(33): p. 24131-45.

82. Martinez-Vicente, M., et al., *Cargo recognition failure is responsible for inefficient autophagy in Huntington's disease.* Nat Neurosci, 2010. **13**(5): p. 567-76.

83. Wong, Y.C. and E.L. Holzbaur, *The regulation of autophagosome dynamics by huntingtin and HAP1 is disrupted by expression of mutant huntingtin, leading to defective cargo degradation.* J Neurosci, 2014. **34**(4): p. 1293-305.

84. Steffan, J.S., et al., *SUMO modification of Huntingtin and Huntington's disease pathology.* Science, 2004. **304**(5667): p. 100-4.

85. Gao, R., et al., *Mutant huntingtin impairs PNKP and ATXN3, disrupting DNA repair and transcription.* Elife, 2019. **8**.

86. Genetic Modifiers of Huntington's Disease (GeM-HD) Consortium, *Identification of Genetic Factors that Modify Clinical Onset of Huntington's Disease.* Cell, 2015. **162**(3): p. 516-26.

87. MacKay, C., et al., *Identification of KIAA1018/FAN1, a DNA repair nuclease recruited to DNA damage by monoubiquitinated FANCD2.* Cell, 2010. **142**(1): p. 65-76.

88. Goold, R., et al., *FAN1 modifies Huntington's disease progression by stabilizing the expanded HTT CAG repeat.* Hum Mol Genet, 2019. **28**(4): p. 650-661.

89. Lu, X.H., et al., *Targeting ATM ameliorates mutant Huntingtin toxicity in cell and animal models of Huntington's disease.* Sci Transl Med, 2014. **6**(268): p. 268ra178.

90. Konca, K., et al., *A cross-platform public domain PC image-analysis program for the comet assay.* Mutat Res, 2003. **534**(1-2): p. 15-20.

91. Williamson, M.P., *The structure and function of proline-rich regions in proteins.* Biochem J, 1994. **297 (Pt 2)**: p. 249-60.

92. Gao, Y.G., et al., *Structural Insights into the specific binding of huntingtin proline-rich region with the SH3 and WW domains.* Structure, 2006. **14**(12): p. 1755-65.

93. Steffan, J.S., *Does Huntingtin play a role in selective macroautophagy?* Cell Cycle, 2010. **9**(17): p. 3401-13.

94. Maiuri, T., L.E. Bowie, and R. Truant, *DNA Repair Signaling of Huntingtin: The Next Link Between Late-Onset Neurodegenerative Disease and Oxidative DNA Damage.* DNA Cell Biol, 2019. **38**(1): p. 1-6.

95. Panier, S. and S.J. Boulton, *Double-strand break repair: 53BP1 comes into focus.* Nat Rev Mol Cell Biol, 2014. **15**(1): p. 7-18.

96. Zheng, Z., et al., *An N-terminal nuclear export signal regulates trafficking and aggregation of Huntingtin (Htt) protein exon 1.* J Biol Chem, 2013. **288**(9): p. 6063-71.

97. Olive, P.L. and J.P. Banath, *The comet assay: a method to measure DNA damage in individual cells.* Nat Protoc, 2006. **1**(1): p. 23-9.

98. Fernandez-Capetillo, O., et al., *H2AX: the histone guardian of the genome.* DNA Repair (Amst), 2004. **3**(8-9): p. 959-67.

99. Rothkamm, K., et al., *DNA damage foci: Meaning and significance.* Environ Mol Mutagen, 2015. **56**(6): p. 491-504.

100. Gusel'nikova, V.V. and D.E. Korzhevskiy, *NeuN As a Neuronal Nuclear Antigen and Neuron Differentiation Marker.* Acta Naturae, 2015. **7**(2): p. 42-7.

101. Porras-Garcia, E., et al., *Purkinje cell loss affects differentially the execution, acquisition and prepulse inhibition of skeletal and facial motor responses in Lurcher mice.* Eur J Neurosci, 2005. **21**(4): p. 979-88.

102. Mashimo, T., et al., *Progressive Purkinje cell degeneration in tambaleante mutant mice is a consequence of a missense mutation in HERC1 E3 ubiquitin ligase.* PLoS Genet, 2009. **5**(12): p. e1000784.

103. Dougherty, S.E., et al., *Purkinje cell dysfunction and loss in a knock-in mouse model of Huntington disease.* Exp Neurol, 2013. **240**: p. 96-102.

104. Singh-Bains, M.K., et al., *Cerebellar degeneration correlates with motor symptoms in Huntington disease.* Ann Neurol, 2019. **85**(3): p. 396-405.

105. Wetts, R. and K. Herrup, *Direct correlation between Purkinje and granule cell number in the cerebella of lurcher chimeras and wild-type mice.* Brain Res, 1983. **312**(1): p. 41-7.

106. Burrows, C.J. and J.G. Muller, *Oxidative Nucleobase Modifications Leading to Strand Scission.* Chem Rev, 1998. **98**(3): p. 1109-1152.

107. Kawanishi, S. and M. Murata, *Mechanism of DNA damage induced by bromate differs from general types of oxidative stress.* Toxicology, 2006. **221**(2-3): p. 172-8.

108. Ben Saad, H., et al., *Potassium Bromate-induced Changes in the Adult Mouse Cerebellum Are Ameliorated by Vanillin.* Biomed Environ Sci, 2018. **31**(2): p. 115-125.

109. Shacter, E., *Quantification and significance of protein oxidation in biological samples.* Drug Metab Rev, 2000. **32**(3-4): p. 307-26.

110. Klionsky, D.J., et al., *Guidelines for the use and interpretation of assays for monitoring autophagy in higher eukaryotes.* Autophagy, 2008. **4**(2): p. 151-75.

111. Kabeya, Y., et al., *LC3, a mammalian homologue of yeast Apg8p, is localized in autophagosome membranes after processing.* EMBO J, 2000. **19**(21): p. 5720-8.

112. Yan, J., et al., *Germline deletion of huntingtin causes male infertility and arrested spermiogenesis in mice.* J Cell Sci, 2016. **129**(3): p. 492-501.

113. Kegel, K.B., et al., *Huntingtin associates with acidic phospholipids at the plasma membrane.* J Biol Chem, 2005. **280**(43): p. 36464-73.

114. Xia, J., et al., *Huntingtin contains a highly conserved nuclear export signal.* Hum Mol Genet, 2003. **12**(12): p. 1393-403.

115. McFadyen, M.P., et al., *Differences among eight inbred strains of mice in motor ability and motor learning on a rotorod.* Genes Brain Behav, 2003. **2**(4): p. 214-9.

116. Shanbhag, N.M., et al., *Early neuronal accumulation of DNA double strand breaks in Alzheimer's disease.* Acta Neuropathol Commun, 2019. **7**(1): p. 77.

117. Lattanzi, G., et al., *Lamins are rapamycin targets that impact human longevity: a study in centenarians.* J Cell Sci, 2014. **127**(Pt 1): p. 147-57.

118. Yan, S., M. Sorrell, and Z. Berman, *Functional interplay between ATM/ATR-mediated DNA damage response and DNA repair pathways in oxidative stress.* Cell Mol Life Sci, 2014. **71**(20): p. 3951-67.

119. Madabhushi, R., et al., *Activity-Induced DNA Breaks Govern the Expression of Neuronal Early-Response Genes.* Cell, 2015. **161**(7): p. 1592-605.

120. Menalled, L.B., et al., *Time course of early motor and neuropathological anomalies in a knock-in mouse model of Huntington's disease with 140 CAG repeats.* J Comp Neurol, 2003. **465**(1): p. 11-26.

121. Andre, E.A., *Structure/Function Analysis of the Huntingtin N-terminus Encoded by Htt Exon 1 Using Knock-In Mouse Models*, in *Neuroscience*. 2017, University of Virginia.

122. Neveklovska, M., *Generation and Characterization of Knock-in Mouse Models Expressing Versions of Normal (7Q) and Mutant (140Q) Huntington with Deletions of the Proline-rich Region*, in *Neuroscience*. 2012, University of Virginia.

123. Sanchez-Martin, P. and M. Komatsu, *p62/SQSTM1 - steering the cell through health and disease.* J Cell Sci, 2018. **131**(21).